Università
Ca'Foscari
Venezia

Master's Degree

in Digital and Public Humanities

Final Thesis

Remote Sensing and Digital Methods in Archaeology

The Necessary Means to Uncover a Bronze Age Settlement in North-Eastern Italy

Supervisor
Ch. Prof. Federico Bernardini

Assistant supervisor
Ch. Dr. Massimo Calosi
Ch. Prof. Elena Leghissa

Graduand
Samantha Hunter Broking
Matriculation number
893248

Academic Year
2021 / 2022

Table of Contents

0. Introduction

The rise of digital tools within the field of archaeology has drastically changed the exploration and understanding of the past. The primary temporal focus that has dominated archaeological study has expanded and transformed into a spatiotemporal analysis. Instead of investigating with the perspective of history through time, today, technology allows for the study of the environment and its relationship with nature and human surrounding the past. There are several digital practices demonstrating value within archaeological study including Airborne Laser Scanning (ALS), Structure from Motion (SfM) photogrammetry, 3D Ground Penetrating Radar (GPR) and thermography. These non-invasive techniques can provide detailed, high-resolution topography and detect buried anomalies corresponding to archaeological features. The use of these tools provides the opportunity to make new discoveries that may not have been possible solely using traditional methods, like stratigraphic excavations. This is the case for the recently uncovered protohistoric hillfort in northeastern Italy; without employing digital techniques, this settlement would likely still be unknown.

The Karstscape Project, a campaign to explore the Karst region, began in 2020 with a goal to reconstruct the progression of the ancient landscape. The project used ALS, SfM photogrammetry and 3D GPR to document findings. Within the area of Dolina, an Italian commune that borders Slovenia, evidence pointed to remains of a large protohistoric hillfort and archaeological fieldwalking that resulted in some surface-level pottery findings, furthered suspicions. The initial results allowed for reconstructing the settlement and in the highest, best-preserved sector, an additional investigation ensued. This took place at the eastern region of the settlement, henceforth referred to as Trmun hilltop, and used ALS, SfM photogrammetry, 3D GPR and thermal imaging to better define archaeological features. To ensure a comprehensive analysis of the Trmun hilltop, a stratigraphic excavation followed the digital investigation in summer 2022 and confirmed protohistoric occupation. As a whole, the Trmun campaign consisted of three stages: the original detection during the Karstscape Project, further investigation with digital methods and finished with a stratigraphic excavation.

The results from the Trmun campaign will be examined in detail to exemplify the impact digital methods, in particular remote sensing tools, can have in the field of archaeology. The first section of this paper provides sufficient explanation of the four digital tools utilized in this campaign: ALS, SfM photogrammetry, 3D GPR and thermal imaging to grasp a better understanding of how they are used and the kinds of results they can generate. This section will begin with information on Global Navigation Satellite Systems because it is incorporated in the digital methods. The remaining sections are dedicated to the Trmun campaign from initial investigative results to the stratigraphic excavation that revealed a chronological timeline and confirmed protohistoric occupation. The combination of digital and traditional methods helped uncover a Bronze Age settlement and the Trmun campaign can be used as an example for future archaeological studies that prove such a combination is imperative for the clearest results.

1. Digital Methods in Archaeology

1.1. Global Navigation Satellite Systems

Before discussing the four digital methods, it is important to highlight global navigation satellite systems (GNSS). The majority of remote sensing technologies in archaeology are accompanied with GNSS and provide precise location information to help analyze results. Therefore, knowledge of GNSS will allow for a deeper understanding of the digital methods.

1.1.0. Introduction

GNSS is more commonly referred to as, global positioning systems (GPS) (Boeser, 2019). GNSS and GPS have been used synonymously for decades, in actuality though, they are different. GNSS is the general term used to describe satellite constellations in a medium earth orbit around the globe. These systems provide positioning, navigation and timing services at various levels of accuracy. GPS is solely the navigation system created and operated by the United States; its prevalence, compared to other GNSS, across the world has fashioned the synonymous usage between GNSS and GPS. Specifically for archaeology, GNSS allows for very precise location information for topographical data that can be used with software to help interpret study areas, whether it be to discover anomalies or create 3D models. Understanding GNSS is an essential part of using various techniques for data collection.

GNSS refers to satellite constellations, or a group of satellites working together, that provide position and time data. There are four main GNSS constellations: GPS, GLONASS, Galileo and BeiDou. GPS is the most utilized navigation system and will be the most referred to throughout this paper. GLONASS is the satellite constellation operated by the Russian Federation, Galileo by the European Union and BeiDou by China. All four of these systems have at least 24 satellites in operation to ensure global coverage and moreover, each provides free usage of their systems. There are two smaller regional systems, NAVIC from India and QZSS from Japan. These are satellite constellations that provide location services in their respective regions but are not large enough to provide global-scale coverage.

GPS is one of the main navigation resources used throughout the world by both governmental organizations and the public. A GPS receiver that is positioned anywhere on or near Earth's surface is fed location and time information from satellites in a medium earth orbit. This type

of orbit offers high accuracy while maintaining a wide coverage area. GPS, along with the other three GNSS, have at least 24 functioning satellites at all times to guarantee coverage (Boeser, 2019). This specific number of satellites derives from the need to have at least four satellites for calculating position on earth and having 24 satellites is enough to provide total coverage around the sphere. The United States guarantees approximately seven meters of accuracy 95% of the time and to ensure this, GPS operates a total of 31 satellites (National Coordination Office, 2021). The extra seven satellites provide backup to the core constellation of 24 satellites.

1.1.1. Components and Usage

GNSS satellites act as reference points for GNSS receivers that are positioned somewhere on or near earth's surface. The satellites emit radio signals that contain two specific pieces of information, the time the signal left the satellite and the position of the satellite at that particular moment. The GNSS receiver then takes the travel time, the total time from satellite to receiver, and multiples it by the speed of light to calculate distance. This will take place over a total of at least four satellites in a method known as trilateration to calculate location (fig. 1) (Boeser, 2019). While having distance data from three satellites would in theory give a 3D position, this is not the case for a GNSS receiver. All satellites are equipped with an atomic clock, which is a clock that has extreme precision. Atomic clocks though, are cost prohibitive and not used commercially. Because a GNSS receiver does not have an atomic clock within its system, only using three satellites would cause significant error and an inaccurate location calculation. Instead, if the measurements from a fourth satellite were taken, this would allow for error adjustment in the receiver's clock and an accurate position could be calculated. In addition to clock error, there are other types of error that can occur which include radio signal interference in the ionosphere and troposphere, unpredictable atmospheric conditions and multipath errors caused by a signal taking multiple paths to reach the receiver due to possible reflections off obstacles (Boeser, 2019). The use of a fourth satellite helps alleviate these errors along with the postulation that while satellites seem far apart from one another, they are close enough to assume they are affected by the same errors, and some can cancel each other out (fig. 1).

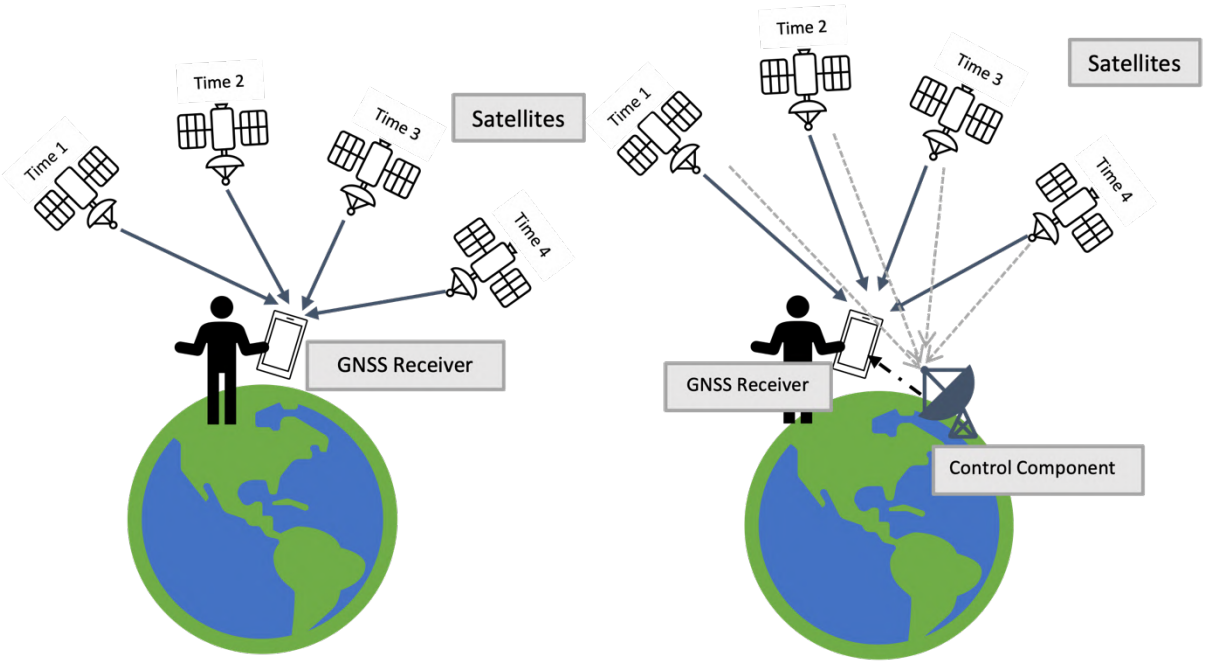

Figure 1. (Left) Position of a mobile device calculated using time and location information from 4 satellites. (Right) When a control unit is used to increase accuracy, the control unit acquires information from the satellites, and relays that information to the GNSS receiver.

1.1.2. Types of GNSS

GNSS receivers have various grades of accuracy and systems differ based on data acquisition needs. There are three categories of GNSS receivers: navigation, mapping and survey (fig. 2). Navigation grade systems are the most basic form of GNSS (fig. 2a). These are hand-held devices that provide general navigation information, similar to what is used in smartphones. Devices cost in the hundreds of dollars and is therefore a wise choice if only a low level of accuracy is required, as in several meters. The general public may use navigation grade devices to help with directions to get from one place to another (Pearson et al., 2015). The second type of GNSS is a mapping grade device (fig. 2b). These systems provide a higher level of accuracy; depending on the device, this could be just a few meters. Cost generally ranges in the low thousands and consists of a hand-held device with a data logger inside. These are the devices often used by agencies that want a higher level of accuracy for detailed landscape analysis and target identification (Pearson et al., 2015). The third type of GNSS is a survey level system (fig. 2c). These devices offer the highest accuracy; however, they are the most expensive, ranging in the tens of thousands of dollars. When centimeter-level accuracy is required for mapping, this is the preferred level of analysis. Normally, two receivers are used to generate position in a method known as differential GPS (DGPS) (Pearson et al., 2015). This

technique is becoming more popular for archaeological analysis because of the absolute accuracy that can be obtained for 3D model creation.

Figure 2. (a) Navigation grade device, (b) Mapping grade device, (c) Survey grade device, Differential-GPS. Note, images (a) and (b): Pearson et al., 2015.

1.1.3. Differential GPS

In general, GPS consists of a stand-alone receiver that collects signals from satellites to help pinpoint a location. Accuracy can range from several meters down to just a few depending on the device. For example, smartphones can determine a position within several meters of accuracy (Bettinger & Merry, 2019). A decent level of precision can be achieved at an affordable price. However, there will be circumstances where centimeter-level accuracy is required, and this can be achieved through survey grade devices. Differential GPS enhances the GPS system to acquire very precise location information (fig. 2c). DGPS improves accuracy through the addition of fixed ground points (Boeser, 2019). Two receivers are used for this method, a base receiver and rover receiver. The base receiver is fixed at a known point with predetermined coordinates. This receiver is static and collects and transmits satellite data to the rover. The rover, which is mounted on a pole and is mobile, is carried around an area to gather data (Pearson et al., 2015). The rover also collects satellite data throughout the survey; however, the coordinates will only be a rough estimate. Because the base station is at a fixed

location it can take the standard errors that occur during data collection, such as the ones that happen for a standalone GPS receiver like atmospheric conditions and clock error and compute a series of position corrections. Once calculated, these corrections are sent to the rover, and this allows the rover to correct its rough position estimate. The base and rover maintain a close distance, not exceeding 10 to 15 kilometers (km). This is purposeful because with such a close distance, it can be assumed that the receivers acquire signals from the same GPS satellites and therefore experience similar atmospheric conditions. These assumptions lead to error cancellation and help improve location accuracy. The ability to cancel error, along with using relative fixed points in a study area, allows DGPS to provide centimeter level accuracy. Archaeologists greatly benefit from this with the capacity to build highly accurate 3D models of study areas.

To go one step further and obtain even higher accuracy, real-time kinematic GPS (RTK GPS) can be used. RTK is seen as a branch of differential GPS because location is calculated essentially by the same method. Both require a base and rover receiver to gather data and communicate instantaneously. The only differences are that the corrections from the base receiver take place in real time and some of the internal computations change (Boeser, 2019 and Pearson et al., 2015). These calculations help further eliminate errors of atmospheric conditions or from satellite clocks. RTK GPS can give accuracy up to just a few centimeters, the only downside is that these devices cost significantly more than a DGPS system.

1.1.4. Conclusion

GNSS has significantly advanced data collection in archaeology. Archaeologists can collect position information with centimeter level accuracy in a short amount of time. Position data can be collected from RTK GPS devices and implemented in software such as Geographic Information Systems (GIS). GNSS can also be placed on digital tools for methods like Airborne Laser Scanning or Ground Penetrating Radar that will collect location data as a survey is conducted. Collecting GNSS data provides archaeologists with the opportunity to further 3D model creation, like elevation models, and deepen analysis.

1.2. Airborne Laser Scanning

1.2.0. Introduction

Airborne Laser Scanning (ALS) is a remote sensing technology that uses a laser profiling and scanning system to measure elevation. The addition of elevation figures within data collection allows for the creation of precise and accurate 3D models of the earth's surface known as Digital Elevation Models (DEM). These DEMs provide archaeologists with spatial information without ever needing to step foot on the study area. Using ALS in archaeological analysis helps create the surrounding environment of a study area and gives a better context of geological features.

Generally, ALS is referred to as Light Detection and Ranging (lidar, LiDAR) (Luo et al., 2019). While this is acceptable, it is important to note that lidar does not imply ALS. Lidar is a remote sensing method used to examine the surface of the earth; however, it does not need to be airborne. Lidar systems can also be attached to ground-based devices known as Terrestrial Laser Scanning (TLS) (Historic England, 2018). ALS is more commonly used to scan large areas, whereas TLS is better for smaller study areas. Lidar is similar to other scanning technologies like Sound Navigation and Ranging (Sonar) and Radio Detection and Ranging (Radar). All three techniques send signals to and from targets to calculate distance, they just use different mediums; lidar emits light pulses to understand the earth's surface and features, sonar uses sound waves to map the ocean and radar transmits radio waves for tracking movement in the sky or ground.

There are two types of airborne lidar, topographic and bathymetric (Luo et al., 2019). The latter uses a green light-based laser that can penetrate water; this is helpful to measure seafloor or riverbed elevations. Archaeologists mostly work with topographic lidar that uses a near-infrared light to map land. Near-infrared light, which is safe for human eyes, is utilized because these wavelengths, or types of light, reflect strongly off vegetation (Historic England, 2018).

ALS is an active remote sensing technique that uses light pulses to measure elevation of the ground, forest or buildings. In general, remote sensing methods observe targets on the

surface or subsurface of the earth by using non-direct contact devices (Luo et al., 2019). This gives archaeologists the opportunity to understand the geographical context of an area in a non-invasive way. An active remote system produces its own radiation, unlike passive systems that capture naturally occurring radiation. Passive systems detect natural energy, most commonly reflected sunlight, that is emitted or reflected by the target or study area. Active systems have their own light source that is used to illuminate an object or study area. A pulse of energy is sent from a laser to the target, then the target absorbs some of that energy and the remaining is reflected back to the system. The system records this backscatter to attain the elevation information. Since active systems create their own radiation, they can be used under various weather conditions and during the night (Luo et al., 2019).

1.2.1. Components and Usage

There are four main components that make up an airborne laser system: the lidar unit, a GPS receiver, an inertial measurement unit (IMU) and a computer. All four components are necessary for precise data collection. For the instance of archaeology, the laser unit consists of a near-infrared laser to scan the ground. The laser scans from side to side as the aircraft flies with a pulsed laser beam. The unit also includes particularly sensitive detectors that measure the reflected light (Monnet, 2012; Historic England 2018). An aircraft's natural movements produce data results in a zigzag-like pattern, unlike the standard grid-like collection. However, the data composed in this manner can still be processed and used to produce 3D models. The second component of an ALS system is the GPS receiver. This tracks the altitude and location of the aircraft. Knowing these coordinates allows the system to determine where the lidar reflections take place as it hits a target (Historic England, 2018). In terms of a coordinate system, the location is tracked as an (*x, y*) coordinate and the altitude is tracked as a *z* coordinate. The third component is the IMU. As an aircraft flies, movement and turbulence inevitably occur. The IMU monitors the orientation of the aircraft which includes the roll, pitch and yaw (Monnet, 2012). The IMU device may differ depending on aircraft type, but all observe the same information. The roll tracks the tilt of an aircraft from left to right; think of a plane's wing dipping to one side or the other. The pitch tracks the up or down movement; for example, tracking if a plane's nose increases or decreases in height. The yaw tracks rotation around the vertical axis; imagine a plane in a steady position and its tail wiggles left or right. Keeping track of this data assists the GPS receiver to determine the

actual position of the pulses as they hit an object or the ground. The fourth and most essential component of an ALS system is the computer. The computer collects and stores the data, in particular the height data. The critical height information allows for the complete construction of an elevation model (Historic England, 2018). Depending on the type of aircraft used or the goals of data collection, there may be additional components of the ALS system. Yet, in order to obtain meaningful data, these four components are necessary.

1.2.2. Data Collection

The process of acquiring ALS data takes place over several steps. First and foremost though, it is important to note an ALS system is mounted on an aircraft, hence the *airborne* in ALS. For large areas, planes and helicopters are utilized and in instances of smaller studies, Unmanned Aerial Vehicles (UAV) also known as drones, are suitable.

To begin, the aircraft flies around a specified area from side-to-side and sends a laser pulse out to scan the earth (fig. 3). There will be a few instances when the pulses are sent at nadir, as in directly below the aircraft, however most pulses will travel off-nadir, or at an angle from the aircraft. Some of the active light energy will reflect when it encounters an object, known as return.

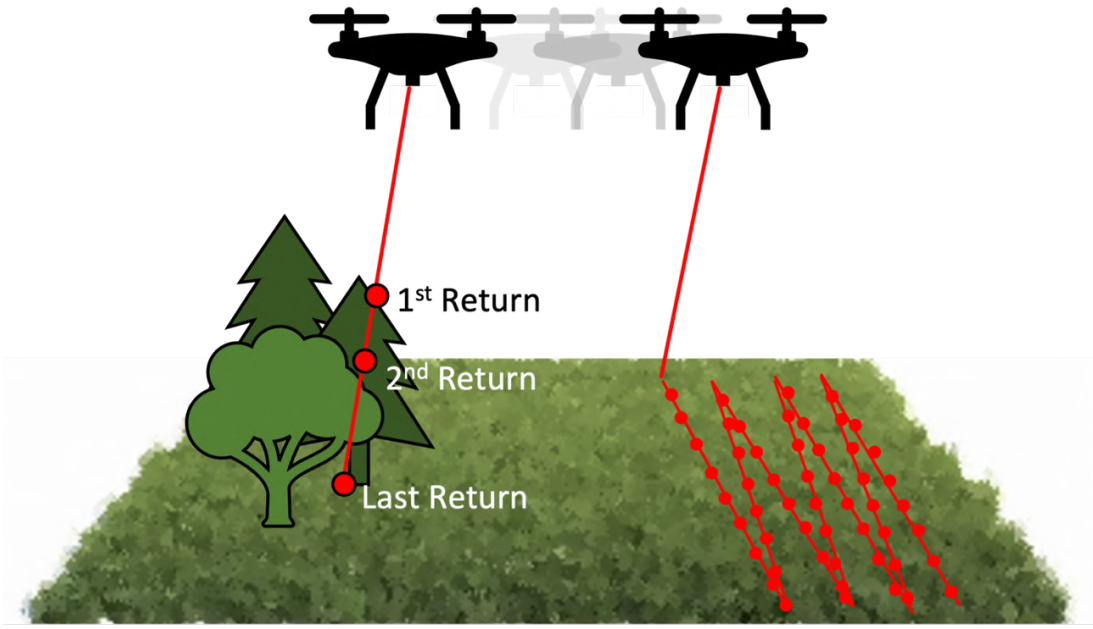

Figure 3. Illustration of the ALS process. An aircraft has an onboard GNSS and IMU for calculating position and orientation. (Right side) The red lines with circles demonstrate the path of scanning across the ground (x, y direction), with the circles representing the actual ground return footprints. (Left side) An example of multiple returns when the pulse hits an object(s) before reaching the ground (z direction).

The second step is to calculate the distance from the aircraft to the target. This takes place by recording the return times of the reflected energy, or the time it takes a pulse to travel to a target and back (Historic England, 2018). A single pulse of light can produce multiple returns and the sensor in the lidar unit records this as a continuous signal (fig. 3). As light passes through the canopy, reflections can occur off branches or leaves; the initial reflection is known as the first return (Historic England, 2018). It is only when the pulse hits the ground that the returns cease; the final reflection is referred to as the last return (Historic England, 2018). The numerous returns can offer meaningful insight about vegetation, like tree shape, leaf density and possibly shrubs or other plants that surround the trees. Once the total time (*t*) is recorded, distance can be calculated by a simple equation using the speed of light (*c*):

$$distance = \frac{t}{2} \times c$$

Time is divided by two because the travel time (*t*) takes the entire pulse journey into consideration, from the time it leaves the aircraft until it returns, and only a single journey is required for calculations. This formula gives the distance from the aircraft to the target with a high degree of accuracy, typically between 100-150 millimeters (mm) (Historic England, 2018).

The third step in ALS is computing elevation. During this stage it is important to recall two facts, turbulence unavoidably happens, and a pulse, most of the time, leaves the aircraft at an angle. Both of these can affect accuracy of elevation data and therefore are monitored by the IMU onboard the aircraft. The computer system takes the IMU measurements into consideration along with the information recorded by the GPS. The GPS receiver tracks the altitude (*a*) of an aircraft, which is the total distance from the aircraft to the earth's surface. The distance formula used in the second step calculated the distance (*d*) from the aircraft to the reflection. Knowing these two numbers will give elevation by the following formula:

$$elevation = a - d$$

Once elevation is calculated, the remaining GPS information, location of reflection, is calculated during the fourth step. To understand how a GPS system calculates location see section 1.1. With the elevation and location data in hand, the process of creating DEMs can commence.

One last interesting piece of information that can be determined through ALS is the material or composition of a target. The sensors within the lidar unit can record the intensity of a reflection, or the return strength of the laser pulse. This is done by looking at the intensity of returned radiation, as in the fraction of photons returned to the aircraft (Historic England, 2018). The number of photons is controlled by the material properties of the target surface. Surfaces provide different absorption rates and deliver a certain amount of reflection back to the sensor. The use of a near-infrared laser for archaeological purposes is intentional because the wavelengths created at those frequencies give high intensity returns when in contact with vegetation. This means vegetation is highly reflective and appears very bright in final products. Another example is black asphalt; this surface material absorbs much of the near-infrared wavelength and gives a low intensity return. On final products, asphalt appears rather dark in color (Historic England, 2018). For more information on the specifics of intensity calculations, refer to the Ground Penetrating Radar section, 1.4.2.

1.2.3. Data Processing

As lidar data is collected, it is initially stored in a point cloud format (denoted as an (*x, y*) location and *z*-value as an attribute, specifically elevation). This format provides the groundwork of 3D information about the topography of a study area. A point cloud is a collection of points with no relationship to one another; the points are merely floating in space (Historic England, 2018). This is due to the zigzag-like pattern caused by the aircraft. The light pulse emitted from the aircraft is not spaced in a regular grid-like form. Therefore, the goal is to convert the zigzag-like pattern into a grid which will allow for the formation of DEMs, among other outputs. Open-source software, like System for Automated Geoscientific Analyses GIS (SAGA GIS), are available to assist in data transformation. These software convert point cloud data into usable data structures for output creation.

The computer within the ALS system stores the point cloud data as a LAS (.las) file (Historic England, 2018). Once the LAS file is uploaded to the software, different types of surfaces can be generated; the two main ones are raster and a triangular irregular network (TIN) (fig. 4) (Historic England, 2018). Raster, or gridded, data are stored as a grid of values rendered on a map. Think of taking the point cloud data, which has points randomly dispersed in space, and placing a grid over it (fig. 4). This grid is made of cells, also called pixels. The pixels represent

an area on the ground (denoted as an (*x, y*) location) that all have the same spatial dimensions, for example a pixel might represent a 0.5 meter (m) x 0.5m area on the ground. Due to the point cloud data being scattered, some pixels will have many points and others may have none; those are referred to as “no data” values. When multiple points exist in a pixel, typically the average of the height values is taken (denoted as an attribute, *z*-value). However, to eliminate “no data” values, data points can be interpolated. Interpolation takes the values of points inside the cell, as well as the points surrounding the cell, to calculate a value by using statistical operations. Interpolation can provide some form of prediction for values, specifically in those “no data” pixels (Luo et al., 2019).

TIN is a second type of surface that can provide high precision models, however, takes much more computer power and processing time than a raster surface. TINs are considered a type of vector-based data representation that connect data points in a triangular facet (Historic England, 2018). TIN perceives the point cloud data as nodes that have *x, y* and *z* values. Because this data is non-uniform, three nodes are connected to form triangles of varying size and shape (fig. 4). Unlike raster, TIN keeps every data point and does not create or lose points through interpolation; this causes the long processing time because of utilizing, and maintaining accuracy of, the whole dataset. The triangles are interconnected, do not overlap and have a continuous surface (Historic England, 2018). TIN is helpful for surface areas with high variability because the triangle nodes can be placed irregularly.

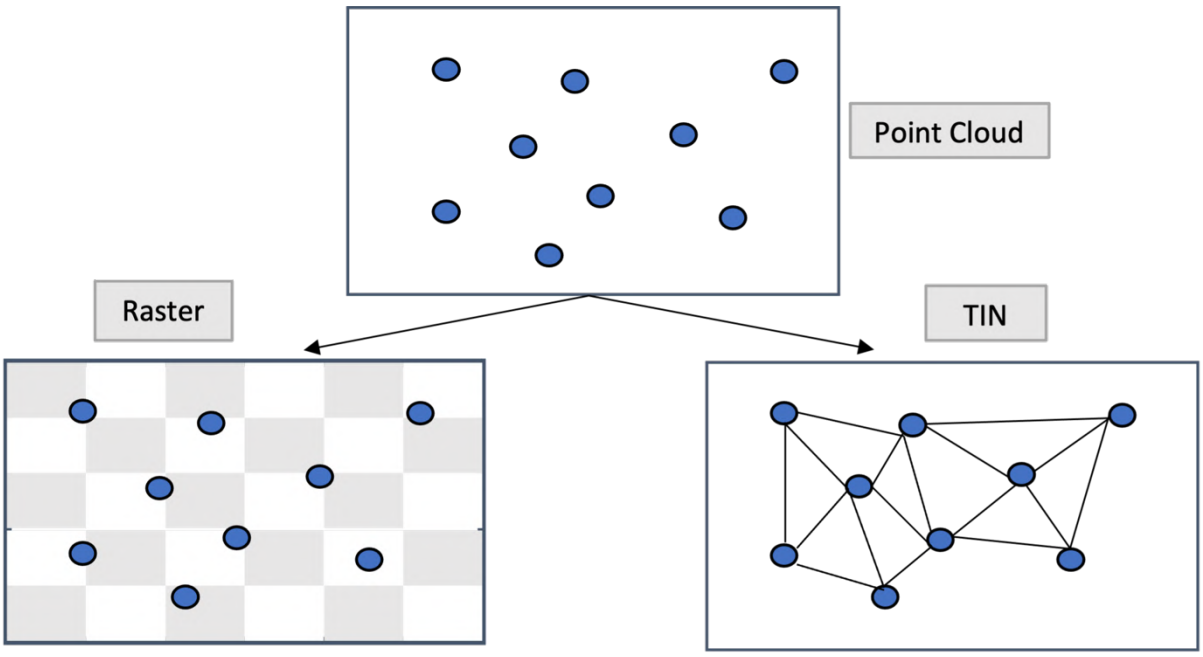

Figure 4. When ALS data is uploaded to software, it is in a point cloud format, with no data structure. The point cloud data can be converted into a raster format (left). The grid shows there can still be empty pixels with "no data" values. Data can also be converted into a TIN (right). Here, points are all interconnected to create a continuous surface.

1.2.4. Visualizations via LiDAR

The end products of ALS data revolve around reconstructing the topography of a specific area of the earth's surface. There are helpful software to better visualize these outputs such as Quantum Geographic Information System (QGIS) and Relief Visualization Toolbox (RVT). A Digital Elevation Model is the most common and useful product of lidar data. This model represents the bare surface of the earth, with vegetation, buildings or other structures excluded. DEMs can be split into Digital Surface Models (DSM) and Digital Terrain Models (DTM) (Luo et al., 2019). Both types further analyze the topography of an area by focusing on values related to specific laser pulse returns. DSMs are generated from the first pulse return. This model uses the highest elevation values to show the top canopy. This could be trees in a forest, manmade structures or even water surface height. DTMs are made from the last pulse return and represent the bare earth. This model gives information about the surface texture of the ground by taking out all vegetation or structures. In dense forest areas, a DTM can provide a meaningful glimpse of topographic information that would otherwise be difficult to gather.

The resolution of DEMs can vary depending on pixel size. In general, the smaller the pixel size, the higher the resolution. Although, if the pixel size decreases too much, the end result could contain many null pixels, or pixels that do not contain any data. Therefore, the goal is to obtain the smallest pixel size while maintaining a low number of empty pixels. Resolutions can range from under one meter to over one-hundred meters, each can be appropriate depending on study needs.

Once a DTM is constructed, it can be further analyzed through software, such as QGIS. This software offers several visualizations that can expand interpretation of a study area. Some standard visualization types are shaded reliefs, slope analysis and contour maps (Luo et al., 2019). A shaded relief, also known as a hillshaded map, is one of the most common outputs within archaeology because of the enhanced picture it can provide of the topography (Luo et al., 2019). By modifying light conditions of a DTM, for example the angle of the sun, various features of the topography can be enhanced depending on the desired focus. Slope analysis gives height information about terrain and an output can provide a color scale to visualize the elevation changes. Contour maps are another visualization that can be derived from a DTM. These maps use contour lines to enhance elevation changes in the terrain (Luo et al., 2019).

The products of ALS derived data, along with the expanded visualizations, improve the topographical understanding of a study area. However, it is essential to verify all results with field walking. It is possible for lidar data to pick up certain information that was interpreted incorrectly. This is especially the case for archaeological surveys; what may look like anomalies could just be part of the natural vegetation. With a simple walking survey, results can be confirmed as accurate.

1.2.5. Conclusion

ALS has many benefits such as quick and highly precise data collection, extremely sensitive lasers that record even minute anomalies, penetrate dense vegetation and has active sensing that allows for use day or night. Because this is a non-contact method, areas can be surveyed without human contact; this can be particularly valuable for cultural or heritage sites (Luo et al., 2019). Another advantage is cost, which is relatively economical, however for surveys of smaller areas the cost increases and may no longer be the best solution (Historic England,

2018). Only few other disadvantages exist, such as the inability to penetrate water and its impractical use in arable environments due to worn earthworks that may be undetectable.

Within archaeology, ALS has become an invaluable method that is causing a shift in analysis. Traditional archaeology typically focuses on a temporal analysis and relies on artifact findings, radiocarbon dating or comparing results of one site with nearby sites. However, with remote sensing technologies, a spatial analysis has emerged that takes the surrounding environment into consideration and leads to a more detailed analysis of an entire study area (Luo et al., 2019). Questions about location or examining how man may have affected an area can be answered. Spatial analysis certainly does not trump temporal analysis, instead they should be used in junction with each other. Combining ALS with the more conventional archaeological methods will provide a deeper and more complete analysis of a site.

1.3. Structure from Motion Photogrammetry

1.3.0. Introduction

Structure from Motion (SfM) photogrammetry is a passive remote sensing technique that uses a set of 2D photos to create 3D models of physical objects or the environment (Arrowsmith et al., 2021). SfM offers accurate and high-resolution outputs, similar or even better to other remote sensing methods like ALS, and therefore has become a popular option for archaeological analysis. The low cost is an additional incentive for usage, along with an easy-to-follow structure for acquiring SfM products like DEMs and orthophotos.

In general, photogrammetry is the practice of photography for surveying and gathering information of an object or area. Traditional photogrammetry requires a lot of information prior to data collection. The camera's height and focal length must be known, as well as the exact position and orientation of where the photos are taken. After photo collection, the computer work requires matching features and measuring distance between features. SfM photogrammetry has eliminated these requirements and allows data acquisition without knowledge of location or camera angle (Arrowsmith et al., 2021). Images can be taken with relative ease because today's software can take the 2D photos and process them to make 3D visualizations. The software is capable of identifying and matching features automatically and can process photos even at different acquisition angles and orientations. In traditional

photogrammetry, the camera needs to be stable to produce accurate results, however SfM photogrammetry allows for some instability in photo acquisition, like taking photos from a drone that may be affected by weather conditions (Arrowsmith et al., 2021).

1.3.1. Components and Usage

The components required for SfM photogrammetry are minimal. A camera and lens are the two most important aspects to consider. The resolution of SfM products like orthophotos are dictated by camera quality, therefore depending on the desired output, certain cameras may perform better than others. Mayank Sharma et. al, formulized a study on the effects of camera resolution and its sensor type to the accuracy of point cloud generation and georeferencing (Sharma et al., 2022). This study compared six consumer-grade cameras that would all be viable options to use for SfM photogrammetry. The cameras were fixed to a tripod with a GPS receiver above the camera. Assessment consisted of one building that had ten measured coordinates from a Total Station. Each camera captured 35 images with the same focal length (Sharma et al., 2022). The cameras ranged from 2 megapixels (MP) to 24.3MP. The point cloud generation, along with the georeferenced points, garnered quite interesting outcomes. The 2MP camera generated such poor-quality results compared to the rest that it was excluded from the final outcomes (Sharma et al., 2022). Overall, this study found that camera resolution directly impacts the accuracy of point cloud generation. Resolutions that fluctuate between two megapixels of each other will not significantly affect accuracy, although as resolution increases beyond 2MP, point cloud accuracy will be positively impacted (Sharma et al., 2022). The 24.3MP camera gave the highest level of accuracy, but the 10.2MP and 12.9MP cameras produced suitable accuracy between .25m and 0.5m. Therefore, the study determined that cameras ranging from 10-12MP produce point clouds that are sufficient to use for detailed analysis (Sharma et al., 2022). As an additional reference, the latest iPhone 14 Pro model is equipped with a 48MP camera system, making a cellular device a viable option for acquiring SfM images (Apple Inc., California).

Aside from selecting a camera, there are other optional components that can be added like a GNSS receiver. One option is to have a camera mounted on a tripod and place a GNSS receiver on top of the camera. Like in the previously mentioned study, this allows for georeferencing to take place. Georeferencing is the act of placing geographic information onto a digital image

that can later, with the help of mapping software like GIS, be transformed into actual real-world coordinates on Earth (Arrowsmith et al., 2021). Ground control points can also be collected for the target object or study area through a Total Station or RTK GPS.

The use of UAVs for SfM photogrammetry in archaeology is expanding. Cameras are firmly situated onto drones, or may be built into drones, making image collection easier and quicker. Some drones are even equipped with an RTK system that allows for a very high level of accurate georeferencing. This means that with every image capture, its metadata includes a georeferenced location (Arrowsmith et al., 2021). This eliminates the need for ground control points, even though they could still be beneficial to obtain and can only strengthen data analysis. Another benefit of drone SfM photogrammetry is flight planning software. Some drones come with programmed flight software that ensures parameters are maintained throughout a flight. Although, the downside to these features is the lack of flexibility. A user may not be able to customize the software, or even the hardware onboard the UAV (Alevizos, 2019). This includes the possibility of an onboard camera. Users that have a drone fixed with a camera are stuck with that camera's specs and cannot change them, even if a higher resolution were to be preferred. Battery life of drones is important to keep in mind. An average camera-carrying drone has approximately 20-30 minutes of flight time, thus flight plans must be made accordingly (Alevizos, 2019). This could mean multiple flights must occur to acquire data for the entire target; fortunately, by using drone software it is possible to program a UAV to make identical flights under the same parameters. Overall, drones suitable for SfM photogrammetry cost in the hundreds to low thousands making this a cost-effective option for archaeologists. This price range includes drones equipped with cameras and/or built in GNSS. As for cameras that could be mounted on tripods, those have a similar range, although cameras with 10-12MP resolution could be purchased in the mid to upper hundreds.

1.3.2. Data Collection

The process of SfM photogrammetry takes place over four steps. Although, SfM is technically only a part of the process, multi-view stereo (MVS) is a second essential step that allows for dense cloud creation. Therefore, the whole process should be considered as SfM-MVS. The initial image capture follows feature detection through software, then SfM completes a

bundle adjustment and lastly, MVS algorithms produce a dense cloud. Once a dense cloud is made, various outputs can be generated like a DEM, orthophoto or orthomosaic.

Image collection may seem like a simple procedure, however there are many factors that can influence an image data set (fig. 5). The first consideration is the camera lens. The lens should always be set to a fixed length throughout the duration of image capture. Any kind of zoom will confuse software (Arrowsmith et al., 2021). It is the *motion* of the camera that provides the depth information as a sequence of photos is taken, so keeping the lens at a constant length is necessary. This does not mean that images need to be taken at the same distance; image collection can include multiple rounds with the camera at various distances, as long as the lens length remains the same (Arrowsmith et al., 2021). A second consideration is the camera's geometry, or how the camera is positioned and oriented (fig. 5). SfM requires a large amount of image overlap, at least 50-60% to produce meaningful results (Bemis et al., 2014). Although many datasets have an even higher overlap percentage. This overlap allows the software to identify features of interest and create accurate 3D models. The camera's geometry affects the amount of possible overlap. The camera can take photos in a divergent, convergent or parallel manner. Divergent image capture is the least suitable for SfM because of the error it leaves in software processing. Divergent images are taken from a single point while the camera is spun around. A parallel position offers adequate overlap by taking a camera across pre-determined straight lines. Convergent collection is the best solution by moving the camera in an arch-like way around the target (fig. 5). A combination of these three positions can be used in data collection (Arrowsmith et al., 2021). The next consideration is camera orientation. A camera can be oriented in a nadir or oblique position. Nadir provides image capture straight down from the camera to the target and is most useful for flat surfaces. An oblique camera takes pictures from an angle, not in a perpendicular fashion, but at various angles like 45-degrees. Oblique is best for areas that have ranging elevations (Arrowsmith et al., 2021). As with using a variety of camera positions, data collection is best when using both nadir and oblique camera angles.

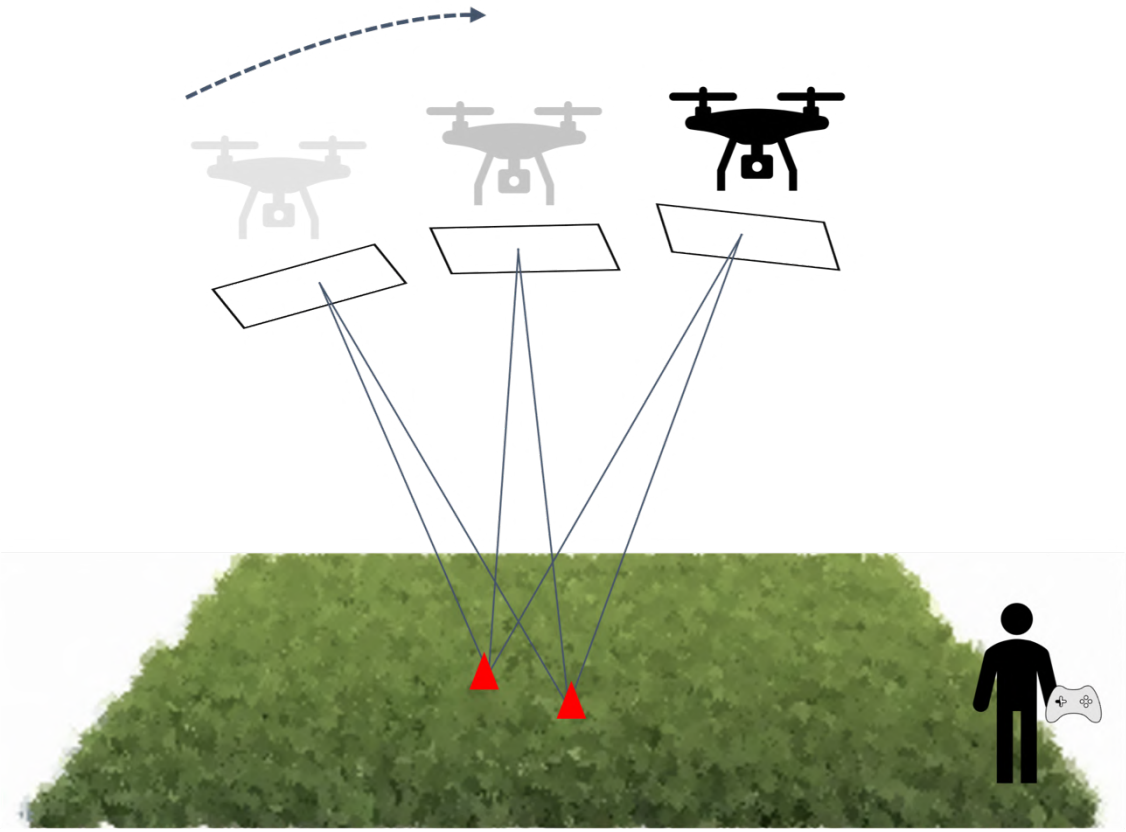

Figure 5. Illustration of the SfM photogrammetric process. The "structure" refers to both the camera positions and orientation, along with the topography. The "motion" of the camera provides the depth information. A UAV takes a sequence of photographs. The rectangular boxes show the positioning of photos being taken as the UAV flies in an arch-like path from left to right. The red triangles represent the features matched in multiple photos.

1.3.3. Data Processing

The first few steps in SfM-MVS post image collection deal with the SfM technique. These steps include feature detection, feature description, keypoint creation and matching, finished with a bundle adjustment (Arrowsmith et al., 2021). Photos are uploaded to a software, commonly Agisoft Metashape, and processed using various algorithms (Agisoft LLC, St. Petersburg). Scale-invariant feature transform (SIFT) is a frequently used algorithm that is specifically used to detect and match features within images (Lowe, 1999). SIFT spots features in images and creates points within the images that provide descriptive information including orientation and scale. These descriptors can identify points from different perspectives and conditions. The next step is keypoint creation. SIFT refines the feature points to create keypoints, these points are automatically detected by the software as having distinctive contrast. Keypoints are identified throughout all images and are then tied, or matched, across all images in which they appear. The last step that involves SfM is the bundle adjustment. The bundle adjustment attempts to recreate the scene structure by comparing an image's camera geometry and the

positions of keypoints into its calculations (Förstner, Wrobel, 2016; Iglhaut et al., 2019). Once the bundle adjustment is complete, a sparse cloud is created. A sparse cloud is a representation of all the tie points, or image pairs, that have sufficient overlap with each other. When visualizing a sparse cloud within Agisoft Metashape, it is possible to add camera orientation to see the paths of the images and the angles they were taken from (Arrowsmith et al., 2021). A sparse cloud does not consider the elevation, therefore should always be considered as a starting outcome used to make accurate models.

Next, MVS is used to build a dense cloud. MVS takes the calibrated overlapping images obtained from SfM and applies dense image-matching algorithms to reconstruct the target in 3D (Iglhaut et al., 2019; Arrowsmith et al., 2021). The algorithms group images based on proximity and compute each bunch separately to help with processing time. A dense cloud is a collection of points visualized in a 3D space. It takes all the points used in a sparse cloud and attempts to fill in the empty areas (Arrowsmith et al., 2021). There may be so many points generated that a dense cloud may appear as a *solid* surface but zooming will show the cloud as a collection of pixels.

Another interesting aspect of the SfM-MVS process is georeferencing. Georeferencing gives the points used in dense cloud creation a known location (Iglhaut et al., 2019). Without georeferencing, the points are merely floating in space without any kind of positional information. Georeferencing happens in two ways. The first is through the information collected from a GNSS receiver either mounted with a camera on a tripod or fixed to a drone. The second, a more accurate way of georeferencing, happens indirectly with ground control points. These points are acquired using DGPS and can be directly added into software like Agisoft Metashape. Ground control points can even be added and labeled on the outputs to further analysis.

1.3.4. Visualizations via SfM Photogrammetry

A dense cloud is the initial output of the SfM-MVS process that allows for the construction of several other products like a mesh, textured map, DEM, orthophoto and orthomosaic. A mesh takes the dense cloud a step further to provide a more continuous surface. Interpolation is done to create a mesh, which uses algorithms to make elevation predictions. For this setting,

interpolation happens when a point with unknown elevation takes the known elevation information of surrounding points to predict its own elevation (Arrowsmith et al., 2021). A textured map provides color to enhance certain features. DEMs are another output of SfM that can be generated in software like Agisoft Metashape with the click of a button. DEMs are generated in a rater format, or a grid of pixels. The DEM itself can be considered a 2.5D product because of the height data (*z*-coordinate). In a 2.5D setting, an (*x, y*) point only has one *z*-coordinate, whereas in 3D, *z* can contain multiple points. An orthophoto is an aerial image that provides an accurate map projection by removing distortions, camera tilt and any topographic relief from the area. An orthophoto uses the 3-dimensionality to make the appropriate projection and allow for distance measuring in a 2D photograph (Arrowsmith et al., 2021). One of the last main products that can be created from SfM-MVS is an orthomosaic. This takes a series of dissected orthophotos and stitches them together to make one orthomosaic photo, deriving from the mosaic technique in art. An orthomosaic gives very high details and accurate topographic information. DEMs, orthophotos and orthomosaics are most useful for archeological analysis because of the detail and accurate topographic information they can provide.

One final remark on the SfM-MVS process is that it is important to keep resolution in mind. Agisoft Metashape will build many outputs for a user, however processing time greatly varies depending on resolution selection. The higher the desired resolution, the longer the processing time and multiple days may be required. In general, a medium quality resolution will still provide adequate results and may save precious time, computer power and storage space (Arrowsmith et al., 2021).

1.3.5. Conclusion

Structure from Motion photogrammetry transforms sequences of overlapping 2D images into 3D models that can be used for detailed topographical analysis. SfM photogrammetry is a relatively cheap and flexible technology that is gaining popularity in archaeology. Only a camera and software are needed to transform pictures into meaningful products like DEMs and orthophotos. Unlike traditional photogrammetry, SfM does not require any knowledge of camera positions or coordinates in order to generate results allowing for more efficient data collection.

There are only a couple of limitations in SfM photogrammetry. First, SfM is not ideal in places that are difficult to photograph, like densely vegetated areas. Second, computer power and storage can be a hurdle during data processing. If camera resolution is high, or results like DEMs or orthophotos are desired in high resolution, a computer with very high processing power is required. Even with a high-power machine, processing time can still be extensive. Once the outputs are generated, storing them may be problematic. Some results take up a lot of memory on a computer and make conservation tough. Overall, a medium resolution will be sufficient in most cases.

SfM photogrammetry provides archeologists with a model of a site before any physical work begins, or could produce an accurate 3D representation of a specific piece of cultural heritage. Other benefits of SfM in archaeology include stratigraphical documentation. Stratigraphy is typically recorded manually and in areas where soils offer only slight differences, SfM can provide clarity. Cameras and drones can be purchased for a relatively low cost, especially in comparison to other techniques like ALS. Additionally, compared with ALS, SfM photogrammetry at times can offer even higher precision. Therefore, it is always a wise choice to incorporate multiple remote sensing methods in an archaeological analysis.

1.4. Ground Penetrating Radar

1.4.0. Introduction

Ground Penetrating Radar (GPR) is an active geophysical method used to gather subsurface information. Geophysical techniques allow for a better understanding of the physical earth properties of a study area (Johnston, 2021). This can be exceptionally useful in archaeology because much of history lies below the surface from years of natural and manmade effects. Breaking down GPR, the *ground* ranges from soil and rock to wood or concrete, amongst almost any type of surface aside from metal, which cannot be penetrated. *Radar*, which in itself is an acronym for Radio Detection and Ranging, is a system that uses radio waves to detect objects in relation to a site. *Penetrating*, for the instance of GPR, means using radar to pierce through the ground to find a target. Altogether, GPR is a method that releases radio waves into the ground and records the reflected pulses to build a subsurface image of a study area (Conyers, 2016, 2018; Johnston, 2021).

GPR has become one of the most used geophysical ground-based remote sensing methods in archaeology, however there are some other noteworthy similar methods that can produce meaningful results. Magnetometry is a technique that uses a magnetometer to record information on local magnetic fields throughout a site (Fassbinder, 2016). This device can detect subtle changes to acquire possible anomalies below the surface. A similar technique is gravimetry that measures gravitational acceleration with a gravimeter (Sarris, 2016). Both methods are passive, in that they use their own energy sources for data collection. Two other geophysical techniques are resistivity and the very-low-frequency electromagnetic method. These methods are active, in that they produce their own radiation and use probes placed in the ground to measure how electrical currents pass through materials (Tabbagh, 2016). Archaeologists may use any of these methods to help with a non-invasive investigation of a study area, however, the use of GPR is most prevalent due to its ability to provide precise depth information. GPR data analysis offers information on where and how deep objects are detected, and this gives archaeologists the steppingstones to formulate excavation plans.

As is the case of airborne laser scanning, GPR is an active remote sensing technique. Recall, remote sensing techniques collect data in a non-invasive manner, so for this method, no digging would be required to find a target under the surface. Being an active method means the system produces its own radiation (Conyers, 2016). GPR systems use radio waves, which are on the same electromagnetic spectrum as the near-infrared light used in ALS, only radio waves produce much longer wavelengths at lower frequencies. These differences shift the outcomes of both methods. ALS is used for accurate 3D mapping because of the precise data it can provide regarding a target's shape, size and location. While GPR is most helpful for detecting objects; rather than a goal of target analysis like size, GPR can provide assurance that *something* is beneath the surface (Johnston, 2021).

1.4.1. Components and Usage

GPR devices vary in shape and size, but all have three main components, a control unit, an antenna and a survey encoder (Johnston, 2021). The control unit holds the electronics that help generate and control the energy pulses. The unit also has a computer, or the capacity for an external computer connection, that collects and stores the data as it is taken. Additionally, nearly all control units have a display monitor. This provides a surveyor with data

in real-time and results can be checked on the spot with preliminary findings (Johnston, 2021). The second component is the antenna. The antenna is equipped with a transmitter and receiver. The transmitter sends radio signals into the ground as a series of pulses. As the pulses hit objects, parts of the radio waves will return back to the antenna and the receiver will collect this information that includes two-way travel time and the signal's amplitude (fig. 6) (Johnston, 2021). The data is then sent to the control unit to be recorded and saved. For most systems, the data is immediately displayed on the monitor in real-time. The survey encoder, the third component of a GPR system, is a small sensory device that helps track path information throughout a survey. These devices are also known as odometers or distance measuring instruments. The wheels on a device are calibrated to help the survey encoder calculate distance traveled. Moreover, the wheel calibration lets the system know it is moving and once a certain wheel rotation distance is met, the system triggers another pulse into the ground (Novo et al., 2008).

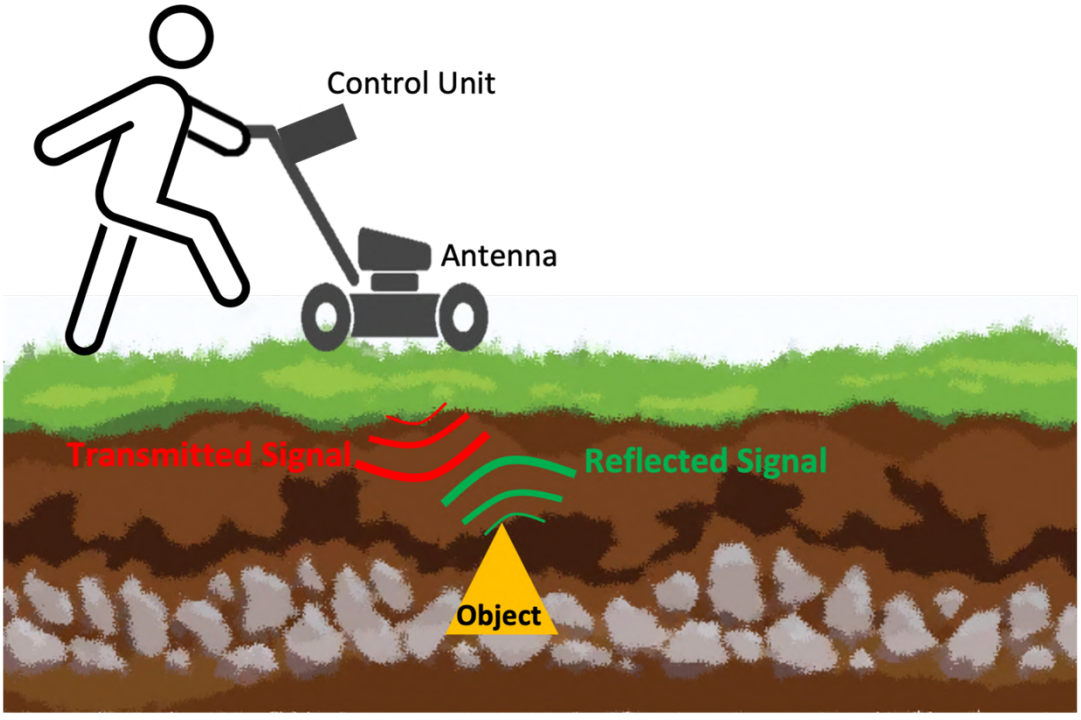

Figure 6. Illustrates the GPR process. As the device goes along the grid-like pattern established during the survey setup, the antenna sends a pulse into the ground and when an object is sensed, the reflected signal is returned. The control unit will display the data in real time.

There are numerous GPR models that cater to a variety of data acquisition needs. Some systems are rather large and are mounted on a trolley to be pulled or even attached to tractors. Most systems are similar to the size of a push lawn mower and require a user to push the device as he walks, while some devices are small enough to be used only with hands. The goal is to find a system that will provide the desired information regarding depth and resolution of a study area. This can be accomplished by selecting the appropriate radio signal frequency (Conyers, 2016). GPR systems transmit a wide swath, or range, of radio signals that vary in frequency. Typically, GPR devices are referred to by their center frequency. For example, a device that is centered at a frequency of 500-Megahertz (MHz) would be labeled as a 500-MHz GPR system. Additionally, the size of the device usually depends on the antenna size. A 500-MHz system is physically smaller than a 250-MHz system because the required antenna to generate a 500-MHz signal is shorter. It is important to note that as frequency capability increases, the resolution quality also increases, however the penetration depth will decrease (Johnston, 2018, 2021). When shallower depths or smaller targets are desired, higher frequencies may be a good option, whereas lower frequencies may be a better solution if desired penetration depths are deeper, or targets are larger. As a general rule of thumb in archaeology, ranges between 250-MHz and 500-MHz offer a good balance between depth and resolution (Johnston, 2021). Within this range, high-resolution images can be generated and interpreted by archaeologists.

1.4.2. GPR Survey Set Up

The process of acquiring GPR data starts with a proper survey setup. This can be completed in two steps. First, the target needs to be examined to understand the material, size and approximate location and depth underground. This allows for proper configuration of the GPR device, including the appropriate frequency selection. The second step is planning the physical survey; this involves choosing a grid pattern and determining the number of scans. Once the initial setup is complete, the data can be collected and post-survey analysis can be conducted.

The first step of survey setup is to analyze the target. It is especially important to have an idea of the target's type of material because this could affect the GPR system configurations and pulse reflections (Johnston 2018, 2021). Radio waves reflect off targets when there is a

contrast of materials, this is referred to as reflectivity. The more contrast there is between materials, the more energy that will be reflected back to the GPR system (Johnston 2018). It is also important to consider the dielectric difference between the target and the surrounding materials. Every material has a specific dielectric permittivity (*k*), which in simple terms for the case of GPR, means every material is given a value according to how reflective it is. The more reflective a material, the higher the *k*-value. Thus, when a GPR system is scanning the ground, the target needs to have a different, preferably a highly contrasted, *k*-value from the surrounding materials (Johnston, 2018). One example is a metal object located in dry soil. Metal has an infinite *k*-value because it cannot be penetrated by radio waves and is 100% reflective. Dry soil has a low *k*-value and therefore, because of the vastly different *k*-values, the antenna's receiver will record a high amplitude value, demonstrating the metal is highly reflective, and the monitor will display strong data collection at that point. On the contrary, if a target has a similar *k*-value to its surrounding material, the data will be weak and not well defined or visible.

In addition to gathering material information, it is also important to have an estimate of target size and subsurface depth. This helps determine which frequency to select. If the object is deep under the surface, selecting a low frequency may be best. However, if the object is deep and the target is large, selecting frequency may require more thought, and possibly be best to survey a couple of times with varying frequencies (Johnston, 2018, 2021). Overall, analyzing the target information is a critical first step in starting a GPR survey to get a better idea of how data may be collected.

The second step is planning the survey on the land (fig. 7). The two main aspects to consider here are grid pattern selection and determining the number of scans to be completed. All GPR systems collect data in a line-scan mode (Conyers, 2016; Johnston 2021). This means that data is collected by taking the GPR device along pre-determined individual lines in a grid formation. Grids allow an area to be surveyed thoroughly by collecting data from equally spaced parallel lines from two directions. While surveys may be conducted only using one direction, recording data from perpendicular angles generally provides clearer results. The grid pattern is set up using right angles and styled in a square grid. GPR software typically generates this automatically. Line spacing is another factor that determines how much work must be done.

If grid spacing is smaller, as in lines are closer together, more work will take place. Selecting a distance for line spacing may seem tricky, however the antenna length can be used to make this step easier. In general, the grid data can be collected using the length of the device's antenna (Conyers, 2016; Johnston 2021). For example, if a 500-MHz antenna is 20 centimeters (cm) long, the line spacing would ideally be 20cm. If time was a constraint and 20cm would take too long, the line spacing could be increased, although this would create a data gap which could cause some data loss. On the other hand, it is possible to have a data overlap where the line spacing is smaller than the antenna. Adjustments can be made depending on data collection needs, but overall, the target should be crossed over as many times as possible (Johnston 2018). One last consideration is to acquire data beyond the survey area. Expanding the survey to include some data from the outskirts could give a wider picture of the area and help with general background analysis.

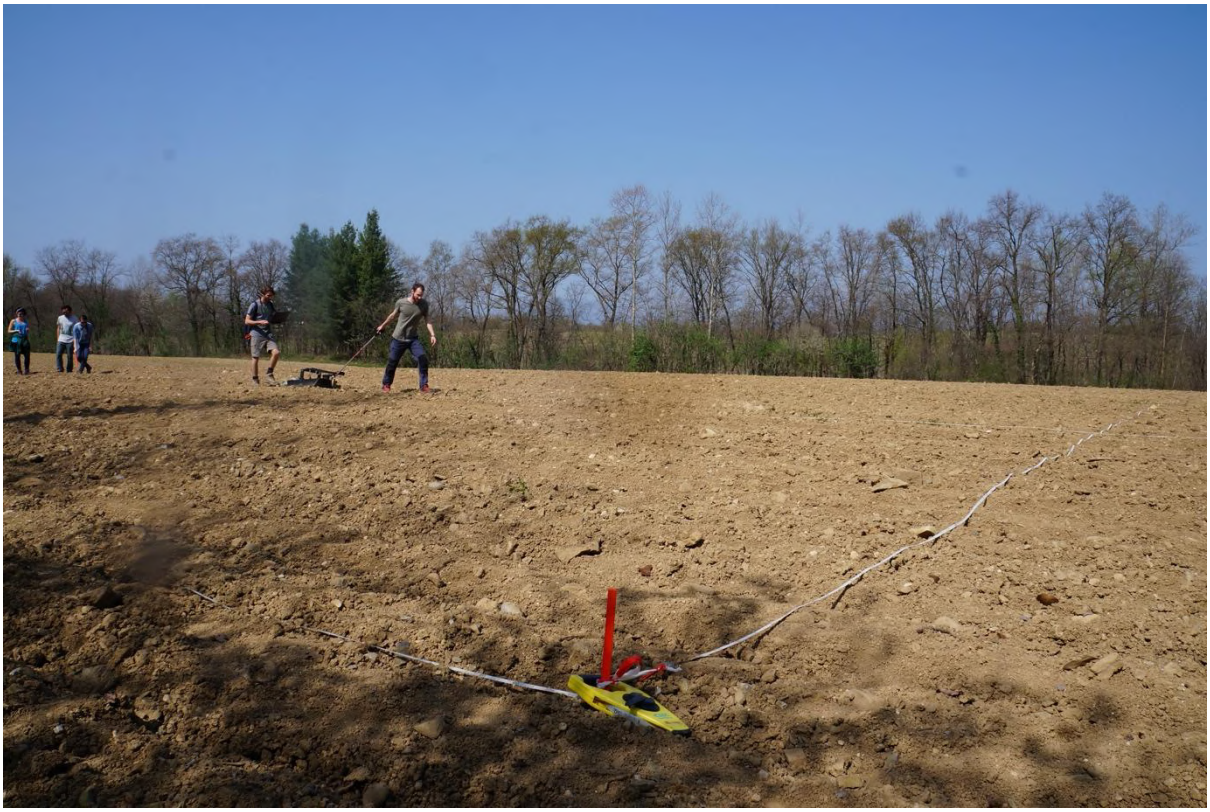

Figure 7. Example of a GPR device being pushed along a previously established grid. A surveyor walks behind the device to look at the data as it is being recorded and processed in real time. Image provided by: Forte, E., Pipan M.

To take survey planning a step further, pseudo-grid surveys can be conducted that include the use of GNSS. Some GPR systems are equipped with GNSS that greatly enhance data collection. The most desirable system would be an RTK GPS to allow for centimeter level position accuracy (Conyers, 2016). By incorporating precise location information, a more in-depth analysis of data could be conducted that provides further details of where objects were detected and for the case of archaeology, help with excavation plans.

1.4.3. Data Collection

Once the GPR device is properly configured and the grid pattern is established, data collection can commence. The GPR device is either pushed or pulled along the precise straight lines that were defined during the survey set up (fig. 7). As the wheels of the device turn, pulses are sent into the ground (fig. 6) (Johnston, 2018, 2021). The transmitter then generates and releases a pulse. A pulse can instigate one of four specific actions as it encounters a target, transmission, reflection, refraction or diffraction. Refraction occurs when the light pulse strikes an object and bends as it passes through it. Light is diffracted if it hits an object and spreads out. For the case of GPR, transmission and reflection are the most considered (Conyers, 2018).

When the GPR device releases a pulse, the radio wave either transmits, as in it goes through the ground or object, or it is reflected and sent back to the device. When this happens, the antenna's receiver collects this information, specifically time and amplitude (Conyers, 2016; Johnston 2018, 2021). The time is measured as the total travel time of the pulse as it left and returned to the device. The amplitude records the strength of the reflected pulse (Conyers, 2018). This can possibly help provide information about the target's properties. Furthermore, one of the most significant features of GPR is the ability to view data in real time. As data is collected by the receiver, it is immediately displayed on the system monitor. This allows for instant interpretation and gives the possibility to make modifications if necessary. It is important to keep in mind, the image produced from this data is a mere ambiguous and distorted image; it does not look like a regular picture taken from a camera. The monitor will show targets in the form of hyperbolas, an inverted U-shaped line. Hyperbolas are created because when the energy pulse enters the ground, it spreads in a cone-like shape; this is unlike a laser beam from ALS that shoots out in a straight line (Conyers, 2016). The cone

shaped energy causes the system to record some of the pulse return that occurs both ahead and behind the device. The tip of the hyperbola represents the time when the device is directly above the target. Hyperbolas will continue to form as long as the pulse is able to reach part of the target (Conyers, 2016).

When the GPR device reaches the end of the grid line, there is a slight pause to move and adjust the device to the next line. Think of mowing a lawn by going back and forth, taking a few seconds to turn the mower to face the other direction. If an RTK GPS system is active, the data collection can be continuous without the need to pause (Johnston, 2018). Depending on the size of the area and line spacing, data collection can be completed quickly, or could last hours or even days.

1.4.4. Data Processing

Once the data is collected, the main goal is to transform the distorted hyperbola-filled images into usable, interpretable images. These images are referred to as GPR slices. Various software are available that convert the data into slices simply by uploading the data held in the GPR control unit. When a dataset is uploaded into a software, along with adding the applicable acquisition information like survey dimensions and direction of the GPR device as it scanned, the transformation process starts. There are several algorithms and calculations that take place within the software that leave a user with various options to visualize the data.

The most common output for archaeologists is a horizontal depth slice. A depth slice is visualized as a sort of aerial image of the study area at one specific depth (Conyers, 2016; Johnston, 2018, 2021). These images can be color-coded to show reflectivity strength and to indicate where anomalies were sensed. The term anomaly is often used because GPR data only indicates that *something* is at a particular spot, it cannot give any kind of target details. Therefore, it is up to the archaeologist to interpret the anomaly. It is common for multiple depth slices to be generated to give a better picture of the subsurface. For example, having depth slices at 0.5m, 0.75m and 1m. These depth slices will most likely show different data because some targets may be visible at one depth, but not at another. If the target was a knife buried around 0.5m below the surface, the slice at 0.5m would indicate an anomaly at that depth, while a slice at 1m would most likely not show any reflectivity data at the exact spot.

Another way to further analysis is to superimpose a GPR slice onto an aerial image of the study area (Johnston, 2021). This visualization helps illustrate where the anomalies are in comparison to the surface. One other useful output for archaeologists is a vertical slice. This can be useful to further investigate a specific spot within the study area (Conyers, 2018). Keeping with the knife example, a vertical GPR slice could show the depth where the reflections occurred. If the knife is visible at a 0.5m horizontal slice but not at 0.75m, a vertical slice could indicate the deepest reflections occurred at 0.6m and that is why a 0.75m horizontal slice does not show any information.

1.4.5. Conclusion

Ground penetrating radar is becoming commonplace in archaeology because of the precise subsurface information it can provide. This method is non-invasive and gives archaeologists the chance to learn about an area without disrupting the land or possible material. The most important aspect to remember about GPR is that the data only indicates that *something* is below the surface. An archaeologist remains tasked with interpreting anomalies and deciding on possible further investigation. GPR data can confirm anomaly suspicions and roughly specify how deep an excavation would need to be in order to physically hit the anomalies or targets. Furthermore, GPR has allowed archaeologists to go beyond studying cultural heritage and investigate the surrounding environment. Understanding the geological aspects of a site can greatly aid in analysis. Paired with other remote sensing methods, GPR is a great technique to help understand the subsurface of an area.

1.5. Thermal Imaging

1.5.0. Introduction

Thermography, also known as thermal imaging, is a technique that has been around for nearly a century yet has only recently been integrated into the field of archaeology. Commercial availability and a significant drop of camera cost has allowed this remote sensing method to assist in historical and cultural analysis (Thomas, 2018, 2019; Casana et al., 2014; McLeester et al., 2018). Thermal imaging detects variances in ground temperatures to expose subterrestrial remains. Surveys can be completed quickly while covering a large area, making this technique a popular choice among other geophysical methods. Additionally, the results

produced from thermal image surveys are comparable with those created from other geophysical ones.

Thermal imaging is a passive, non-invasive technique that uses radiation to detect features beneath the surface. It can be coupled with similar imaging methods like multispectral imagery (McLeester et al., 2018). Both use electromagnetic radiation to monitor changes in ground temperature. The electromagnetic spectrum is the complete range of radiation wavelengths and frequencies. The lowest frequencies, which have the longest wavelength, are radio and microwaves and are used for applications like televisions or phones. The highest frequencies with the shortest wavelength are gamma rays; these rays are used in cancer treatment. In the middle sits the visible light spectrum, the light that can be seen by human eyes. Surrounding visible light is infrared and ultraviolet (NASA, 2010). A thermal camera uses infrared energy for detecting anomalies in the ground and multispectral can employ infrared, visible and ultraviolet energy in its survey (McLeester et al., 2018). Depending on the desired analysis, having multiple energy ranges can increase subsurface detection, however for most cases thermal imaging will suffice, as infrared has the capability to produce meaningful results.

1.5.1. Components and Usage

Similar to SfM photogrammetry, the components of thermal imaging are few and include a camera and possibly, a mounting device. The most important parts of the camera are the lens and sensor. These cameras are known as radiometric thermal cameras because the integrated sensor monitors radioactivity (McLeester et al., 2018). For the case of archaeology, the sensor measures and records the intensity of infrared energy to obtain ground temperatures. Thermal cameras can acquire a wide range of temperatures. For archaeologists, FLIR, one of the most well-known companies for thermal surveys, has cameras capable of detecting temperatures from -20°C – 400°C (-4°F – 752°F) (Teledyne FLIR, 2023). As for the lens, using a relatively short focal length will obtain the best results. A shorter focal length allows for a wider view, covering more ground in one image. Although the sensor's capabilities must be kept in mind; its range could affect image coverage (Casana et al., 2014). Camera sensors may also include a cooling feature that attempts to cool the internal sensor temperature to reduce *noise*, the radiation that may be coming from unwanted objects (Casana et al., 2014).

Until recently, cameras with these kinds of specifications and capabilities were too expensive to use for archaeological investigations. However, not only have thermal cameras become affordable, UAV technology has also improved to incorporate thermal surveys into its systems. Drone usage has become commonplace in archaeology, covering various methods like ALS and SfM photogrammetry. Now, drones can be used for thermal imaging by adding a radiometric camera to its system (Casana et al., 2014). This also allows for accurate location data to be collected as thermal images are taken. Additionally, flight planning software can be used for ease of data collection.

It is possible to mount thermal cameras onto devices such as helicopters, planes, kites, helium blimps and even a man-powered parachute (Casana et al., 2014). As thermal technology is novel in the archaeological world, only few studies have been published on the matter (e.g., Casana et al., 2014; McLeester et al., 2018; Casana et al., 2017; Ángel et al., 2020). One study, the Zagora Infrared Photogrammetry Project conducted a survey to compare drone-based data acquisition with ground-based. A thermal camera was mounted onto a pole while a surveyor walked around the site in a predetermined route (Thomas & Williams, 2019). Results showed that the ground-based thermal survey produced slightly stronger results than the one obtained from the aerial survey (Thomas & Williams, 2019). This leaves promise that with more thermal camera experimentation, new possibilities will be discovered, and common practice may be refined.

1.5.2. Data Collection

On paper, the process of collecting thermal data is simple. A thermal camera is turned on and as it moves about an area it detects and records the infrared energy of the ground, including energy of possible subsurface objects. The camera then converts the infrared data into an image that displays the surface temperatures. The differing temperatures represent possible anomalies beneath the surface (Casana et al., 2014). This process though, requires precise analysis of the surrounding climate conditions because of the direct impact weather has with infrared energy in materials. This analysis is difficult and can cause the need for multiple surveys. This issue will persist for some time until more studies are conducted, and more definitive conclusions can be made.

All objects emit varying amounts of infrared radiation dependent on the temperature of the object, this is known as emissivity (Casana et al., 2017). For example, water has a high emissivity because it absorbs infrared energy. This means water, or anything wet, can greatly impact thermal survey results. If a soil has a higher water content, and the target object absorbs high amounts of infrared energy, there is a possibility that because of the similar emissivity levels, the target will not be differentiated enough from the soil to be documented by thermal analysis. This is where tracking weather conditions factors in. A wet environment will likely produce poor results; therefore, a survey must be conducted during drier conditions (Casana et al., 2019). For the Zagora Project, surveys had to be conducted in the evenings because the morning dew negatively impacted results (Thomas & Williams, 2019). Furthermore, the temperature of materials varies throughout the day depending on the diurnal cycle. The diurnal cycle is all of the patterns that recur with every full rotation of Earth, or the 24-hour period it takes for the Earth to complete one axis rotation. The Earth's rotation causes temperature and weather fluctuations throughout each day, and this affects the emissivity of an object (Casana et al., 2017). The sun emits an immense amount of radiation, thus, as the sun rises in an area, the temperature of soils and objects, even ones beneath the surface, increase. The thermal camera will pick up radiation reflected by the sun, creating poor results if acquisition takes place during daylight (Casana et al., 2019). As the sun sets, temperatures gradually decrease, leaving nighttime as the favored time of day to organize surveys. It can take months-long observations to properly understand preferable acquisition times and even then, adjustments will most likely need to be made.

Detecting archaeological features occurs when there is sufficient variance of emissivity between the features and surrounding soil. The features will most likely possess different internal temperatures and emit varying amounts of infrared energy, which means the diurnal cycle will affect features and soils differently (Casana et al., 2017). Taking multiple thermal surveys will provide an overall picture of a study area and allow for possible anomalies to be detected during different times of the day. A study in Cáceres, Spain took multiple surveys throughout the course of a diurnal cycle and results indicated that time could affect how archaeological features are seen (Ángel et al., 2020).

Ground control points (GCP) are one way to enhance thermal imaging products. GCPs give accurate location information and produce stronger results. For thermal imaging, it is important to use an appropriate material that will not affect data collection. A case study at the Chaco-era Blue J community in New Mexico used GCPs made of aluminum sheets due to metal's low emissivity (Casana et al., 2014). The Zagora Project used cardboard, as the material's emissivity differed enough from the ground (Thomas & Williams, 2019). Another option is using the internal GNSS of a drone to georeference thermal images.

1.5.3. Data Processing

Thermal imaging data is processed in a similar manner to SfM photogrammetry. Using software like Agisoft PhotoScan and its internal algorithms, results can be obtained quickly. Images are processed for feature recognition and then matched throughout the set of images. Then the camera's parameters are considered, along with location coordinates, to create a point cloud. From here, a dense point cloud and mesh model are made to allow for final output generation. The most common products of thermal imaging are orthophotos and orthomosaics (Casana et al., 2014). Recall, an orthophoto is a single image that has removed distortions, while an orthomosaic combines all orthophotos together to create one complete image with distortion correction and typically is color balanced. During thermal image analysis multiple surveys are completed during various times of the day. Outputs like orthophotos allow for easy comparison amongst the different surveys.

In general, data is processed into a grayscale image, using brighter shades for hotter temperatures and darker shades for cooler temperatures. However, software has made it possible to transform grayscale photos into color images, where typically hotter temperatures are represented in yellow and cooler temperatures are blue, with a color scale for in-between temperatures. It is interesting to note that thermal cameras may come with a self-calibration function to help maintain a constant internal temperature. While overall helpful, this may cause a color drift in the image; for example, the top of an image produces vibrant colors, but progressing towards the bottom of the image, the colors slightly fade. Most likely, this would not hinder results. One potential solution could be to acclimate the camera to the surrounding temperatures by turning it on prior to commencing image collection (Casana et al., 2019).

To further analysis, thermal images may be compared with other aerial photos of a study site, in particular historical aerial photos (McLeester et al., 2018). Aerial photography has been used in archaeological analysis for quite some time. Many historic aerial collections started in the beginning to mid 20th century as a way to document various landscapes. Looking at photos from the past can help establish a timeline of a study area, as well as observe possible changes made throughout time (Historic England).

1.5.4. Conclusion

The recent availability and affordability of thermal survey equipment has brought a new way to study the subsurface for possible archaeological feature detection. With the few studies that have incorporated thermal imaging into investigations, results show a promising outlook for the impact it could have on archaeological analysis in the future. Thermal imaging expands the understanding of a surrounding environment and can help detect subsurface features. Filled in ditches, suppressed architecture and concentrations of artifacts are all possible discoveries with thermographic analysis (Casana et al., 2017). Thermographic data is proving to compete with other geophysical methods like ground penetrating radar, magnetometry and resistivity. Thermal imaging can accompany these methods to strengthen analysis or even be an alternative when terrain is too rough or rugged to perform a ground-based survey (Casana et al., 2014). There is still much to be learned about the impact thermography may have in archaeology. The current experimental phase will likely yield guidelines for conducting the best thermal survey, including guidance on the diurnal cycle and modifications to thermal camera systems. For now, incorporating a thermal survey into an archaeological study can bolster results produced from other remote sensing methods.

2. Equipment and Survey Methods

2.1. Equipment

The Karstscape Project hinted at potential archaeological features at shallow depths near and on the Trmun hilltop. This led to a deeper investigation of the hilltop by means of remote sensing methods including airborne laser scanning, 3D ground penetrating radar, structure from motion photogrammetry and thermal imaging. These techniques provided further evidence to suggest a protohistoric settlement, along with a distinct square-like structure, beneath the surface. An excavation ensued that confirmed suspicions of archaeological features. SfM photogrammetry provided detailed documentation of the excavation phases, along with the site's stratigraphy. The results of all methods were compared amongst each other to strengthen analysis. This following section provides details on the methods used in the Trmun hilltop investigation and excavation.

2.1.1. Airborne Laser Scanning

The ALS data of the Trmun hilltop and surrounding western area was obtained from previously collected data by the Civil Protection of Friuli Venezia Giulia. In 2006, the Regional Infrastructure of Environmental and Territorial Data for Friuli Venezia Giulia was established by the regional government to implement a region-wide project to document the environment and territory (RAFVG, 2023). This open access database, known as the Catalogue of Environmental and Territorial Data, continuously evolves and provides a variety of information such as topography that proved helpful for the Trmun investigation (RAFVG, 2023). The regional administration hired Helica, a company that specializes in remote sensing technologies, to survey the regional territory. Helica used the laser terrain mapper, ALTM 3100 to collect ALS data. ALTM 3100 was released by Teledyne Optech (Ontario, Canada; formally Optech Inc.) in the early 2000s and continues to be a useful system. The ALTM 3100 has the capability to scan from a range of 80m to 3,200m above ground level and can record multiple returns, along with intensity values (Lugari, 2014).

The ALS data of the Trmun hilltop and surrounding western area was extracted and imported into the free open-source software SAGA GIS as point clouds. SAGA GIS is used to edit and manipulate spatial data to produce digital outputs like DEMs. The software took ground

points to interpolate, or estimate, additional points to create 0.5m-resolution DTMs. Additional software, QGIS and RVT were used to further analyze the DTMs and generate other vitalizations like shaded relief models, slope analysis and contour maps. Additionally, historical cartography, specifically a section of the 19th century Franciscan Cadastral maps, was used to further analyze the ALS data. Cadastral maps have been used in geographic analysis to better understand the historical context of an area. These types of maps tracked parcels of land with information on dimension, ownership and value and were generally used for legal purposes (Gajda et al., 2014). These maps also possessed information like borders, roads, agriculture, amongst other useful markings. The Franciscan Cadastral maps encompassed all lands under the Habsburg Monarchy in the 19th century, which at the time included the area of Friuli Venezia Giulia (Gajda et al., 2014). The final step of ALS-derived results involved field walking of the entire Trmun hilltop to ensure the accuracy of all identified features in QGIS.

2.1.2. Structure from Motion Photogrammetry

The equipment used for SfM photogrammetric acquisition varied throughout the campaign. For the investigation phase, a DJI Mavic drone collected data primarily for DTM creation of the entire hilltop (DJI, Mavic 2, Shenzhen, China). The DJI Mavic is a solid model that weighs nearly one kilogram, has a flight time of around 31 minutes and is equipped with GNSS. The onboard camera has a 12MP sensor and a 24-48mm optical zoom lens with an 83° Field of View (FOV). With these specs, flights could be performed at a slightly higher elevation to obtain more coverage while still maintaining a quality image resolution. Two separate flights were planned with FlightPlanner, a specific software created by AeroScientific that assists in flight planning for aerial photography (AeroScientific, Adelaide, Australia). Using software to plan flights alleviates work of the surveyor, saves time and ensures consistent ground coverage. The first flight captured images with the camera perpendicular to the flight path and the second adjusted to a 45-degree angle. The lens zoom remained constant for both flights. A Mavic drone can be purchased in the $1,000 to $2,500 range depending on desired specs, making this a cheaper alternative to ALS, while maintaining high-resolution results.

The excavation site only involved an area of approximately 300m^2 making it possible to use smaller equipment for SfM photogrammetry documentation. The excavation area as a whole

was recorded with a DJI Mini 2 drone (DJI, Mini 2, Shenzhen, China). This drone is lightweight, under 250 grams, and has a flight time of 31 minutes. Like the DJI Mavic, the DJI Mini 2 series has onboard GNSS. Even with this drone model being quite light and compact, it boasts a level 5 wind resistance, 29-38 km/h (National Weather Service). Due to its elevated position, the Trmun hilltop is at times affected by wind conditions, which created some suboptimal survey moments. This did not hinder results, wind conditions only needed to be kept under advisement. The drone's onboard camera has a 12MP sensor and a zoom lens of 24mm with an 83° FOV. Cost of this drone is rather cheap, with prices ranging in the mid hundreds. Documentation took place at various times throughout the course of the excavation. The flights were planned according to the day's weather and the progress of excavated areas.

In some specific spots within the excavated area, a Sony Alpha 6000 camera was used for recording SfM data (SONY Electronics Inc., Minato City, Japan). This method of SfM photogrammetry acquisition slightly differs from a drone. When using a camera, the surveyor walks along a path and takes images rather continuously with a lot of overlap. Although, the surveyor does not need to be completely steady during image capture, as software can detect the exact angles in which images were taken. The Sony Alpha 6000 has a 24MP sensor, delivering especially high-quality results. Additionally, this camera is capable of taking 11 frames per second that allows for quick, time-saving documentation.

After each survey, the images were uploaded to Agisoft Metashape to go through the SfM-MVS process. The photos taken during the initial investigative period were used mainly for the building of terrain models, specifically a 0.02m-resolution DTM. For the excavation phase, those images were processed to create a series of orthophotos. The images taken via drone produced orthophotos of the entire excavated site and the photos captured by camera made orthophotos of specific areas within the excavation, for example documenting the stratigraphy and the details of the unearthed post-Roman tower.

2.1.3. Ground Penetrating Radar

GPR data was collected using a MALÅ MiniMIRA device. MALÅ, a subsidiary of GuidelineGeo, is a world-renowned provider of GPR equipment. The Swedish company has been studying and developing geophysical technologies for decades and continues to release cost-effective

and safe systems to detect subsurface features (GuidelineGEO, Malå, Sweden). The MALÅ 3D Imaging Radar Array, known as MALÅ MIRA, has been a top choice for archaeologists to perform GPR surveys because of the included instruments that allow for an in-depth, accurate subterranean investigation.

The MiniMIRA is merely a reduced version of the MIRA that offers the same capabilities for smaller study areas. The Trmun site only required a survey under 2,000m^2, making the MiniMIRA a better option than the hefty, tractor-mounted MIRA device. Additionally, the MiniMIRA can record features up to approximately four meters below the surface. This sufficed for the Trmun site, as anomalies were anticipated at shallow depths. The MiniMIRA device weighs 66 kilograms and has dimensions 70cm x 104cm x 47cm (LxWxH) that allowed for a hand-pushed survey (GuidelineGEO, 2021). The device operates with 5 transmitting and 4 receiving shielded antennas at a frequency of 400-MHz. Shielding the antennas helps enhance signal directionality and reject frequencies that are out of band. For the Trmun survey, separately attached equipment included an electromechanical odometer for pulse triggering and an RTK GPS to provide absolute position accuracy. 304 parallel profiles were collected with line spacing set at 8cm. Trace spacing was also set to 8cm to ensure total in-line and crossline coverage throughout the survey. This means that the device transmitted a pulse and received its reflected energy every 8cm. In total, these parameters produced 38 swaths, 56cm wide, that provided sufficient subterranean detail for quality result production.

Raw GPR data is not necessarily user-friendly from a visual perspective. Data is shown in the form of hyperbolas and can also be heavily swayed by background noise, creating the need to *clean* the dataset. The Trmun dataset went through a standard processing sequence that included the use of rSlicer software and some in-house algorithms made in Matlab (Forte et al., 2021). Time-zero adjustment calibrated each pulse to a specific set time to match the device's surface position. Background removal and bandpass filtering were applied to ensure the survey kept focus on reflections from desired features. Amplitude corrections were made for spherical divergence; this considers the potential energy loss that occurs when a pulse is sent into the ground because of its conical-like spreading. Migration took place by means of the Stolt algorithm and swaths were interpolated (Stolt, 1978). In the end, several GPR slices were produced, with focus on subsurface levels ranging from 20cm to 70cm.

2.1.4. Thermal Imaging

Thermal images were taken from a FLIR Vue Pro 336 thermal camera mounted on a DJI Phantom 3 drone. The FLIR Vue Pro 336 has a 25° FOV, a 13mm zoom lens and 9-Hz, meaning the camera can create 9 frames per second (Teledyne FLIR LLC, FLIR Vue Pro, Oregon, USA). The thermal camera can detect temperatures ranging from -20°C to 50°C with a maximum altitude over 12,000m. The images were processed through FLIR Thermal Studio with a resolution of 640x480 (Teledyne FLIR LLC, FLIR TSS). FLIR Thermal Studio is a relatively cheap software that provides tools for in-depth analysis and gives high resolution outputs. Coordinates from the Trmun site were manually georeferenced in the software.

Thermal imaging encompassed only a small part of the Trmun investigation, as acquiring this kind of data can be quite difficult and take several attempts. The results from ALS, SfM photogrammetry and GPR proved most useful and therefore thermal imaging is a mere extra support to those methods.

2.2. Closer Look: Structure from Motion Photogrammetric Data Processing Sequence

The most significant topographical findings from the Trmun hilltop come from SfM photogrammetry (fig. 8). This technique is easy to incorporate into archaeological investigations due to the low cost of equipment and software. Additionally, the process is user-friendly and does not require an expert skill set. SfM photogrammetry is a great companion, or even a worthy alternative to ALS, as it is cheaper and can at times deliver stronger results. The SfM technique proved most valuable amongst all methods for obtaining high-resolution topographic documentation used to analyze the Trmun site; therefore, the following section provides additional insight to the SfM photogrammetric workflow through various software.

Figure 8. DJI Mini 2 drone capturing SfM photogrammetric data of the Trmun hilltop excavation in summer 2022.

SfM data of the Trmun hilltop was processed through Agisoft Metashape. The initial step involved image alignment. The software processed all photos to create a sparse cloud and calculated the camera positions. Two sparse clouds can be seen in Figures 9 and 10. Figure 9 shows the entire excavated area; including over 500,000 points extracted from the uploaded photos. Figure 10 shows the sparse cloud created for stratigraphy documentation. This screenshot also includes six ground control points that were taken to help enhance location accuracy. Figure 11 includes the camera positions. SfM data was obtained from various flights, some perpendicular to the ground, and others at varying angles. The blue rectangles exhibit those angles, along with the adjoining lines.

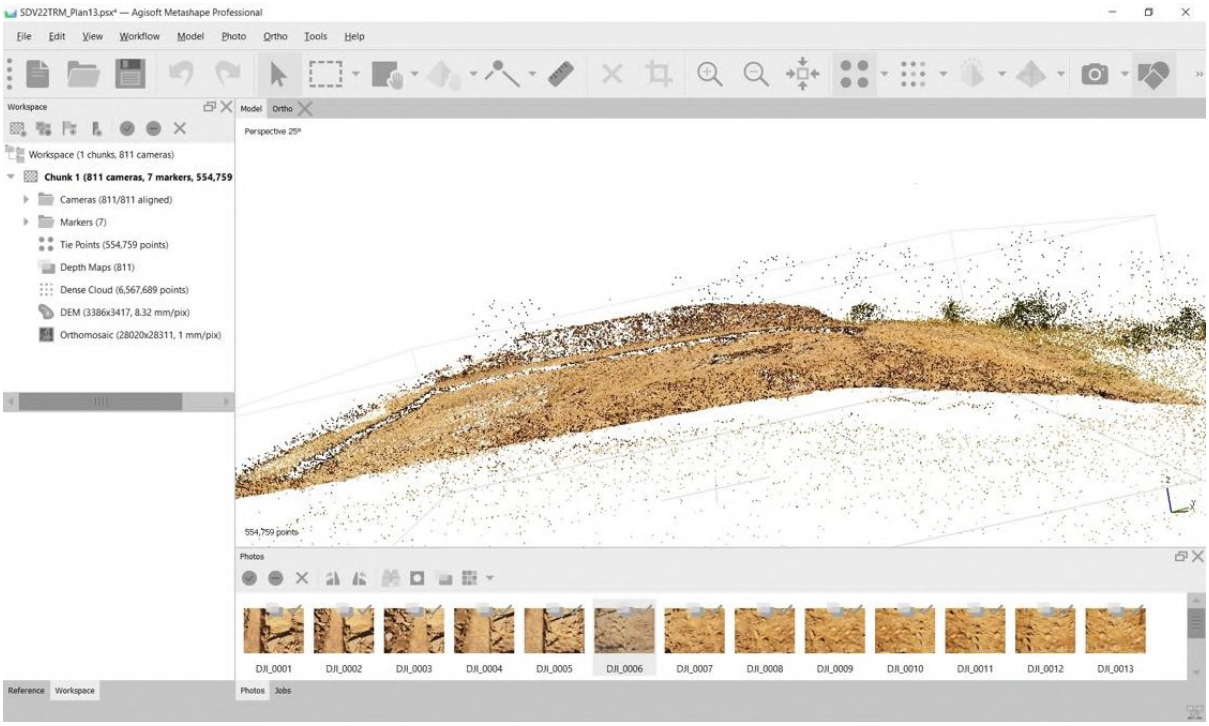

Figure 9. Creation of the sparse point cloud for the entire excavated area at the Trmun hilltop. Notice on the left side panel, the software found over 500,000 points.

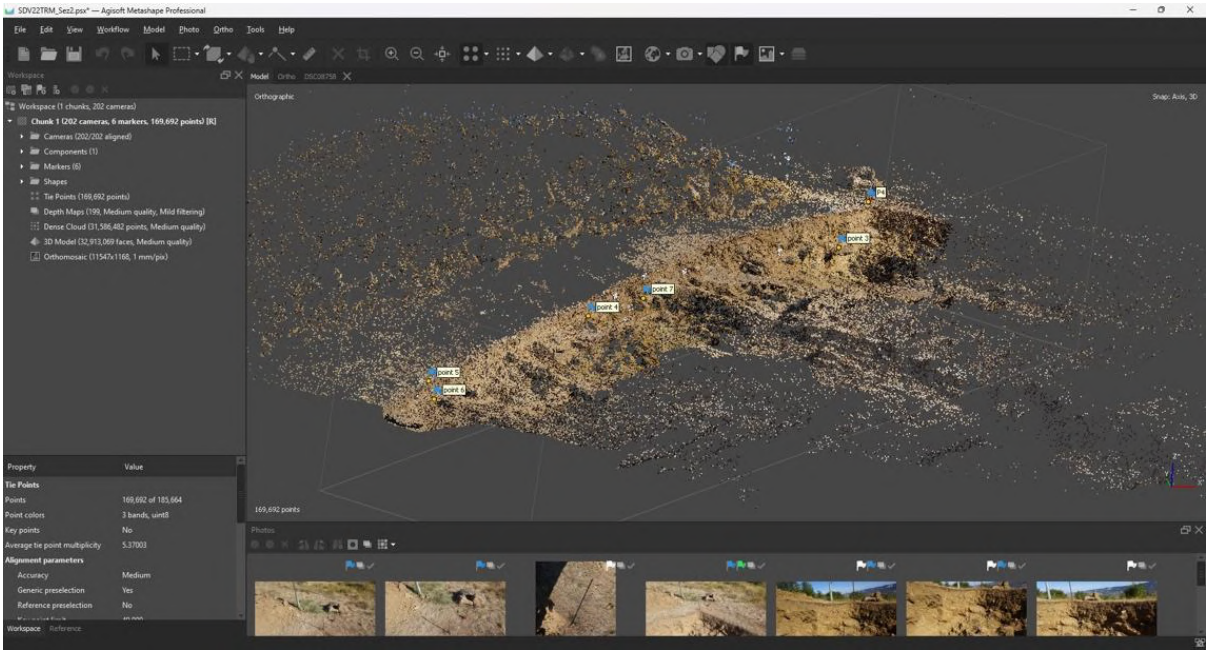

Figure 10. Creation of the sparse point cloud of stratigraphic documentation. Because this section is smaller than the entire excavated area (fig. 9), there are a lesser number of points.

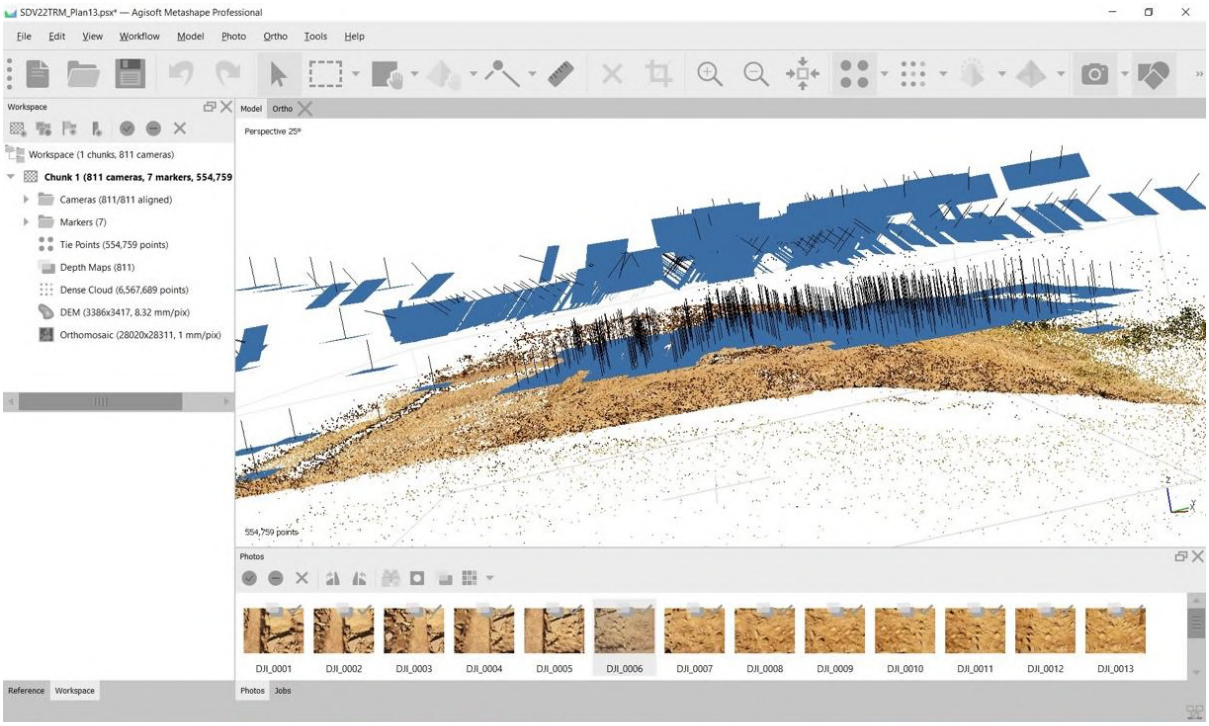

Figure 11. The sparse cloud of the entire excavated area (as shown in fig. 9). Camera positions are represented by the blue rectangles. For this instance, there is a clear distinction of camera height and angle; the lower rectangles appear perpendicular and the higher rectangles are at an angle.

The next step in Agisoft Metashape is to build a dense cloud. A dense cloud takes the sparse cloud and camera positions to build a stronger visualization. Points from the sparse cloud are used to fill in empty areas that were not originally identified in the initial feature detection. The Trmun site dense cloud can be seen in Figure 12 at the same angle as in Figure 9. While this visualization appears image-like, it is important to remember the dense cloud is still a collection of points. Figures 13b, 13c show a zoomed-in section of a dense cloud where some empty space can be seen. It should also be noted that the dense cloud created in Figure 12 is comprised of over six million points, over ten times the number of points used to produce the sparse cloud. Figure 13a shows a different angle of the dense cloud created of the Trmun excavation to give a better visualization of the area as a whole.

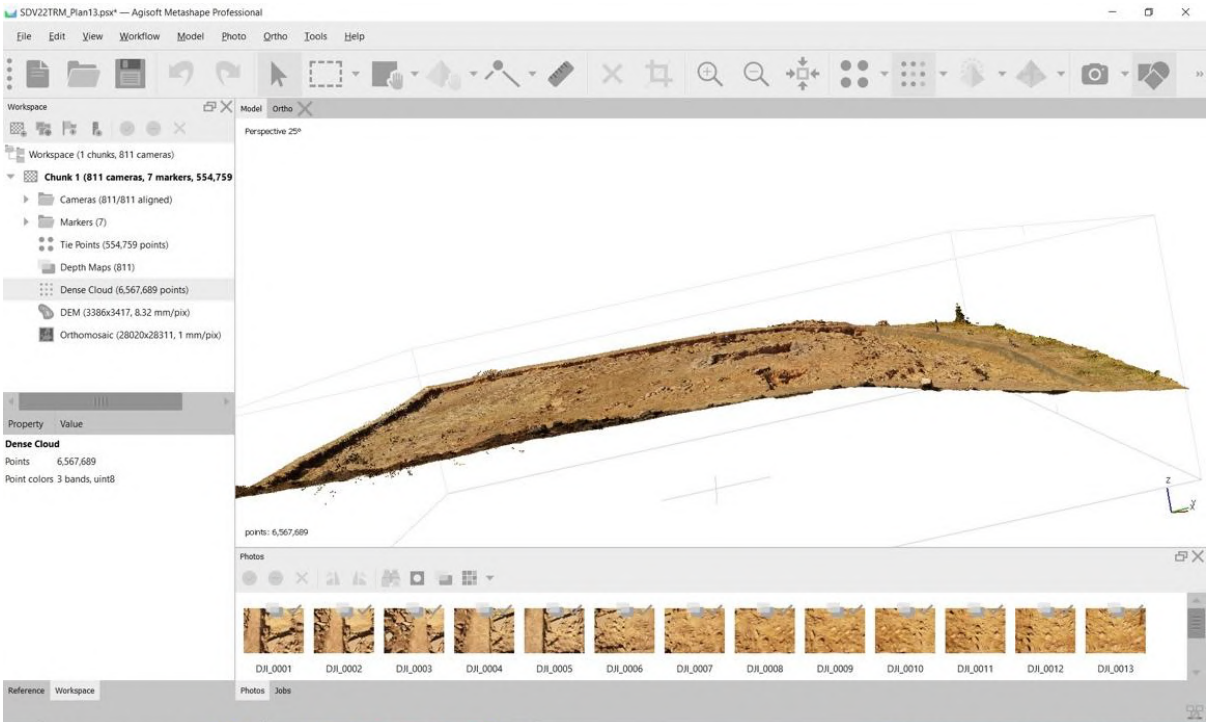

Figure 12. Creation of the dense cloud, using the same data from Figure 9. Note, the dense cloud generates a significantly greater number of points. Here, over six million were utilized to build the cloud.

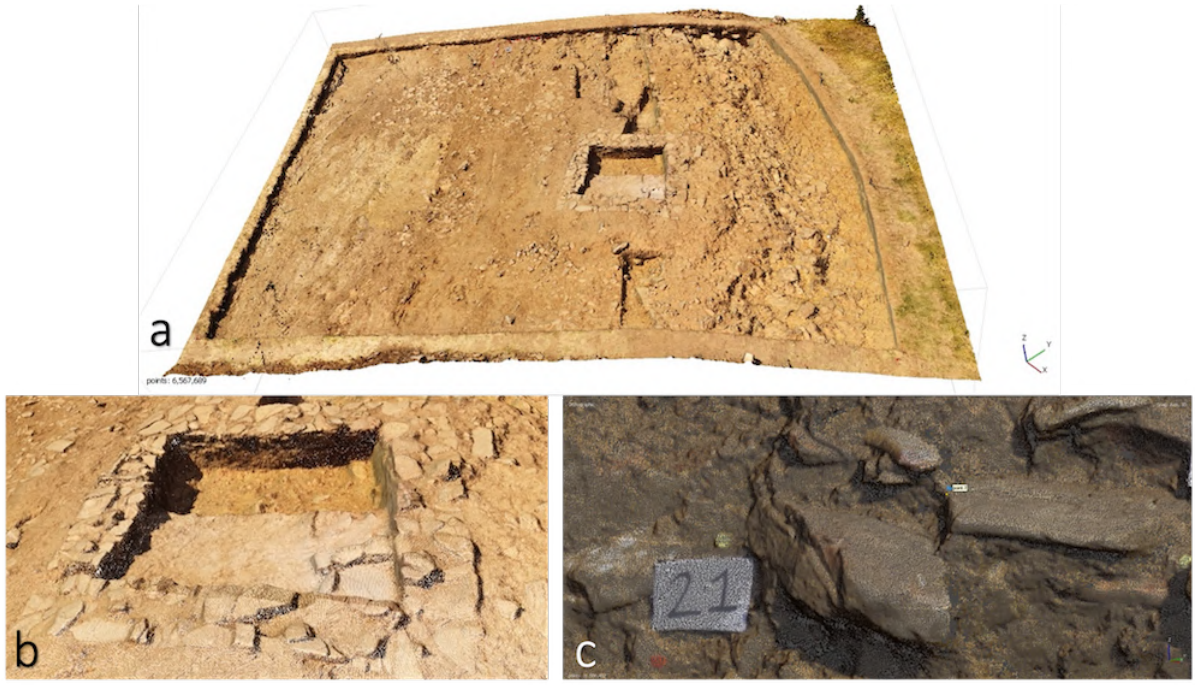

Figure 13. (a) Dense cloud of the entire excavated area from a different angle than seen in Figures 9-12. (b and c) two zoomed in sections to show that the dense cloud is still a collection of points, it is not a continuous, flat surface.

A dense cloud can be further examined through a confidence calculation. Agisoft Metashape has an option to “calculate point confidence,” that essentially ensures the images were taken correctly, are of good quality and determines how well an area was documented (fig. 14). In Figure 14, a new form of dense cloud is seen that provides a color scale based on *confidence*; blue indicates a better surface coverage with more points found by the software, while moving towards red indicates the least amount of coverage and consideration. For the dense cloud in Figure 14, the blue area represents the stratigraphy of the Trmun excavation, verifying most attention went to the appropriate area.

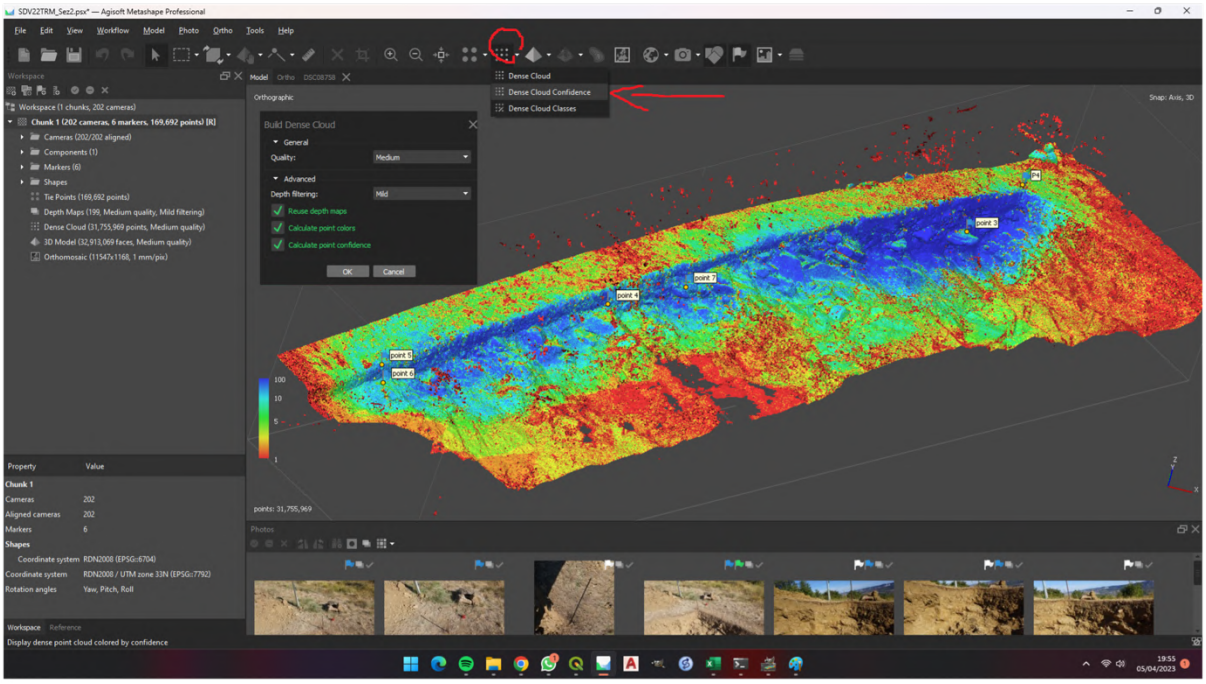

Figure 14. Calculating point confidence. This is an extra step to ensure enough points were taken in the areas of interest. The blue color signifies the most coverage, with red having the least number of images. This screenshot shows the stratigraphic documentation and the blue area is indeed, the main area of interest.

Agisoft Metashape gives the option to create a mesh, which results in a more continuous surface than the dense cloud. This can take a significant amount of computer power and requires a lengthy processing time. Due to these constraints, meshes were mostly left out of the processing sequence, although the stratigraphy section did go through the process at a medium level of quality (fig. 15). Nearly 33 million points were considered that makes this output useful.

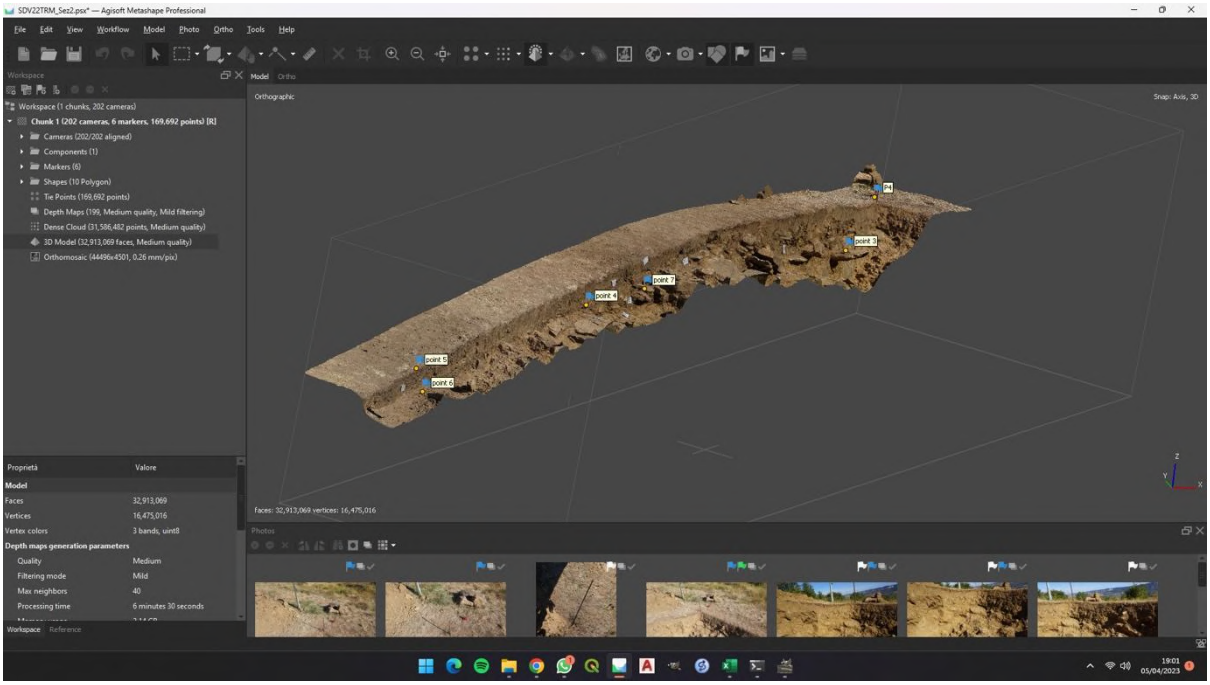

Figure 15. Creation of a mesh that goes one step further from the dense cloud to form a more continuous surface. The processing time for a mesh can be long and high computer power is required. The mesh in this screenshot was created at medium quality.

Once the dense cloud is built, there are a couple of options to produce various end products. Through Agisoft Metashape, DEMs and orthophotos can be quickly generated. Additionally, the georeferenced data can be exported to other software and used to produce other results. Figure 16 shows a DTM created in Agisoft Metashape. The color scale denotes elevation, with red indicating the highest values. The marked points on the DTM are the ground points collected using a differential GPS (fig. 17). Taking ground control points by means of differential GPS significantly increases the precision of location accuracy when yielding results. Figure 18 shows an orthophoto of the Trmun site, including the same ground points. The quality of the orthophotos is extremely high at 1mm per pixel.

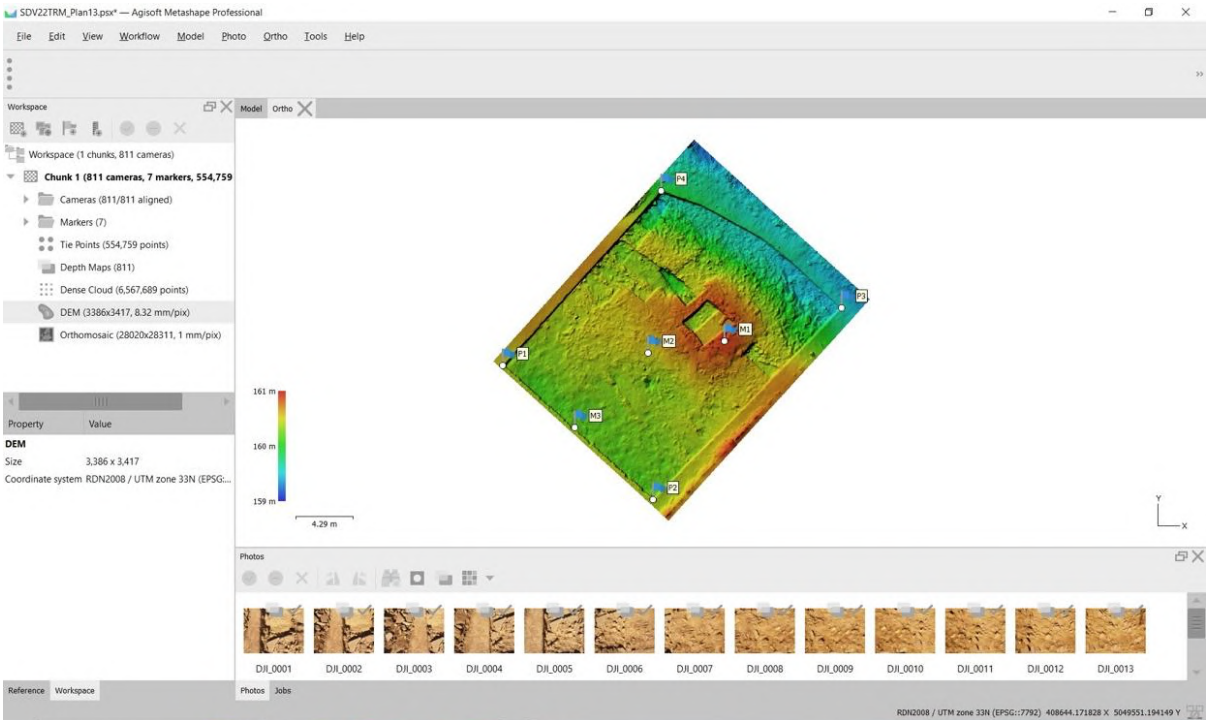

Figure 16. Creation of a DEM. Red represents the highest elevation. There are seven ground control points labeled on this DEM.

Figure 17. Differential GPS used at the Trmun site to obtain centimeter-level accuracy of location.

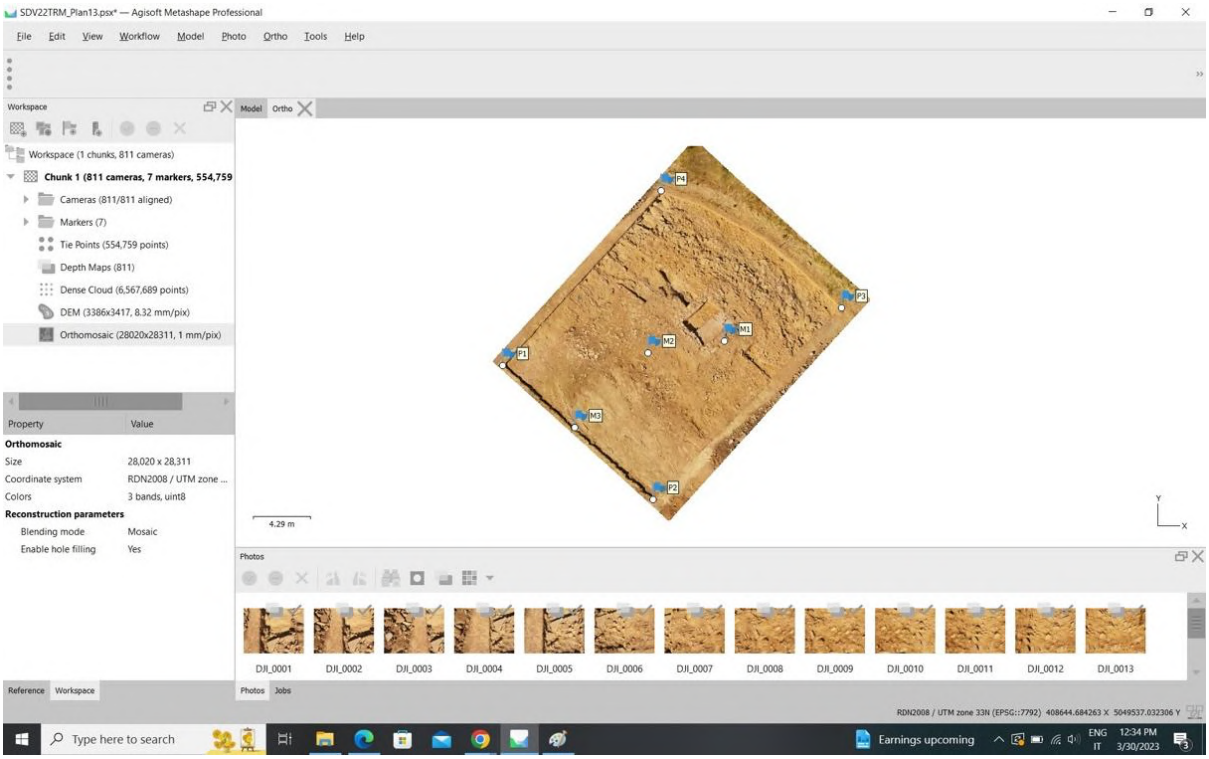

Figure 18. Creation of an orthophoto. This is an aerial image that provides an accurate map projection of the excavated area. Note, the quality is extremely high at 1mm per pixel. This output was the most useful for documentation of the excavation.

Importing SfM data into the free open-source software QGIS is another option to create other end products and further analysis. QGIS offers a range of tools that allows a user to enhance visualizations. For the Trmun site, several orthophotos made in Agisoft Metashape were imported to QGIS to detail the stratigraphy. The georeferenced information remained intact to permit location accuracy in QGIS. Using the same excavation site plan seen in Figure 18, two main stratigraphic vector layers were created to demonstrate some central periods of the site (fig. 19). Figure 19a shows the panel of layers on the left side that were created with vectors. The “Proto_Vita” (proto-life) layer, also seen in Figure 19b, signifies the geographic layer at the time of occupation during the Bronze Age. Details on the stratigraphic layers are discussed in section 4.1. Figure 19c shows the stratigraphic layers post-occupation, after the collapse of the Bronze Age fortification. The addition of these stratigraphic layers in the Trmun analysis offers clear visuals and user-friendly interpretations.

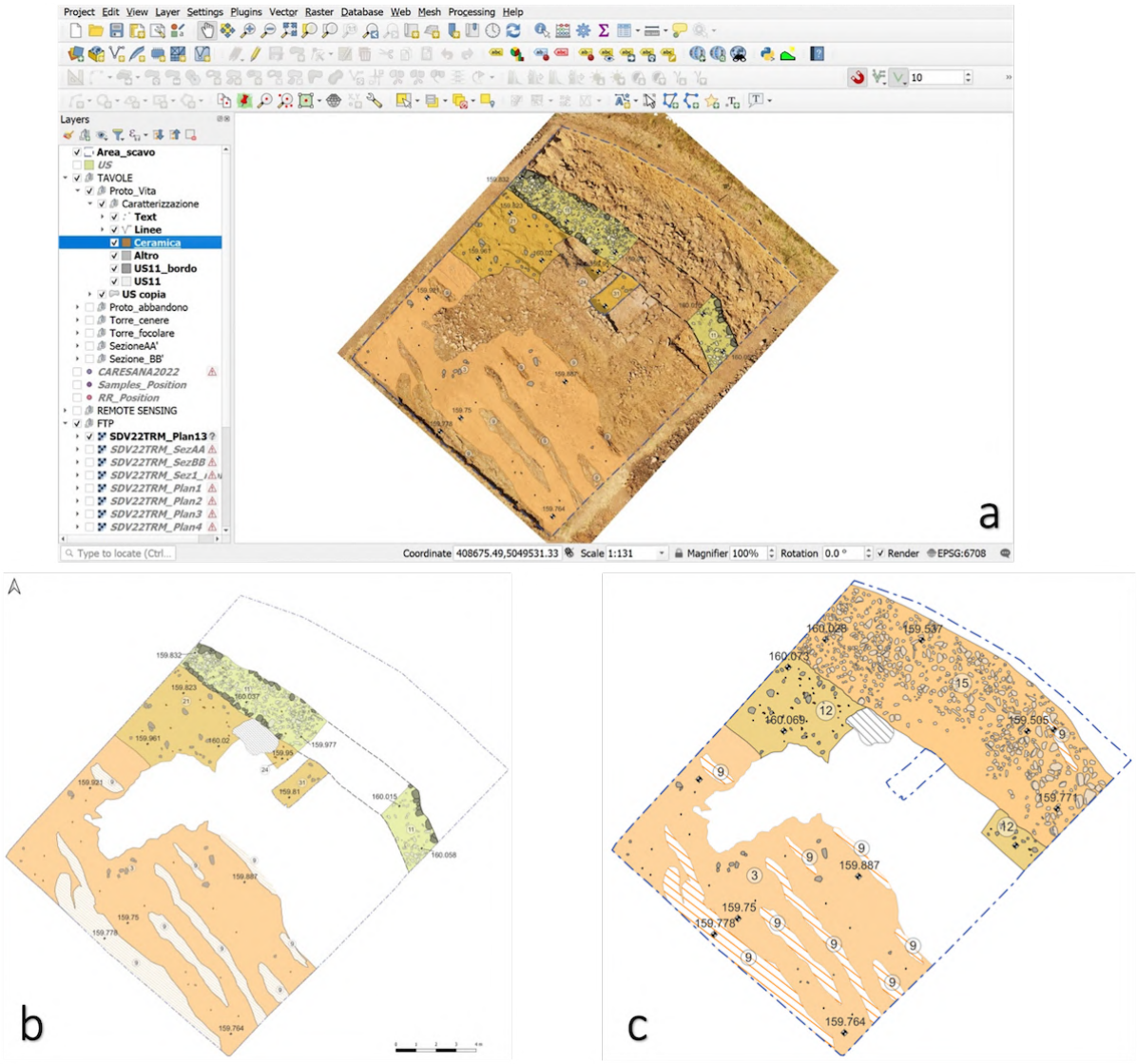

Figure 19. Orthophoto of the excavation uploaded in QGIS to create new visualizations. (a) The uploaded orthophoto with some vector layers to describe the stratigraphic layers. (b) Vector layer of the Trmun hilltop that represents the protohistoric occupation. (c) Another vector layer that illustrates post-protohistoric occupation.

3. Trmun Campaign Results

3.1. Geological and Geographical Background

The Trmun hilltop is located in northernmost Istria, south of the Classical Karst region, an area that includes north-eastern Italy, southwestern Slovenia and some northern parts of Croatia (Jurkovšek et al., 2016). This region has many strong geological traits, with some strata dating all the way back to the Jurassic period. The relief is quite diverse with some high plateaus, steep ascending hills and countless caves (Permanent Delegation of Slovenia to UNESCO, 2015). The area in which Trmun sits is defined by a marly-arenaceous ridge that is part of the Eocene Flysch formation. The Eocene period spans back approximately 56 to 33.9 million years ago, quite younger than some other strata in the region (Geological Society of America, Inc., 2022). The flysch, characterized by silty marls interbedded with sandstones, formed from turbidity currents, underwater events that involve fast-moving water filled with sediment that travel down a slope. Each sandstone-marl pair embodies the effects of a singular turbidity current, leading to the overall continuous alteration of these two rocks (Vlastelica et al., 2018). Of the two, marl is more prone to weathering compared to sandstone, therefore when observing cuts of Eocene Flysch, it is common for the sandstone to slightly jut out higher than the marl layer. This information became extremely useful during the Trmun excavation because the outcrop appeared at shallow depths and noticeably held these flysch appearances.

The Trmun hilltop sits on the Monte d'Oro ridge, which is part of the Eocene Flysch formation, and is located in the northernmost spot of the Istrian peninsula. The ridge runs in an approximate east-west direction and splits the Rosandra valley in the north from the Ospo valley in the south. When descending from the highest point, the ridge spans from the Socerb village in Slovenia to the Stramare landing place in Italy. Additionally, the ridge holds favorable characteristics that include facing the Gulf of Trieste and having access to important routes from both the coast to the interior in an east-west direction and from Trieste to Istria in a north-south direction. In general, this region possesses a strategic geographic and geological position to reasonably justify the large number of protohistoric archaeological sites that lie within this area. The sites span across several epochs, including the time between the Late

Prehistoric era and late Iron Age, the early Roman period and the late medieval and modern times (Mihovilić 2013; Borgna et al., 2018; Bernardini et al., 2013, 2015, 2021).

The campaign carried out at the Trmun hilltop helped confirm the chronology, extension and plan of a protohistoric settlement that had previously never been outlined. The hilltop, which is approximately 40m large, has a circular shape with raised edges and a flat central area (fig 20). Vegetation is generally absent and only a thin layer of grass covers the hilltop, making a campaign more feasible. The hilltop is slightly elevated from the surrounding area and, attractively, marks the highest point of the Monte d'Oro ridge from the coast to the Caresana/Mačkovlje village. Even with no prior formal study, the topography and presence of few surface-level protohistoric pottery fragments suggested Trmun could have hosted a protohistoric hillfort. Furthermore, there are several protohistoric hillforts nearby that elevate hints to a hillfort at Trmun (fig. 21). The Monte d'Oro hillfort is located only one kilometer west of Trmun and was active from the Early Bronze Age to the Iron Age. Three kilometers east, the Socerb and Prebeneg settlements are found. Neither has been formally excavated, however the Socerb hillfort likely dates to the Bronze and Iron Ages based on surface-level pottery findings and an associated cemetery that has been dated to a time between the 6th century B.C. and the 1st century A.D. whereas the Prebeneg hillfort is assumed to come from an era similar to Socerb based on the close proximity, even though chronological data is absent. The topography, surface pottery and closeness to other protohistoric hillforts made the Trmun site an excellent contender for a detailed study.

Figure 20. Geological and geographical context of the Trmun hilltop. The topography is relatively flat, with the surrounding area descending to a lower elevation. The Gulf of Trieste is in the top left corner, signifying a close water source.

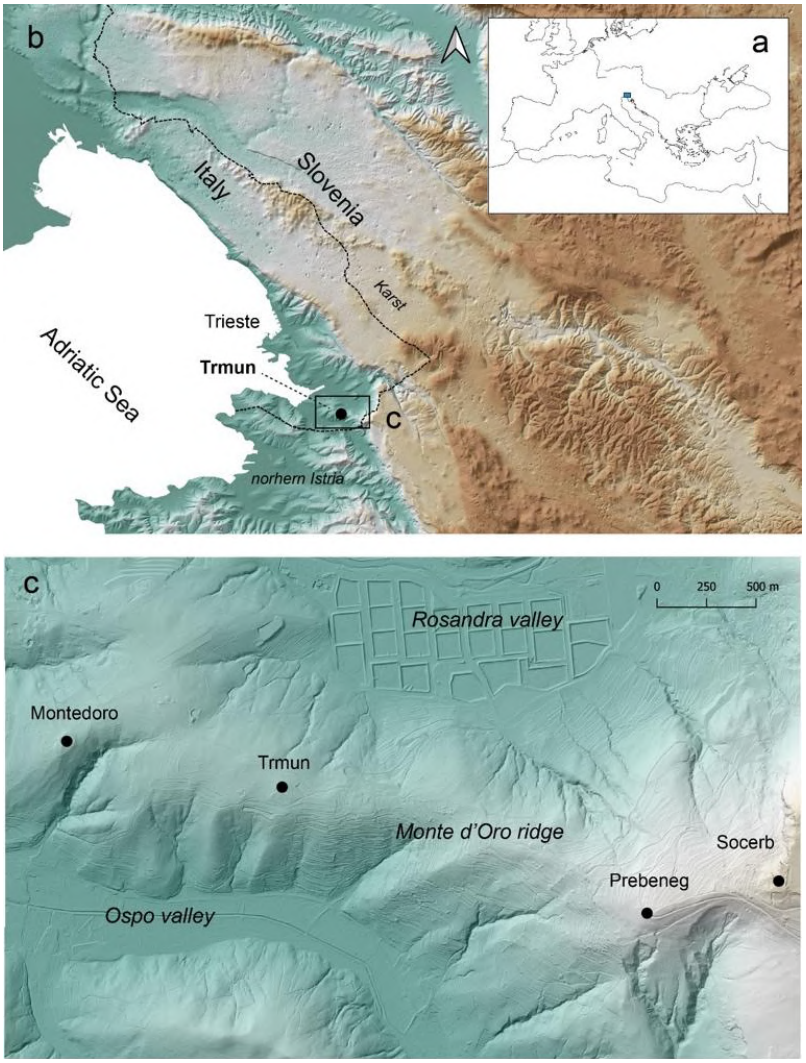

Figure 21. The position of Trmun in relation to other protohistoric hillforts that are located along the Monte d'Oro ridge. Image: (Bernardini et al., 2023, submitted)

3.2. Trmun Campaign Overview

The results section comprises of the investigation and excavation phases of the Trmun hilltop, along with a small peek at the surrounding area. Occupation of the hilltop likely dates back to the Early Bronze Age (further developed in section 4) with the discovery of a rampart and pottery, few flint artifacts and bones from that era. This period can additionally be characterized by terms like protohistoric and Late Prehistoric, which will be used interchangeably in reference to the original occupation. There is also detection of later occupation during the post-Roman period, however the focus of this paper remains on the protohistoric period and therefore the post-Roman findings will only be mentioned briefly. Overall, the Trmun hilltop has been occupied during different time periods and the following results explore the earliest period in detail.

3.2.1. Scope of the Protohistoric Settlement

The documentation and excavation efforts of the Trmun hillfort only includes a small section of the theoretical protohistoric settlement. To gain a better context of the settlement as a whole, some remote sensing data was collected to the west of the hilltop in attempts to define the original extension. Tailored DTMs from ALS data provide evidence of a larger settlement beneath the surface (fig. 23), and the topographic anomalies found in this area have been confirmed by associated pottery findings. Figure 23c illustrates the possible boundaries of such a settlement. Figure 22 provides the situation of 21st century topographical conditions. It is evident that the ancient terrain has been significantly impacted, especially by agricultural activities, therefore, employing remote sensing methods to the area has aided in delivering a clearer context of subsurface features. Due to visible vegetation seen in Figure 22, conducting a laser-based airborne survey provided the best results, unlike a potential GPR or SfM photogrammetric survey that, even if possible, would have likely offered poor results. Moreover, archaeological walking surveys of the Trmun hilltop and some areas to the west have revealed surface-level fragments of Late Prehistoric pottery, furthering suspicions of protohistoric ties.

Delving deeper into the western area, there appears to be a circular fortification below the surface about 230m west of the Trmun hilltop. In addition to Late Prehistoric pottery findings around this area, a portion of the fortification seems to be intact, with dimensions 40m x 10m x (<1m) (LxWxH). A mere 20m north of this fortification, another rampart was partially recognized, as seen in Figure 23b. This slightly curved rampart is approximately 100m long and most likely progressed in an eastern direction; this is predicted based on a modern land division wall that was probably built on top of the remains. From the southwestern tip of the Trmun hilltop, a collapsed wall develops for approximately 50m at a height of roughly 1m and length of 10m, recognized in Figure 23b. Due to these findings, proposed reconstruction of the original settlement is exhibited in Figure 23c. With this sketch, the original hillfort stood around 350m in size and most likely spanned a predominantly flat 5-hectare area.

Figure 22. Google Earth view of the Trmun site. The Trmun hilltop is visibly clear, whereas the remaining sections are covered by vegetation. This made the hilltop preferable for further investigation and an ensuing stratigraphic excavation.

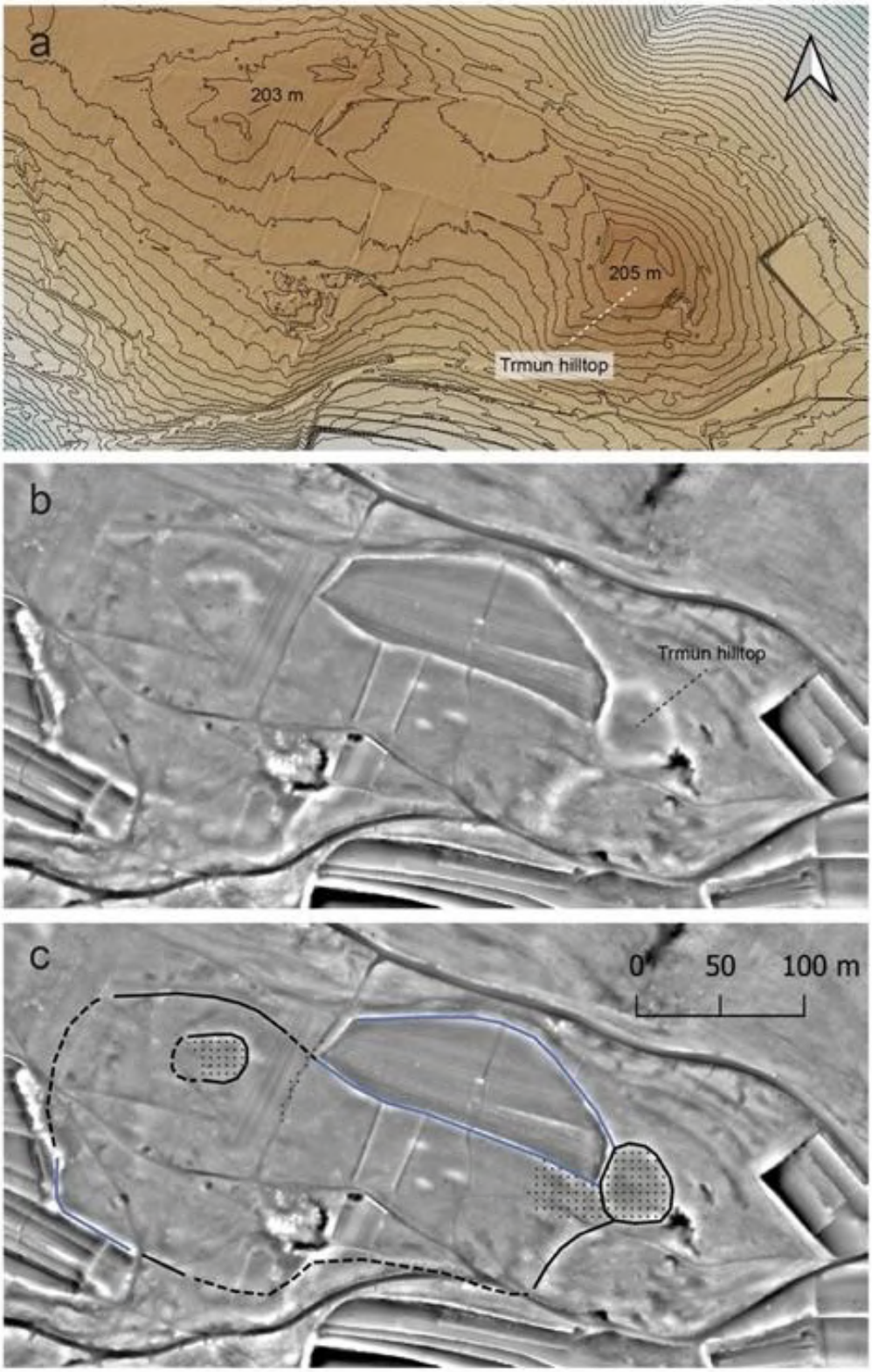

Figure 23. The complete outline of the protohistoric settlement of Trmun. (a) ALS-derived hillshaded image combined with a DTM and 1m contour lines. (b) Local relief model. (c) Local relief model with interpretation of archaeological features. Black lines: preserved ramparts; blue lines: probable ramparts; dashed black lines: postulated position of ramparts; dotted sections: areas of protohistoric surface-level pottery findings. Image: (Bernardini et al., 2023, submitted)

The additional peek into the environment west of the Trmun hilltop is a prime example of how expanding the size of an archaeological investigation can deepen analysis. The detection of a possible larger protohistoric settlement provides a more complete perspective of the Trmun hillfort and helps build a stronger site chronology. While the focus remains on the hilltop, remote sensing technologies make it possible to expand surveys quickly and cheaply. Even with constraints like dense vegetation, there are numerous digital methods that allow for a proper exploration.

3.2.2. The Trmun Hilltop

According to the ALS-derived evidence in Figure 23, the Trmun hilltop only encompasses a small section of the protohistoric settlement. Although, observing the 205m elevation from Figure 23a, it becomes clear that the Trmun hilltop boasts the highest height, marking this a feasible spot for settling due to increased visibility of the whole area. The Trmun hilltop is relatively flat and clear of vegetation, which made this a desirable location for archaeological analysis (fig 24). The most intact section of the Trmun hillfort is located at the eastern boundary of the settlement and became the focus for the investigation and excavation.

Figure 24. Both images exemplify the topographical advantages of the Trmun hilltop. (Left) The highlighted hilltop that is visibly elevated from the surrounding area. (Right) The first day of the stratigraphic excavation in summer 2022, showing flatness of the hilltop.

The small thermal survey of the hilltop unfortunately did not produce any significant results. The thermal image clearly indicates the highest values at the hilltop, however, does not allude to any archaeological anomalies; the values remain nearly the same across the entire hilltop

(fig. 25). Recall, conducting thermographic surveys to obtain meaningful data requires much effort. A proper thermal survey of the Trmun hilltop would have required studying climate conditions of the area to select preferable times for acquisition. Even with that information, it could take multiple survey attempts to gather the appropriate results. Due to the use of other digital methods that would knowingly collect strong data, the thermal survey took a background role, only being used as an additional data source.

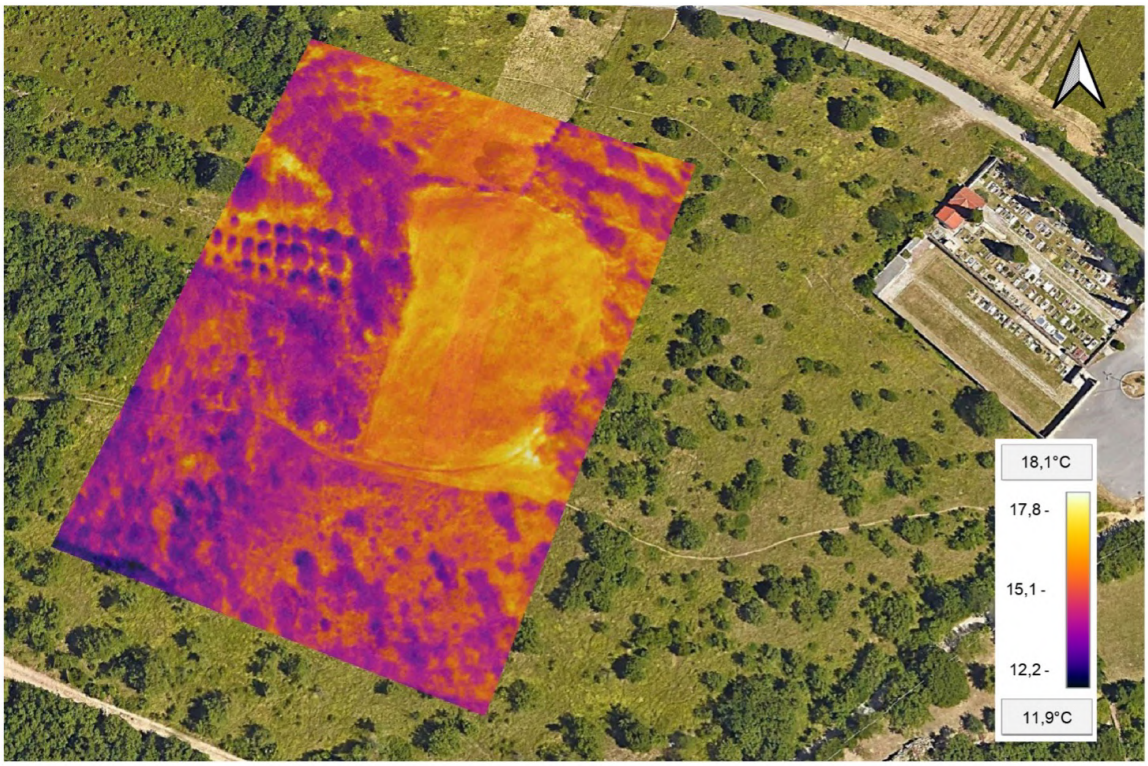

Figure 25. Thermal image of the Trmun hilltop superimposed on a Google Earth overview. The thermal anomalies only seem related to vegetation, not buried archaeological features. Image: (Bernardini et al., 2023, submitted)

The ALS, SfM photogrammetry and 3D GPR methods all produced strong results that assisted in the discovery of a Bronze Age settlement and evidence of post-Roman occupation. Analyzing the three individually and together provide a meaningful analysis of the Trmun hilltop. Of the three, SfM photogrammetry offered the richest high-resolution topographic data with the construction of a 0.02m-resolution DTM (fig. 26c). The ALS data was not strong enough to build the same high-resolution DTM as SfM photogrammetry, however a 0.5m-resolution DTM was created that assisted in verifying the existence of anomalies (fig. 26a). Both creations possess the same color scale of elevation, with the SfM-derived DTM demonstrating extra clarity in feature detection (Figure 26b compared to 26d).

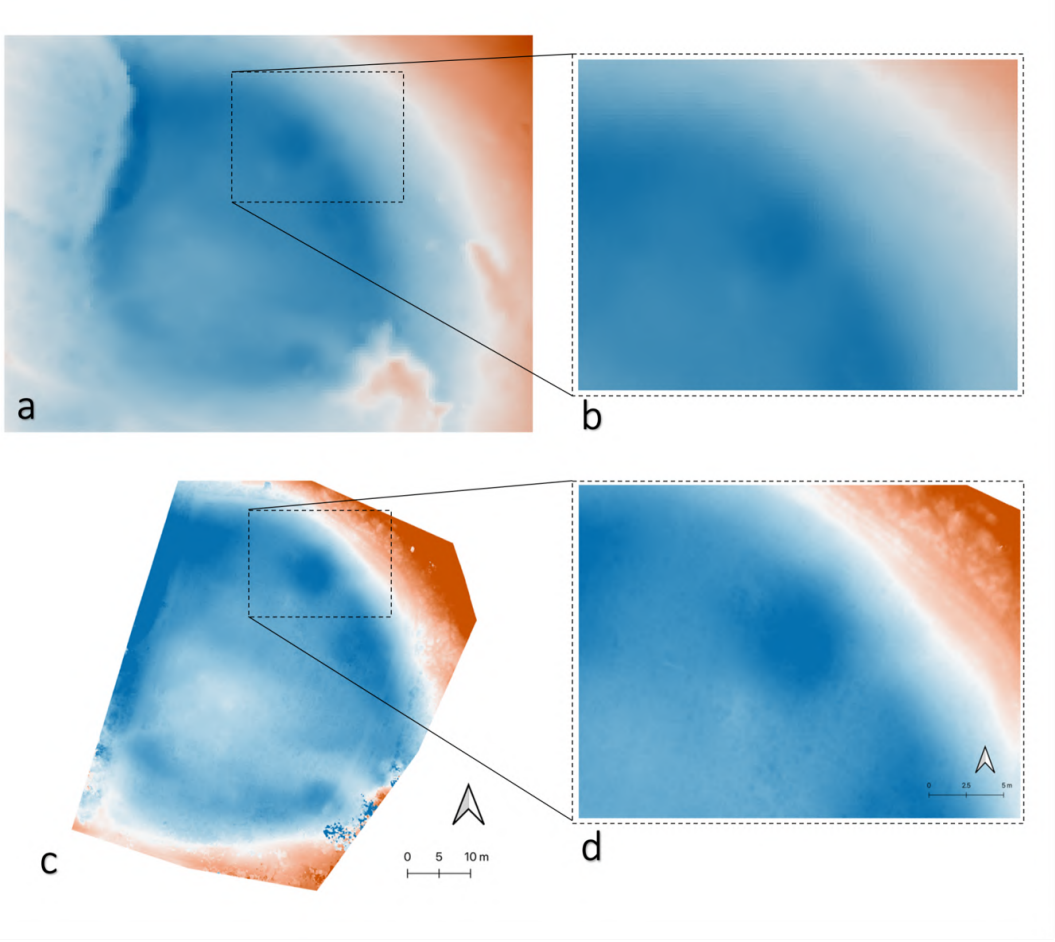

Figure 26. Comparison of (a) ALS-derived 0.5m-resolution DTM and (c) 0.02m-resolution SfM photogrammetry-derived DTM. (b and d) zoomed in view of a sub-circular topographic anomaly (feature 1, F1).

The collection of GPR data provided essential information about buried features. GPR results helped verify the ALS and SfM photogrammetric data, as well as provide the necessary depth figures for a suitable excavation to commence. The GPR end products consisted of horizontal depth slices every 10cm until about 1m below the surface. Figure 27 shows four significant slices at 20cm, 30cm, 50cm and 70cm. Archaeological anomalies were detected starting 20cm below the surface (fig 27a). Additionally, in the middle of the 20cm slice, a hint of bedrock already appears. Both of these instances indicate an excavation would only require digging just below the surface. The 30cm slice best highlights the anomalies, whereas once 50cm is reached, the anomalies almost disappear (fig. 27b, c). By the 70cm slice, only bedrock remains visible (fig. 27d). As detailed in section 3.1, the Trmun hilltop consists of a flysch rock formation and the rather uniformly shaped, thin curved lines that are oriented in a north-west, south-east direction, seen at 70cm below the surface demonstrate matching geological characteristics.

Using the GPR method on the Trmun hilltop not only aided in subterranean anomaly recognition, but also provided essential depth information for planning an excavation. The nearly complete vanishing of archaeological anomalies from 30cm to 50cm, along with the sole flysch terrain seen in the 70cm slice, confirmed a shallow excavation would suffice and reveal the desired targets.

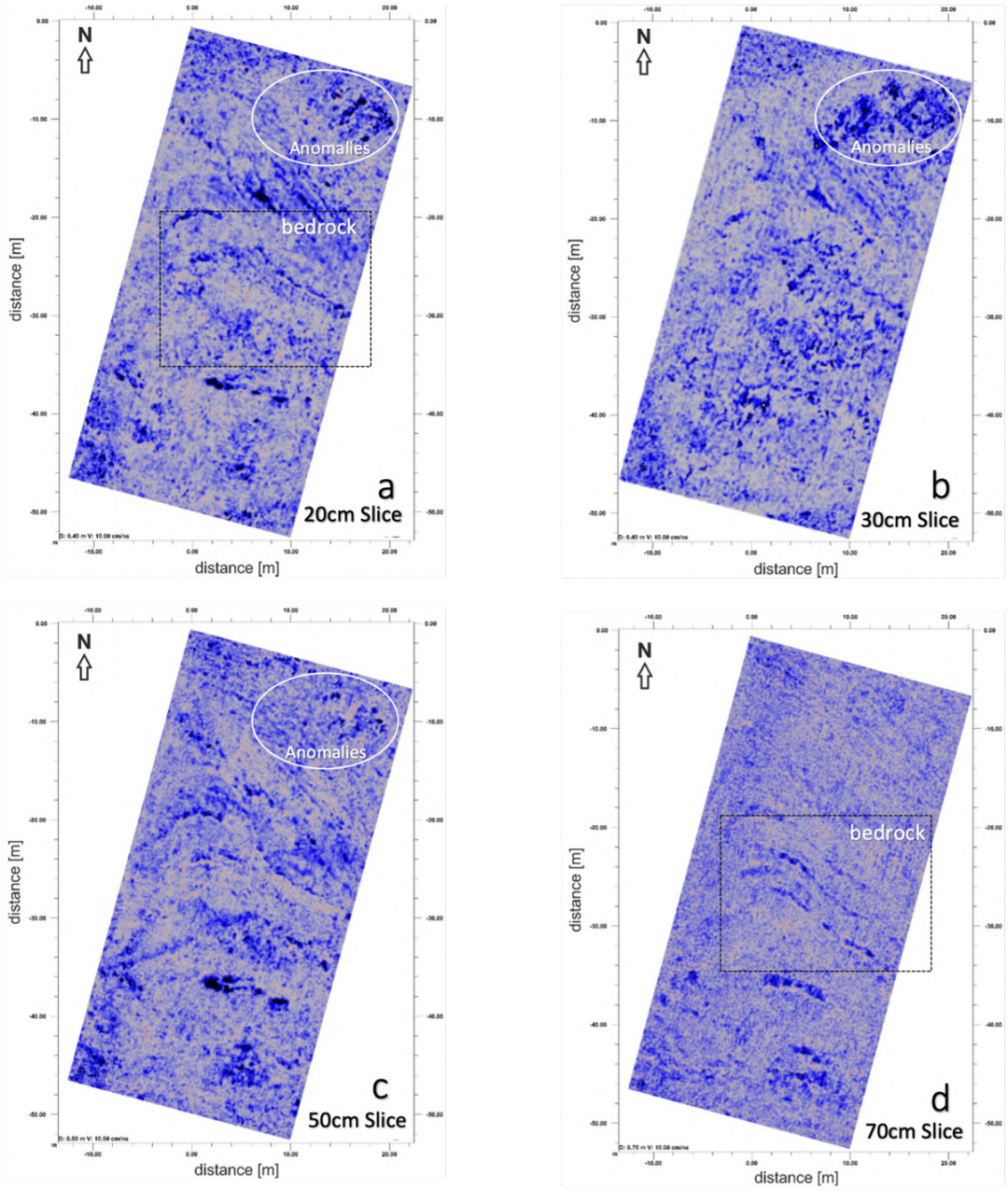

Figure 27. GPR slices that show depth at various degrees. (a) Shallowest slice at 20cm below the surface. The bedrock is already becoming visible, and anomalies appear in the top right corner. (b) 30cm slice, the most useful for archaeological features. Anomalies in the top right corner are strong and clearly indicate archaeological features. (c) By 50cm below the surface, the top right anomalies have nearly disappeared. (d) 70cm below the surface only showed bedrock, which exhibit the typical flysch rock formation.

3.3. Phase I: Investigation Results

The resulting DTMs and GPR slices provide evidence of several anomalies. For clarity of result discussion, the anomalies have been divided into three core features pertaining to post-Roman occupation specifically highlighted in the DTMs and six anomalies sensed through GPR that stretch through multiple time periods, from protohistoric occupation to the second half of the 20th century. The focus of the GPR investigation, along with the subsequent excavation took place at the best-preserved section of the Trmun hilltop. Although, the aerial surveys for lidar and SfM photogrammetric data collection gave a broader coverage of the hilltop. The resulting DTMs, in particular the high-resolution SfM-derived DTM, showcase the possible late prehistoric rampart remains quite well.

The three features, labeled as F1, F2 and F3, in Figure 28 are sub-circular bumps approximately 6m x 6m wide. Theoretically, these features are the buried remains of a post-Roman fortification. All three features appear to be attached to lower passages, of which suspected entrances are marked in Figure 28 as yellow triangles. F1, compared to F2 and F3, showed the strongest variance in color signature, suggesting a high probability of finding buried features. Additionally, F1 vividly appears in the 30cm GPR slice, solidifying the probable existence of a sub-circular feature and implying any digging would not require too much depth (fig. 28).

F2 unfortunately fell outside the GPR survey and cannot be seen on any GPR slices. Though, further analyzing the DTM, there appears to be a mound-like structure around F2, along with some aligned sandstone blocks in the upper part of the area. The GPR survey only acquired a portion of the area surrounding F3 and the covered areas do not show any clear anomalies, leading to a lack of evidence to make any strong conclusions. Overall, these three main features suggest post-Roman occupation with the formation of a small fortification.

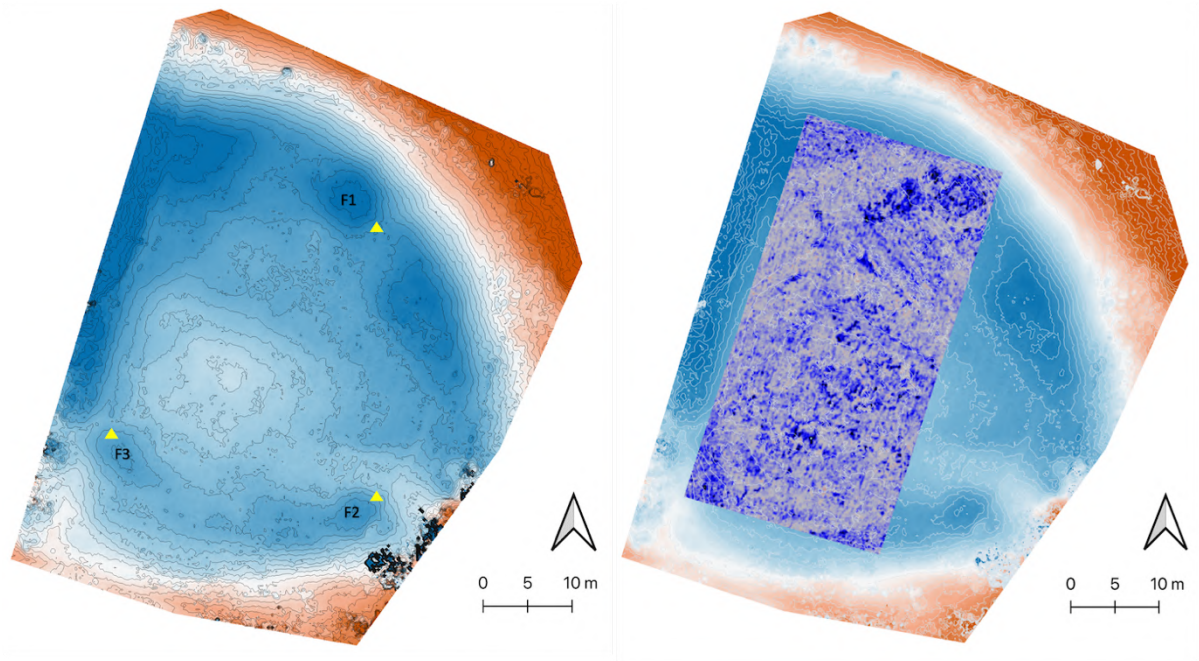

Figure 28. SfM-derived 0.02m-resolution DTM with 10cm contour lines. (Left) Features F1-F3 related to post-Roman occupation. Yellow triangles represent possible entrances. (Right) 30cm GPR slice superimposed on the DTM to show that the anomalies detected through GPR match the area of F1.

The GPR assessment, specifically the GPR slice at 30cm below the surface, revealed six key anomalies, labeled as A1 to A6, some of which offered a more precise interpretation of the features discovered in the aerial surveys (fig. 29, 30). In particular, the GPR data was able to provide further details to the initial feature, F1, identified in the DTM. In the area of A1, as seen in Figure 29, the MiniMIRA GPR device recorded intensity values of the reflected signals corresponding to a probable stone structure. Additionally, the stone structure encompassed a square-like shape approximately 4m x 4m in size. The intensity values, along with the size and location suggest this anomaly could be a tower.

A second anomaly of rectangular shape, A2, appears in the GPR data slightly west of aA1 (fig. 29, 30). A2 recorded similar intensity values to A1, signifying another probable stone material. Additionally, the buildup of reflected signals hinted at either a structure or a possible accumulation of stone, which could be connected to a possible collapse of A1. Between A1 and A2, a third smaller anomaly appears, A3 (fig. 29, 30). The small size makes interpretation difficult, however the anomaly remains quite visible throughout most of the GPR slices, from only a few centimeters below the ground, to almost a meter.

A4 illustrates sub-parallel anomalies going in a north-western, south-eastern direction (fig. 29). These parallel lines likely represent bedrock, as the geological features match the flysch terrain that characterizes the surrounding environment. As seen in Figure 28, the apparent bedrock becomes visible just 20cm below the surface and by the 70cm slice, the flysch-like profiles become obvious. This observation, compared to the other anomalies seen at the 30cm depth slice, indicates that most of the archaeological stratigraphy is present just below the surface.

A5 and A6 were discovered on the boundaries of the GPR study (fig. 29). A5, seen on the northwestern corner of the investigated area, could be associated with the collapse of the Late Prehistoric rampart, however without a complete analysis of the entire area surrounding A5, no definitive conclusions can be made. The same can be said for A6. This anomaly appears on the southernmost part of the GPR slice, covering the eastern and western edges, although because it is cut off from the GPR results, more examination would be required. This anomaly does appear to fall in the precise area of the hypothesized post-Roman fortification, increasing probably of connection to the settlement.

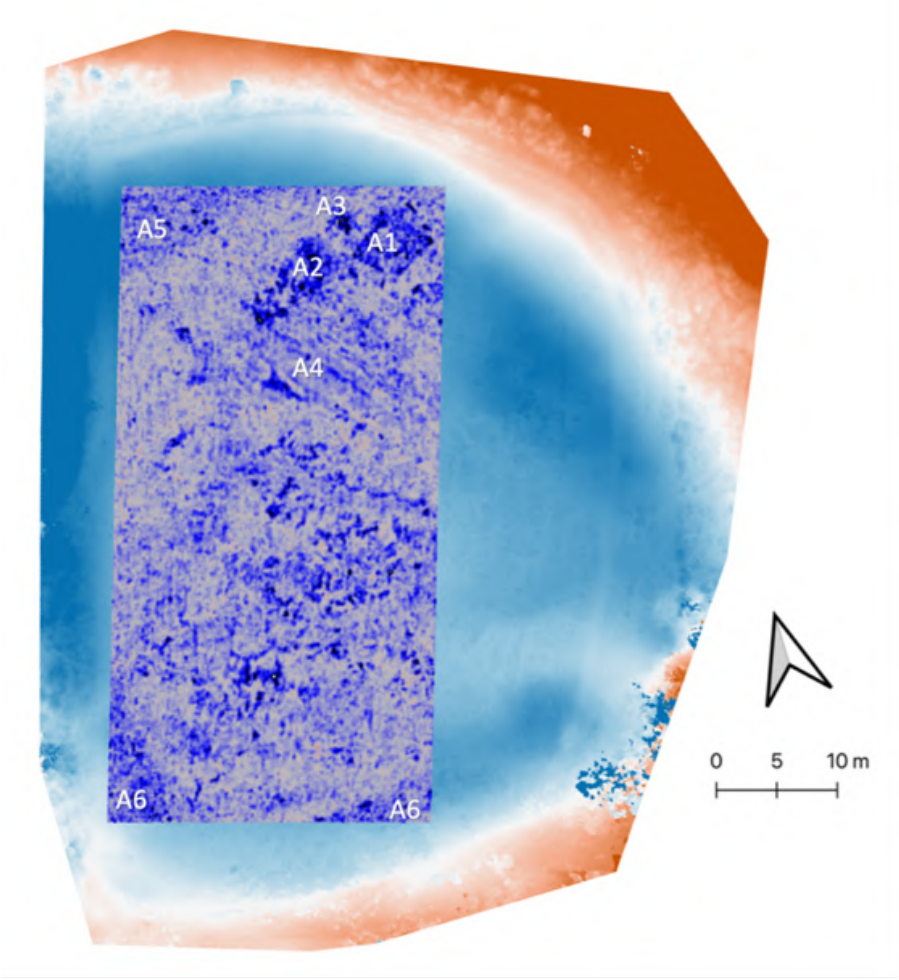

Figure 29. 30cm GPR slice superimposed on SfM-derived 0.02m-resolution DTM. The specific anomalies found in the GPR slice are labeled as A1-A6. A1-A4 fall within the stratigraphic excavation, while unfortunately A5 and A6 were not included.

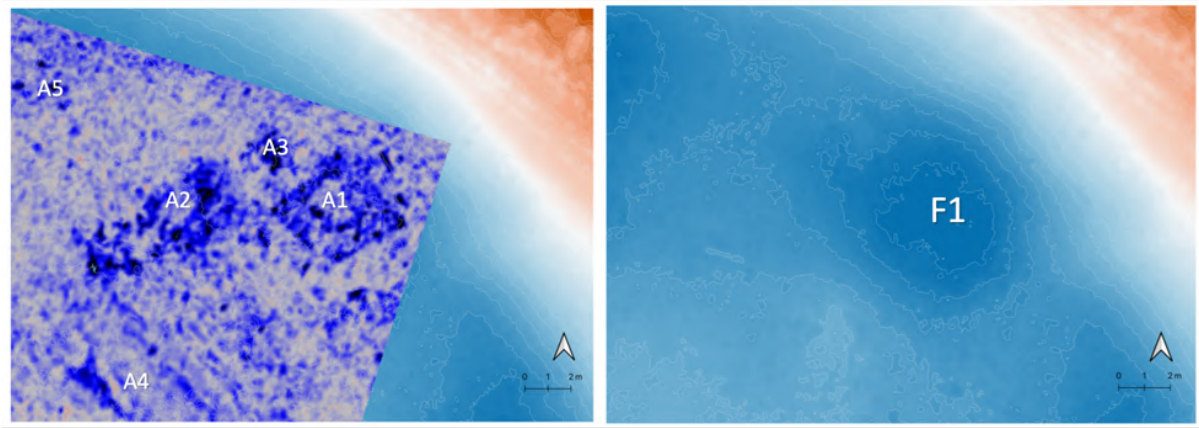

Figure 30. The GPR anomalies are located around the ones found in SfM photogrammetric acquisition. F1 is related to post-Roman occupation, whereas A1-A4 vary with time periods. (Left) Zoomed in 30cm GPR slice superimposed on SfM-derived 0.02-resolution DTM with 10cm contour lines. (Right) DTM without the GPR slice to highlight the feature, F1.

3.4. Phase II: Excavation Results

The investigation phase of the Trmun hilltop provided clear evidence of subsurface anomalies. The DTMs pointed towards specific areas of interest, however the GPR data presented the strongest indication that an excavation would prove valuable for archaeological insights. The 30cm GPR slice directed attention to the northeastern section of the hilltop, and because nearly all GPR slices contained signs of bedrock, even the shallowest slices, only a small layer of soil would need to be removed to come in contact with the archaeological stratification. All of this valuable information led to the planning of an excavation, executed in summer 2022, in an area approximately 20m x 15m in the northeastern section of the hilltop.

Figure 31 illustrates the entirety of the Trmun hilltop campaign to gain a clearer understanding of digital and traditional methods used to pinpoint the area with the highest archaeological significance. The base layer is the 0.02m-resolution SfM-derived DTM that encompasses the entire hilltop. The middle layer entails the 30cm GPR slice that proved to be the most telling of archaeological anomalies that helped develop plans for an excavation. The GPR slice covers a large section of the hilltop, particularly the main feature, F1, identified in the DTM. The northeastern section of the GPR slice contained the most archaeological evidence and thus, an excavation was carried out in that area, as seen in the top layer of Figure 31.

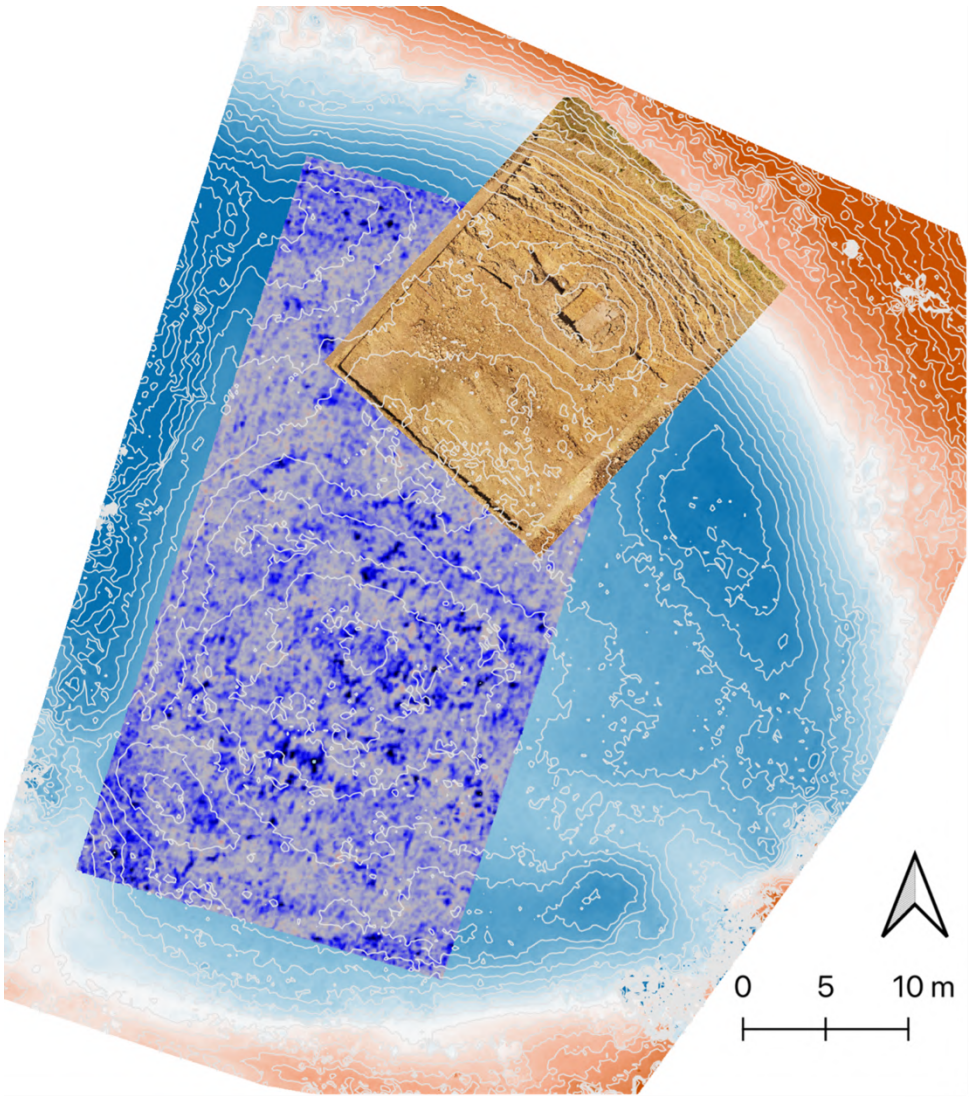

Figure 31. A comparison of the different outputs created during the investigation and excavation phases of the Trmun campaign. The bottom layer is a SfM-derived 0.02m-resolution DTM that includes the whole hilltop. The middle layer is a 30cm GPR slice. The top layer is an orthophoto of the stratigraphic excavation. All layers are overlaid with 10cm contour lines.

Figure 32 shows a comparison of a GPR slice during the investigation phase and an SfM-derived orthophoto of the excavation phase. The anomalies labeled as A1 to A6, in the GPR slice and the archaeological features unearthed during the excavation match well, attesting to the importance of digital methods in archaeology.

The excavation confirmed the details of A1 as the near perfect square-shaped base of a structure made only with sandstone blocks and not mortar; predictably this could have been a watchtower (fig. 32). The base stretched for approximately 50cm below the surface, which matched the GPR data. F1 from the DTMs suggested this anomaly would be larger than it

turned out to be, however this difference could be explained by an earth bank surrounding the stone base. The excavation revealed an earth bank about 1.5m large, likely an intentional accumulation of soil built around the same time as the stone structure. There does not appear to be any collapse of the structure, leading to some hypotheses of the tower's disappearance. One possibility is the material of the structure; wood or other perishable materials may have been built on top of the stone base. A second option is that the stone materials were removed from the site post-abandonment. The structure also contained some wheel-made pottery fragments, along with an iron knife to help establish a possible post-Roman occupation.

A2 featured in the GPR slice, was likely an external area related to the post-Roman tower (fig. 32). The excavation revealed sandstone slabs that could have acted as a sort of footpath leading to a possible entrance on the southwest side of the tower.

The difficult to interpret anomaly, A3, pertains to a modern military foxhole. According to historical aerial photos from 1941 of the Dolina area, this hole did not yet exist, leading to a later 20th century construction (NCAP, 1941).

The excavation confirmed A4 as bedrock (fig. 32). Once a depth of 20cm was reached in the excavation, the bedrock started to appear. Digging continued to around 80cm below the surface to better study the geological traits. A4 is characterized as layers of sandstone and marl. The marl layer is noticeably lower than the sandstone strata, likely due to marl's greater predisposition to weathering than sandstone.

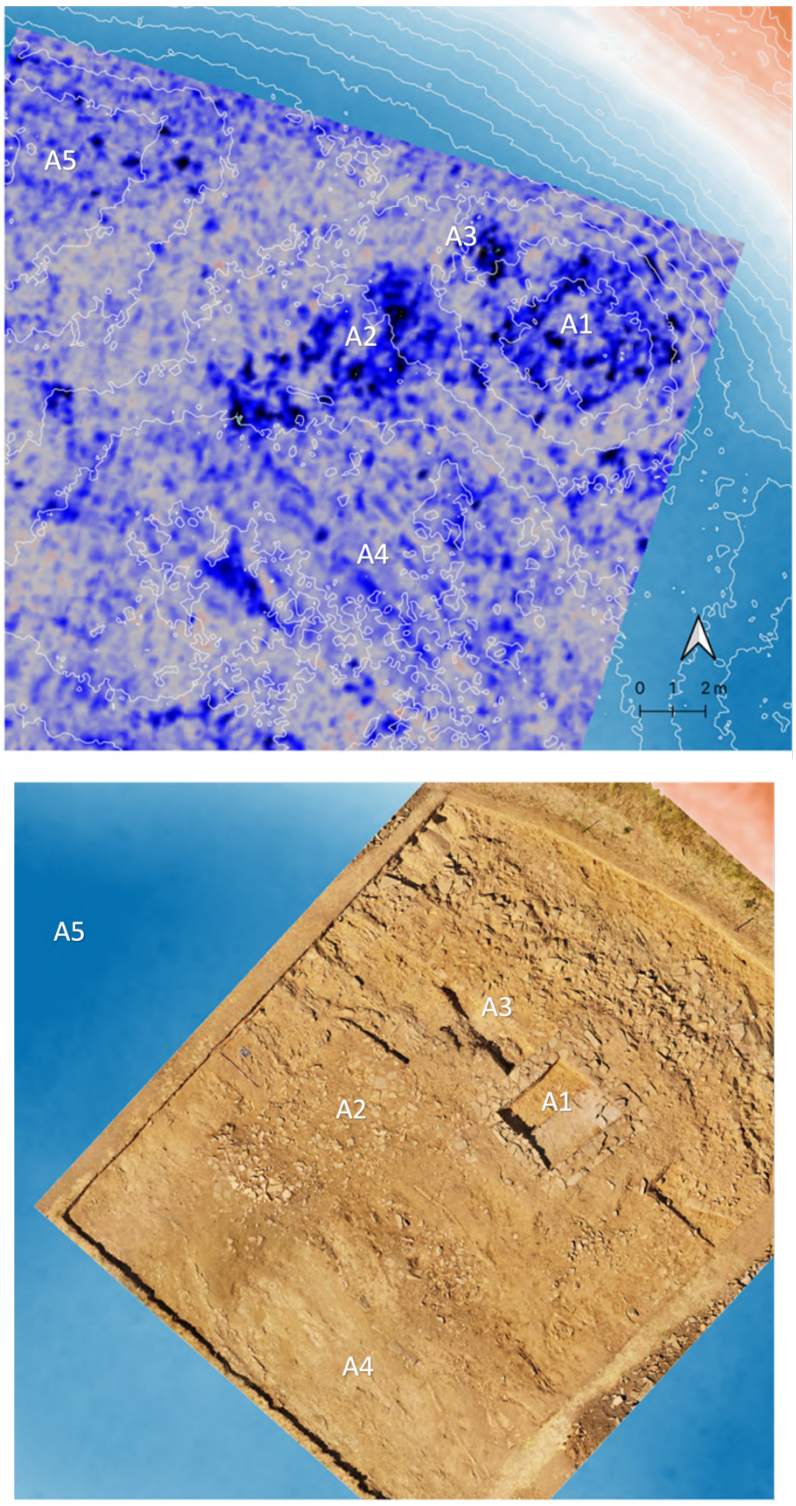

Figure 32. A zoomed in comparison of the 30cm GPR slice with an orthophoto of the stratigraphic excavation. The anomalies detected from GPR clearly align with those uncovered during the excavation.

As a whole, the excavation uncovered the remains of a protohistoric rampart, precisely dating to the early part of the Bronze Age, see section 4 for chronology. The copious amounts of pottery and other significant fragments found in the archaeological layers helped solidify the

time period. The rampart was rather small in size, about 1.6m tall with two external lines of stones (fig. 22). These two lines consisted of rows of stones spaced with soil and smaller stones. In-between the rampart and the central part of the hilltop, a buildup of soil and pottery was likely intentional. From observing the direction of the stones, the rampart collapsed mostly outwards, towards the exterior, which could help interpret A6. Although, because A6, as well as A5, fell outside of the excavation, their initial interpretations from the digital methods largely remain in place. A5, situated at the northwestern area of the hilltop, could possibly be better explained when considering the collapse of the rampart. The excavated area found most of the rampart collapsed directly outside the original fortification boundaries and consisted of large sandstone blocks and slabs with a thickness reaching up to 0.8m.

Figure 33. The protohistoric rampart discovered during the stratigraphic excavation. Dashed white lines represent the outlines of the wall. (Left) A side view and (right) aerial view.

The Trmun hilltop holds favorable characteristics for occupation such as high elevation with a strong panoramic view that stretches many kilometers and boasts a relatively flat surface. These could be prime reasons for a group to settle during the Bronze Age. The raised edges

formed on the outskirts of the hilltop due to the protohistoric rampart became another advantage and helped build some inferences for F2 and F3 revealed in the investigation phase. While these two features were not covered in the excavation, their presence on the hilltop indicate the tower excavated in the area of F1 was likely not isolated and perhaps similar base structures could be found at F2 and F3. F2 has a high probability of such a structure because the DTMs revealed some aligned sandstone blocks near the upper part of the mound. Overall, a post-protohistoric occupation most likely occurred with the construction and usage of a fortlet consisting of two or three towers.

4. Discovery of a Protohistoric Settlement

The excavation of the Trmun hilltop, conducted in summer 2022, not only confirmed the existence of a protohistoric settlement suggested in the remote sensing results, it also provided chronological details of the protohistoric occupation. The excavation also brought evidence of post-Roman ties to light; however, this paper will remain focused on the Bronze Age occupation. There will be some discussion of archaeological stratigraphy in its entirety, including layers relating to post-Roman times. This is only to provide a complete description of layers, as there was a natural mixing of when each protohistoric and post-Roman layer was unearthed.

The excavation involved the northwestern sector of the Trmun hilltop and encompassed an area approximately 20m x 15m. This specific section was selected because remote sensing methods showed strongest connections to a perimeter wall related to a protohistoric fortification and potential reuse during the post-Roman era with the construction of a tower and related structures. In total, 31 stratigraphic layers were identified, also referenced as units of stratigraphy (US). Some of these layers had an abundance of protohistoric pottery, as well as few fauna remains and flint artifacts, that has been studied and can be compared to nearby sites. In general, the protohistoric pottery remains indicate that this settlement belongs to the most ancient chronology of Karst-Istrian fortified villages.

4.1. Stratigraphy

The Trmun site excavation unearthed 31 stratigraphic layers, from the uppermost vegetative layer to the stratums pertaining to the post-Roman and protohistoric occupations. Figure 34 displays the stratigraphy matrix of Trmun that organizes the layers. Typically, during an excavation, layers are uncovered in a nonsequential order. This happens due to uneven topography or stratigraphic layers holding different geologic properties that cause non-uniform formation. The Trmun matrix follows the framework established through the Harris Matrix, a tool for archaeologists to create a structured plan of a site's stratigraphy (Harris Matrix, 2023). The matrix highlights three specific phases of the site, phase 1 corresponding to the protohistoric occupation, phase 2 signifying post-Roman occupation and phase 3 relating to modern layers. These layers were all uncovered during various moments of the

excavation and only once the excavation finished, were the layers examined and grouped accordingly.

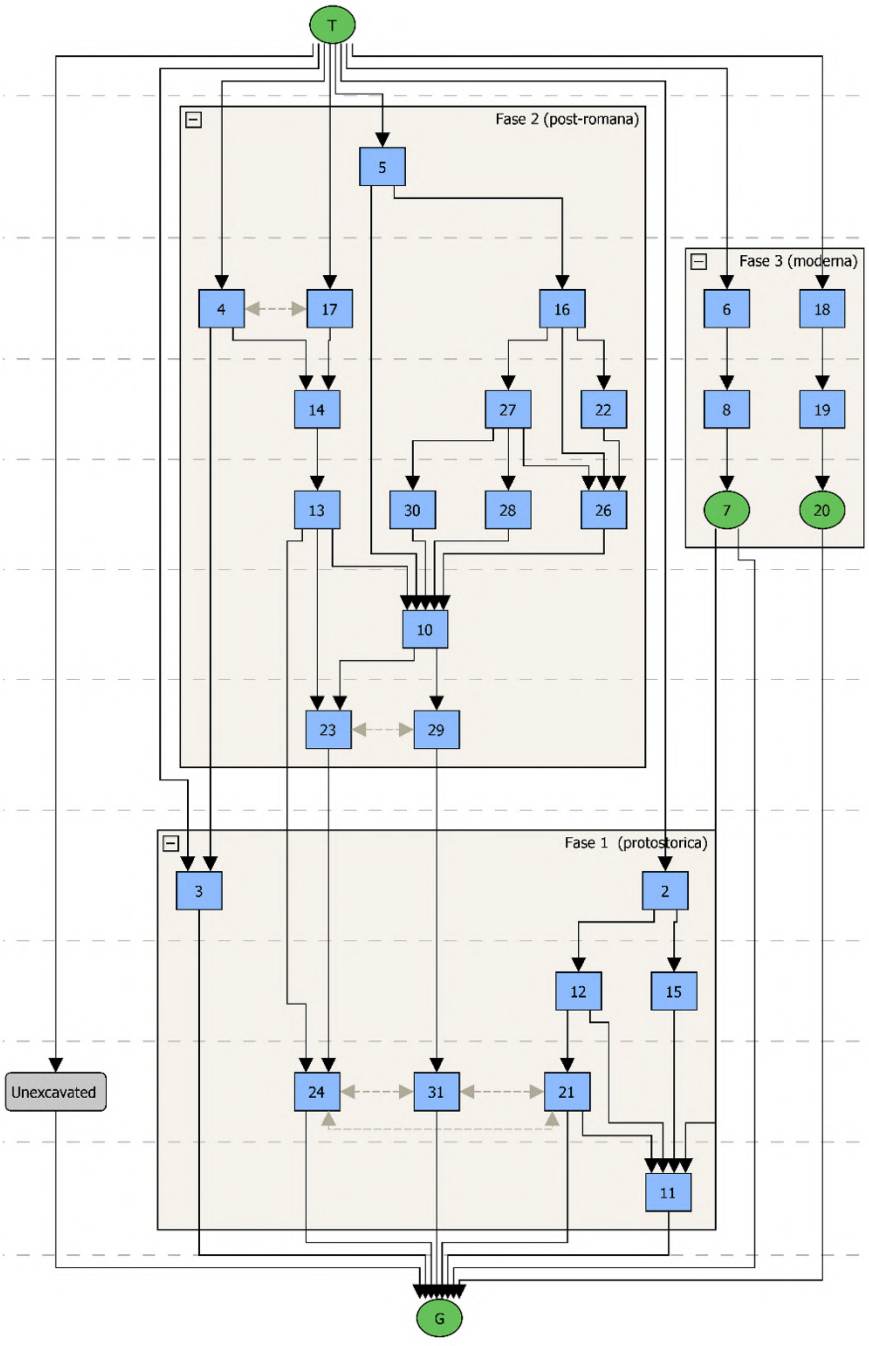

Figure 34. Matrix of the Trmun stratigraphic excavation. The layers (blue squares) are grouped into three phases, each pertaining to a specific time of occupation. T = top, uppermost level; G = ground, deepest level. 7 and 20 correspond to negative units.

The stratigraphic units are uniquely characterized by different geological features and various artifact findings. All layers are described in Figure 35 starting from the uppermost vegetative layer to the deepest level, where bedrock emerges. Just below the top layer, strata from the

modern phase appear. This section only involves a small portion of the excavation and is positioned near the west of the tower. The post-Roman period contains the most layers, as exposing the rectangular structure caused several layers to unfold. Figure 35 provides some detail around and within the tower, including the interesting discovery of a fireplace and remains of ash (US 22, US 26, US 28). The final occupation layer, the protohistoric phase, proved essential for conforming ties to the protohistoric period and assisted in creating a chronology of the Trmun hilltop. The deepest layer contains bedrock, which was found at a shallow depth as the GPR data hinted.

Units of Stratigraphy Identified during the Trmun Excavation	
Vegetation Layer	
US 1	Uppermost layer, with a thin grassy covering.
Modern Phase	
US 18	Located south of the tower, a modern filling of a depression, only partially excavated.
US 19	Large sandstone slabs that appear to border US 20.
US 20	A cut in the bedrock, only partially excavated (uncertain chronology).
Military Post West of the Tower	
US 6	The filling of a modern pit, containing plastic, glass and metal artifacts of a military post (US 7, 8).
US 7	Adjacent to the inner edge of the protohistoric fortification, a pit dug out during the latter half of the 20th century to create a small military post.
US 8	Structure of sandstone blocks, partially covers the US 7 pit.
Post-Roman Phase	
Landscaped Area Southwest of the Tower	
US 4	Layer of sandstone slabs, about 6.5m x 3m wide, covers US 3 and part of the external earthen structure (US 13, 14) leaning against the tower (US 10). This level seems to be connected to the possible access of US 10.
Entrance Area East of the Tower	
US 17	Directly east of the tower, a layer of small stone slabs and blocks. Partially covers the landform (US 13, 14) and around US 10. This is likely an arrangement of the surface layer of the entrance gate associated with the tower.
Tower	
US 5	A very limited shallow collapse of the stone bases related to the tower (US 10), located almost entirely in the internal space surrounded by the structure.
US 16	Sandstone blocks and slabs inside the tower, could be interpreted as a collapse, however more likely is a filling aimed at leveling the ground. This layer covers the fireplace.
US 10	Labeled as the “tower” layer. This is the stone base of the rectangular tower, built *dry* with sandstone slabs and blocks. This layer covers US 23 and US 29 and is supported by the ground platform (US 13).
US 14	A line of elongated stones, which are technically discontinuous, but appear to mark the outer edge of the ground platform (US 13).
US 13	A sub-rectangular platform on the bare earth set against the stone base of the tower (US 10). This layer covers some residual of US 23. Yielded some fragments of fire pots both from the top and from the base of the layer, as well as some protohistoric pottery remains.

US 22	Fireplace located in the northeastern corner of the tower. Consists of large basal slab and is bordered by smaller blocks and slabs. Is associated with a layer of ash a few centimeters thick.
US 27	Layer of sandstone slabs in a horizontal position inside the tower (US 10). This was likely a walking surface in line with the fireplace (US 22), following the first level used in the tower (US 26, 28). Some fragments of rough pottery found here.
US 26	Level mainly consisting of ash below layers US 16, US 22, US 27 and likely in line with US 28. This marks the first level of use within the tower. Various pottery and artifacts found here.
US 28	Burnt area in the northern sector inside the tower, adjacent to a large, vertically placed stone slab. This level is probably in line with the ash level (US 26).
US 30	A small group of sandstone slabs in line with US 26 and US 28 and could likely be equal to US 27.
US 29	Silt clay-like fill that the stone base of the tower (US 10) sits on. This layer corresponds to US 23. Yielded similar pottery found in US 23 and US 13.
US 23	Silt clay-like fill that the stone base of the tower (US 10) sits on. Located west of the tower and comparable to US 29. Represents the lower part of the US 13 platform. The specific pottery found at this layer implies that US 29 = US 23 and, this layer was built almost simultaneously with US 10 and US 13.
Protohistoric Phase	
US 3	Dark brown silt-clayey layer of variable thickness. Located between the grass and base rock in the internal and central part of the protohistoric fortification. Only few fragments of protohistoric pottery found here.
US 2	Thin yellowish silt-clayey layer located between the grass and collapse of the protohistoric wall. Few fragments of protohistoric pottery found, just a few centimeters below the ground.
US 12	Located in the northeastern section of the survey area. Yellowish silt-clayey layer with some small and medium-sized stones and an abundance of protohistoric pottery, the majority of pottery in general, coming from this layer and US 21. Includes elements deriving from a very limited collapse of the rampart towards the inside of the settlement and some materials from within the leveling of the strip located between the rampart itself and the central area of the hill. A small amount of fauna remains found within this layer.
US 15 = US 25	The protohistoric wall collapse towards the outside. Made of blocks and slabs, some with large dimensions and often placed in a vertical position, especially in the areas adjacent to the original base of the defense wall. Some protohistoric pottery fragments found here.
US 11	Original base of the wall, about 1.6m wide. Built with the sack technique, with larger ashlar stones recognizable only along the external side. 3-4 rows are preserved. The internal side is made of smaller stones, randomly placed.
US 21	Located in the northeastern section of the survey, just below US 12. Yellowish silt-clayey layer abundant with protohistoric pottery. This layer shows a voluntary accumulation to level the strip between the rampart and inner part of the hill. A small amount of fauna remains, and flint artifacts found within this layer.
US 24	Located west of the tower. A yellowish silt-clayey layer rich in ceramics. Stratigraphically, this layer corresponds to US 21 and US 31.
US 31	Located below the tower. A yellowish silt-clayey layer rich in ceramics. Stratigraphically, this layer corresponds to US 21 and US 24.
Bedrock	
US 9	Arenaceous marly rock layer consisting of parallel banks of sandstone with a northwest-southeast direction and alternates with bands of marl, more prone to weathering and therefore outcrops at a slightly lower altitude. These features match the Eocene Flysch rock formation that characterizes the area.

Figure 35. Units of stratigraphy uncovered at the Trmun stratigraphic excavation explained. Layers are identified from the uppermost layers to the deepest. US = unit of stratigraphy.

4.1.1. Protohistoric Stratigraphic Layers

Observing phase 1 of the stratigraphy, the protohistoric layers revealed the remains of a fortified protohistoric occupation. This phase of stratigraphy is best split into two specific layers, one pertaining to the period of protohistoric occupation and settlement use, and a second concerning the abandonment period, or post-occupation. Figure 36 illustrates the stratigraphic layers present at the time of Late Prehistoric occupation, including six focal units. These are the units deepest in the subsurface. In general, the land remained flat, with the terrain fluctuating less than a meter to include the protohistoric remains and bedrock. The fortification's perimeter wall (US 11) is clearly visible and spans approximately 1.6m in width. The wall was built using the sack technique with larger, ashlar stones on the external sides, and smaller stones randomly placed on the internal sides. Ashlar is a type of stone that is precisely transformed into a square-shape useful for building structures. There are only a few preserved layers of external ashlar rows. The wall is unfortunately not visible in the northeastern sector for a short distance due to the later occupation and construction of a tower, along with the excavation not pursuing further depth (fig. 36). US 21 offered a wealth of pottery, as well as few fauna remains and flint artifacts, that helped properly date the protohistoric settlement. Additionally, after analysis, US 24 and US 31 proved to be related to the US 21 layer due to similar stratigraphic positioning, soil content and pottery collection. These three layers produced ceramic materials along the entire length of the fortification. Towards the southern part of the survey area, bedrock (US 9) dominates and is recorded with less than a meter difference compared to the perimeter wall (US 11). US 3, a rather shallow layer that fits between the vegetative layer and base level, did have a few pieces of protohistoric pottery that is worth noting.

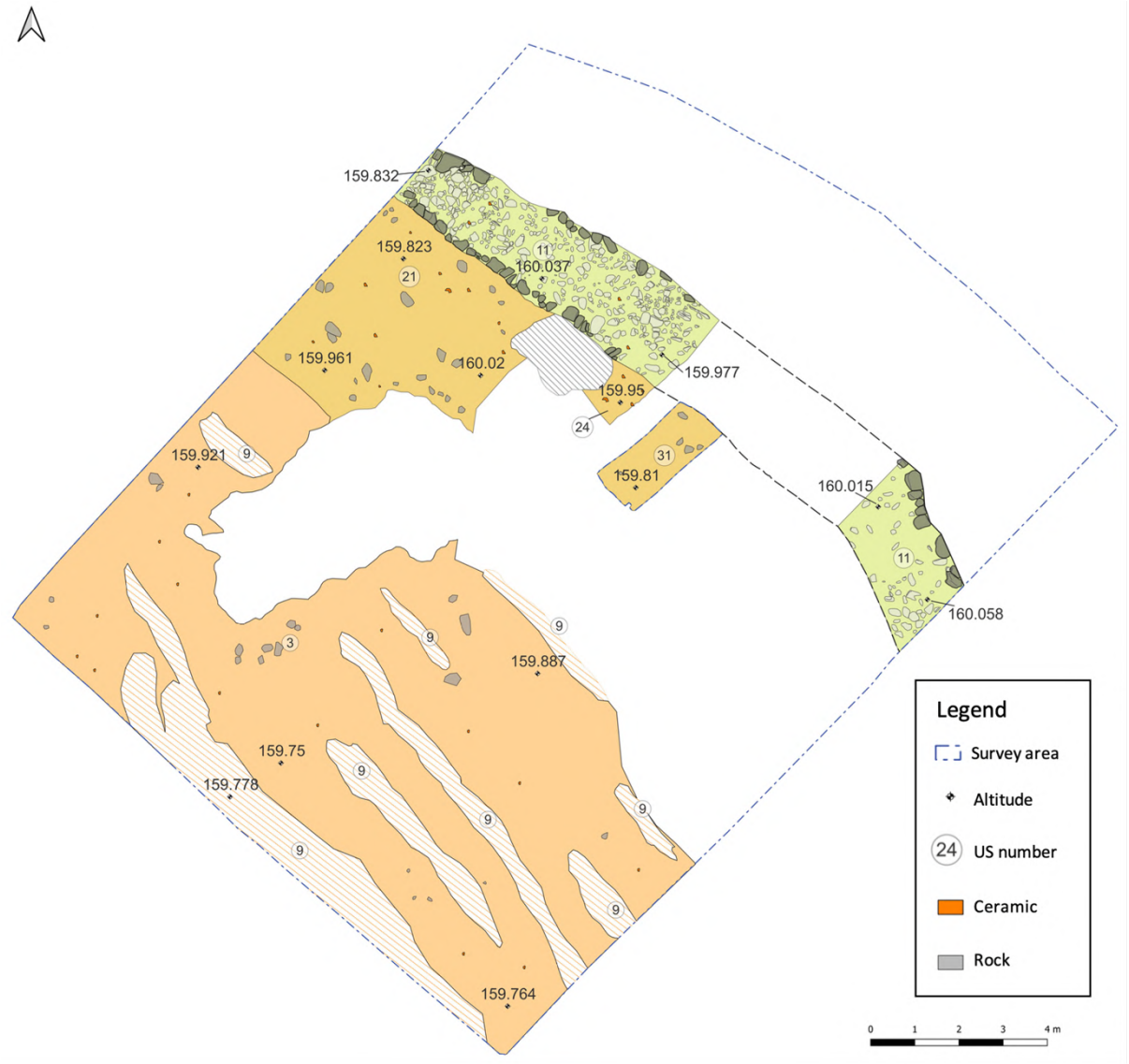

Figure 36. Stratigraphic excavation layers pertaining to the period of active protohistoric occupation. Important layers include: US11, US21=US 24=US31, US 3, US9. Image created as a vector layer in QGIS derived from an orthophoto.

The second protohistoric period is characterized by the abandonment of the settlement. This layer, presented in Figure 37, illustrates the area after the collapse of the fortification and features four main stratigraphic units. As with the occupied phase (fig. 36), the near-surface layer (US 3) and bedrock (US 9) emerges rather quickly. The bedrock even makes an appearance in the collapsed area (US 15) with the typical flysch terrain features including sandstone banks in the northwest-southeast direction interspersed with the more-erodible marl layers. The bedrock emerges around 40cm to 50cm below the surface and a limited amount of pottery was found within the bands, although significantly less than the areas

adjacent to the fortification wall. US 15 represents the collapse of the fortification wall. This layer consists of large blocks and slabs that were vertically positioned, particularly in the areas adjacent to the original base of the defensive wall. Placing slabs vertically and filling the space between them with gravel or small stones, is a characteristic of *castellieri* structures (Mihovilić, 2013). Not surprisingly, some fragments of pottery were found within this layer. Interpreting this area and the materials within it, the fortification wall (US 11) can be assumed to have been quite tall, perhaps between 1.5m and 2.5m. Additionally, the vertical alignment of the collapsed blocks infers a hasty and solitary incident, curiously supposing a deliberate and destructive act. US 12 sits above the original occupied layer, US 21, and contains a vast amount of pottery. Within this stratum, there are some elements implying a limited part of the rampart collapse went towards the inside of the settlement.

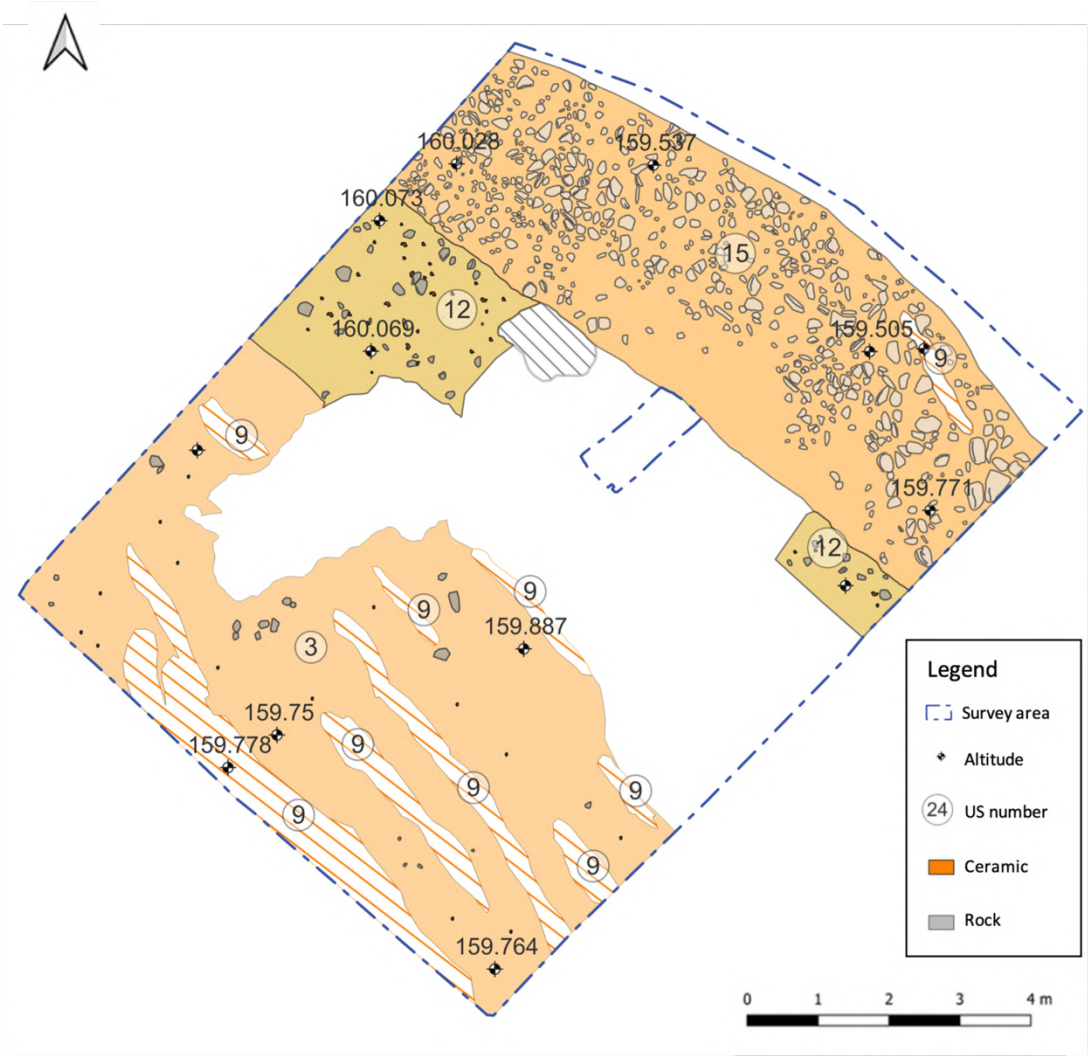

Figure 37. Stratigraphic excavation layers pertaining to the period of abandonment, post-protohistoric occupation. Important layers include: US12, US15(=US15), US 3, US9. Image created as a vector layer in QGIS derived from an orthophoto.

To better highlight the shallow depth required to make contact with archaeological layers, Figure 38 demonstrates the protohistoric levels during- and post-occupation. Figure 38b shows the orthophoto derived directly from the site. The small white squares represent manually labeled layers. Figure 38a dissects the orthophoto to produce an improved, user-friendly visual. There are three georeferenced markings that indicate a mere 1.16m total distance from the topographic layer to the bedrock.

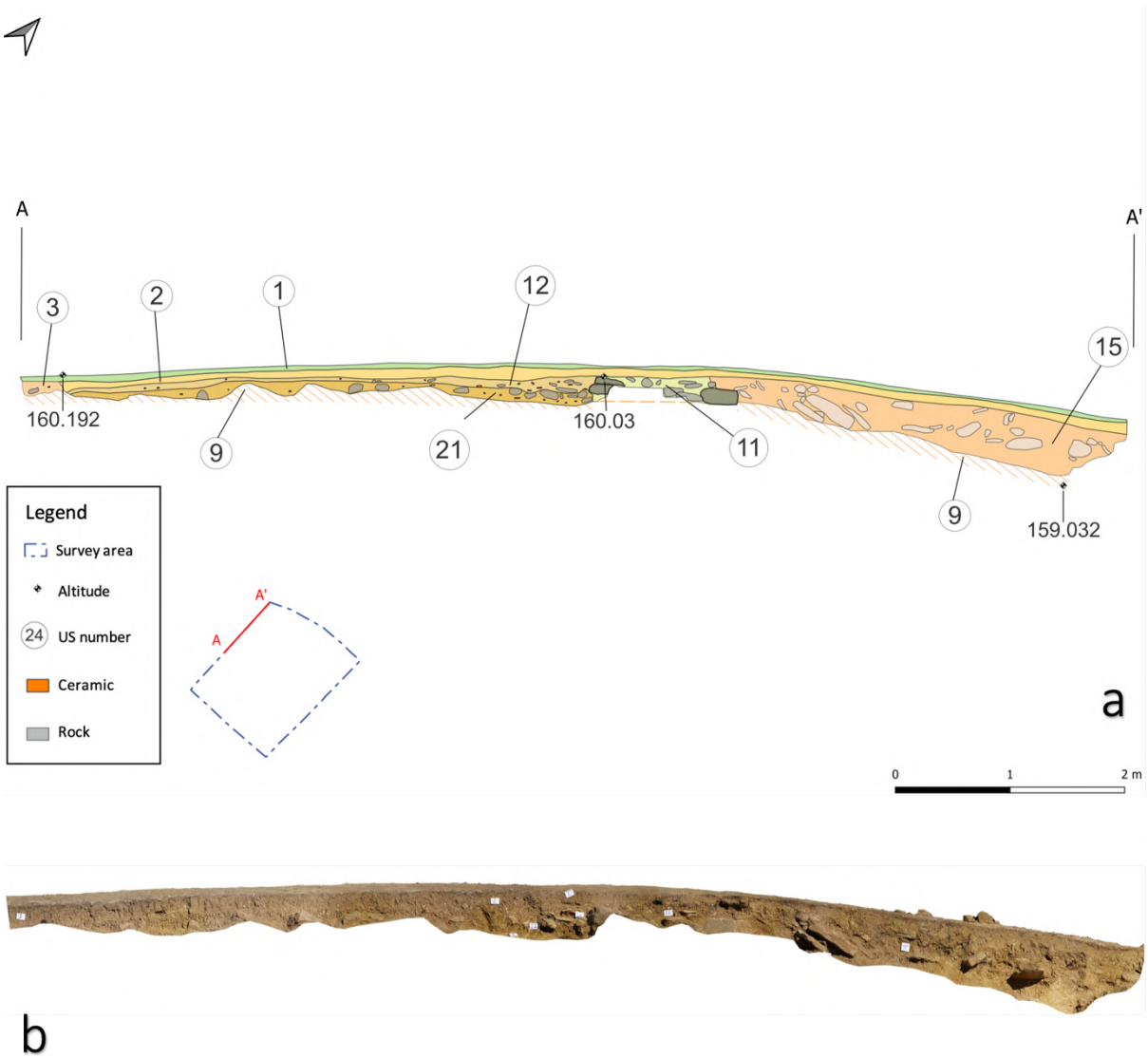

Figure 38. Detailed look at the stratigraphic layers. (a) A vector-based image containing stratigraphic details pertaining to the protohistoric hillfort. (b) Orthophoto used to create the vector-based image (a).

4.2. *Castellieri* Culture

The excavation specific results, including the examination of protohistoric pottery and analysis of a Late Prehistoric fortification, place the Trmun hilltop sometime within the Early and Middle Bronze Ages. This time period is characterized by the *castellieri* culture found in Istria, the Karst and north-eastern Italy. The geological characteristics made Trmun a strategic placement of a settlement and the remains of a rampart imply occupation. There are several other protohistoric settlements that can be compared with Trmun, especially comparing ceramics, to help confirm the time frame.

Castellieri (sing. *castelliere*) describe fortified hill settlements, or hillforts, corresponding to the Bronze and Iron Ages (Mihovilić, 2013). These settlements are located in the northern Adriatic, most commonly in Istria and the Karst region, which encompasses the present-day Italian region of Friuli Venezia Giulia, Western Slovenia and a large sector of northern Croatia. The position of this region, in particular the alpine passes, mild-Mediterranean atmosphere and rather fertile plains, assisted in settlement formation (Marchesetti, 1903; Mihovilić, 2013).

Castellieri embodied proto-urban characteristics by having a clear societal structure and an organized system for building settlements (Mihovilić, 2013). These fortifications were certainly strategically situated; most *castellieri* are nestled on an isolated hill, and some are even positioned near a deep valley or sit on a promontory, a type of peninsula (Mihovilić, 2013). Additionally, it was important for the *castellieri* to be near a bountiful water source and close to key routes (Borgna et al., 2018). These are the same types of geological conditions present in the Monte d'Oro ridge, as described in section 3.1. The Trmun hilltop perfectly fits these characteristics; the Gulf of Trieste is nearby, and the slightly elevated position of the hilltop provides a panoramic view of the area for protection (Mihovilić, 2013).

One prime feature of *castellieri* is the construction of ramparts (Borgna et al., 2018; Mihovilić, 2013). Ramparts are defensive walls that surround a settlement to provide protection. These walls can be substantially high, reaching heights possibly over six meters, ensuring the village is adequately covered (Mihovilić, 2013). For example, in one of the best-preserved protohistoric settlements in the Istrian area, Monkodonja, rampart remains are

approximately two meters tall and are understood as just a small portion of the defensive wall (Mihovilić et al., 2009). Some ramparts featured a complex entrance system, similar to a labyrinth; this provided an extra form of security (Mihovilić, 2013). The rampart served as the primary source of protection because during the earliest phase of the Bronze Age in the Istrian-Karst region, military conquest was not overwhelmingly relevant. Only during the transition into the Middle Bronze Age did warfare rise (Hänsel et al., 2019). This could be a reason as to why many hillforts are dense in pottery findings, yet generally deficient in weaponry. While ramparts usually provided sufficient defense during the Early Bronze Age, by the Middle Bronze Age, these no longer sufficed. Monkodonja is a prime example that met its demise by military defeat and proved the fortification system had become obsolete for the changing times (Hänsel et al., 2019).

At the Trmun site, the remains of a protohistoric rampart, along with an abundance of protohistoric pottery helped confirm protohistoric occupation and ties to *castellieri* culture. The analysis of the hillfort and the examination of protohistoric pottery place the Trmun hillfort sometime between the earliest period of the Bronze Age and the beginning of the Middle Bronze Age (fig. 39). Interestingly, Trmun seems to chronologically cross paths with Monkodonja. Trmun's placement, sometime between 1800 and 1450 B.C., makes this hillfort one of the oldest on the Monte d'Oro ridge and in the Istrian-Karst region as a whole. The Trmun campaign, from the investigative phase to the excavation, has helped provide a further context of the *castellieri* culture.

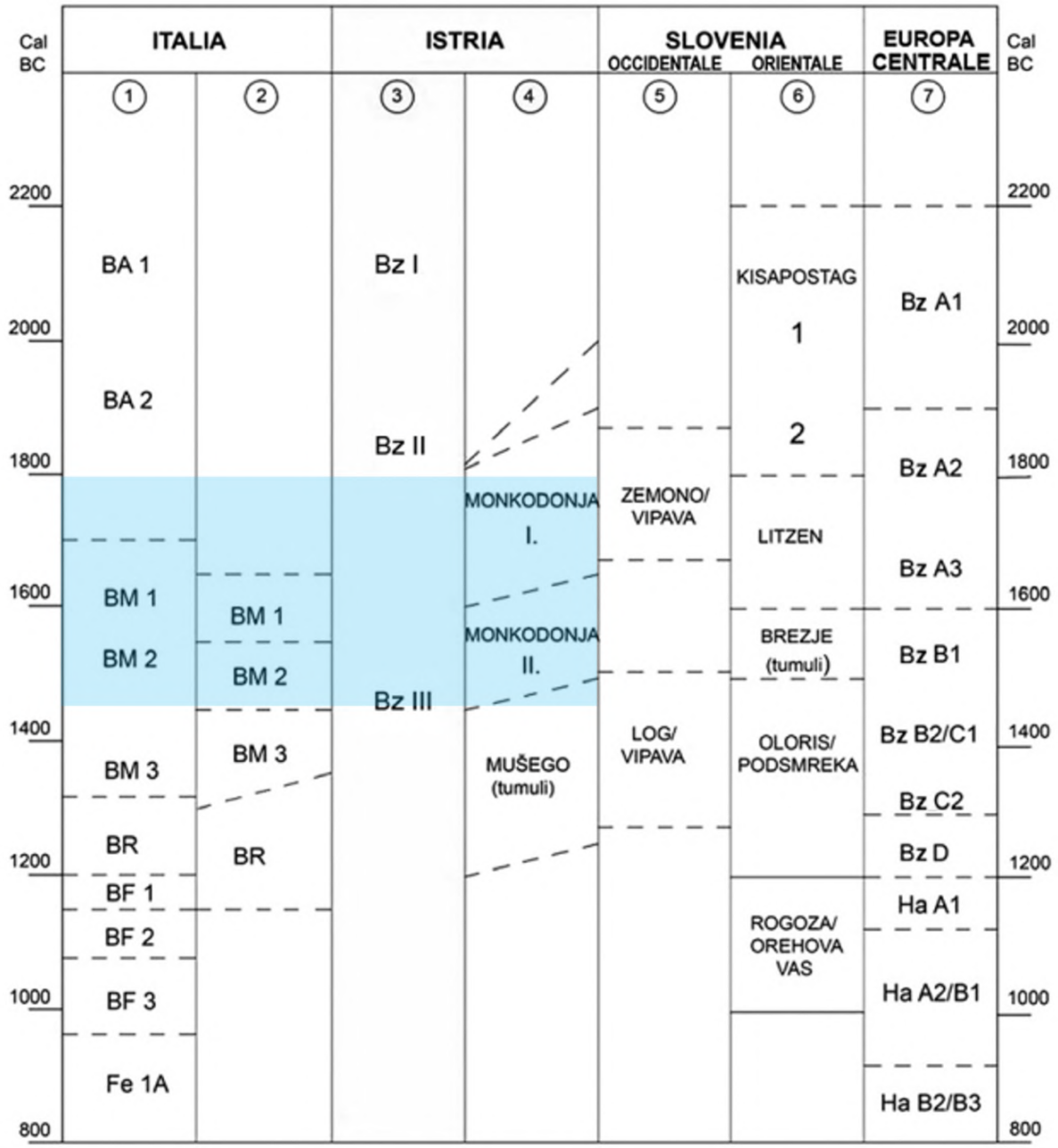

Figure 39. Chronology of the Bronze Age within different areas of Europe. The Trmun site falls within the "Italian" chronology. The area highlighted in blue is the proposed placement of the Trmun protohistoric settlement according to pottery typology. This places occupation at Trmun during the same time as the well-known Monkodonja settlement. (after Borgna et al., 2018, Fig. 3)

4.3. Protohistoric Pottery Analysis

The stratigraphic layers, US12 and US21, both offered an abundance of protohistoric pottery that has been preliminarily analyzed for the article, *Bernardini et. al., 2023 (submitted)* and has vitally assisted in constructing the history of the Trmun hillfort. While other layers also had pottery fragments, these two units remained central. Looking at the chronological aspect of the pottery, the Trmun hilltop can be placed in the Early and Middle Bronze Ages (fig. 39). The ceramics discovered at Trmun are comparable to several surrounding protohistoric settlements, along with other *castellieri* in the nearby region.

In general, the unearthed pottery maintains a similar texture, surface, firing method and form. The vessels were fired in an oxidized environment with coarse or medium-grained pastes, with only few showing a fine-grained texture. Due to the archaeological layers' proximity to bedrock, the clay material shows some angular insertions of varying sized marl, up to a few millimeters. Overall, the vessels fit into three main categories: large and medium sized pots, which were the most common type of vessel (fig. 41: 4-6; fig. 42: 1-2), bowls (fig. 40: 2, 4, 5, 7) and cups (fig. 41: 1).

Inspecting the vessel rims, some have a funnel shape (fig. 41: 4-6). These funnel rims were common during the Early Bronze Age and are similar to ones found in Monkodonja, the site with matching chronology (e.g., Hellmuth Kramberger, 2017, Ta. 4: 1, 3, 4; Ta. 5: 2). Within the area surrounding Trmun, there are some hillforts, such as Elleri, that also have rims of a comparable funnel-shape (e.g., Lonza, 1981, Ta. 7: 4-6, 18; Ta. 13: 5; Ta. 14: 5; Ta. 15). There is further evidence of such a vessel type within Karst caves (e.g., Gilli, Montagnari Kokelj, 1992 and Turk et al., 1993, Ta. 17: 2). The cup, Figure 3: 1, holds a funnel rim and is remarkably similar to a small jar from the archaeological site, Zemono near Vipava, located northeast of Trmun in Slovenia. A sample of charcoal found in the pit where the vessel laid, went through a Carbon-14 analysis and was dated between the 19th and 17th centuries B.C. (e.g., Bratina, 2014, fig. 35.4: 1).

Many fragments discovered at Trmun included interesting lugs and handles that were typical of the Early and Middle Bronze Ages. In particular, some tongue-shaped lugs adorned with a finger impression (fig. 41: 3; fig 42: 1) were found that can be compared to other sites. In

particular, the finger impression spotted in Figure 42: 1 resembles one found at Sv. Križ, a Bronze Age hillfort in Istria (Percan, 2021, fig. 8: 11). This type of lug is commonly seen in the *castellieri* culture and predominated as one of the main lug types (e.g., Borgna et al., 2018, fig. 5; Lonza, 1981, Ta. 11: 2-4, 7; Ta. 17: 3; Hellmuth Kramberger, 2017, Ta. 33: 1; Ta. 76: 2, 3; Ta. 102: 3). Lugs of similar stature have been uncovered in Istrian and Karst caves, as well as the Zemono near Vipava site (e.g., Bratina, 2014, Fig. 36.6: 16, 17 and Gilli, Montagnari Kokelj, 1992, Fig. 59, 60, 62, 64). A bowl with a carinated rim-to-wall transition (fig 40: 4) has a notable "X" handle located below the rim. These sorts of handles also portray *castellieri* culture and a general comparison can be made in ceramic findings from the Elleri settlement (e.g., Zendron, 2017, Fig. 17 and Hellmuth Kramberger, 2017, Pl. 20: 1, 2; Pl. 74: 7, 8; Pl. 101: 3). The placement of an "X" handle or tongue impression that faces upwards may have been used to help carry larger vessels (Zendron, 2017). Another kind of handle included from the Trmun site is one that has a triangular cross-section and narrows towards the top (fig. 41: 2). This is a distinctive handle-type of *castellieri* and already appeared in the Early Bronze Age (e.g., Zendron, 2017, Fig. 114 and Lonza, 1977, Ta. II: 3-7, 8-11; Ta. XIV: 4, 6-7). Observing other protohistoric settlements, the triangular cross-section became more widespread in the Middle to Late Bronze Age. One concluding significant handle discovered at Trmun features a semicircular shape (fig. 41: 7). When looking from the top of the vessel, there is a trapezoidal shape that corresponds to the upper plate. This handle is central because it provided the basis of handles made for overhand plates that began to appear in Istria by the end of the Early Bronze Age. It would not be until the Middle Bronze Age that these types of handles became widespread (Borgna et al., 2018).

Bowl fragments provided additional support in chronological determination of Trmun. Some fragments deriving from conical-shaped bowls appear to have a smoothed inner surface and roughly abraded outer surface (fig 40: 2, 3). It is likely that this type of bowl belonged to the collection of *briquetage*. This is a specific type of very-coarse-pottery used for salt extraction from seawater (Harding, 2014). Similar bowl fragments can be seen in nearby *castellieri* (Zendron, 2017, Fig. 121). Another conical-shaped bowl with a particularly flat shape with no curvature in the rim (fig. 40: 7), appears similar to one found in Elleri with a flat bottom (Zendron, 2017, Fig. 121).

A small number of fragments resemble parts of a tripod, also identified as legs (fig 40: 6, 8). These have emerged in several other sites within the Istrian-Karst area (Hellmuth, 2017, Ta. 11: 2-4; Ta. 23: 5; Ta. 58: 3; Ta. 71: 5). At the Sv. Križ settlement, some tripod pieces have been found with similar appearance (Percan, 2021, fig. 16: 4). In Monkodonja, there is evidence that indicates tripod use as part of a mobile fireplace due to burn marks directly on the ceramics, opposed to underneath (Percan, 2021; Hellmuth Kramberger, 2017).

Pottery fragment analysis clearly indicates the Trmun hillfort belongs to the most ancient phase of the Karst-Istrian *castellieri*, a period between the Early and Middle Bronze Ages. The types of vessels uncovered during the excavation align with those from surrounding, relevant sites.

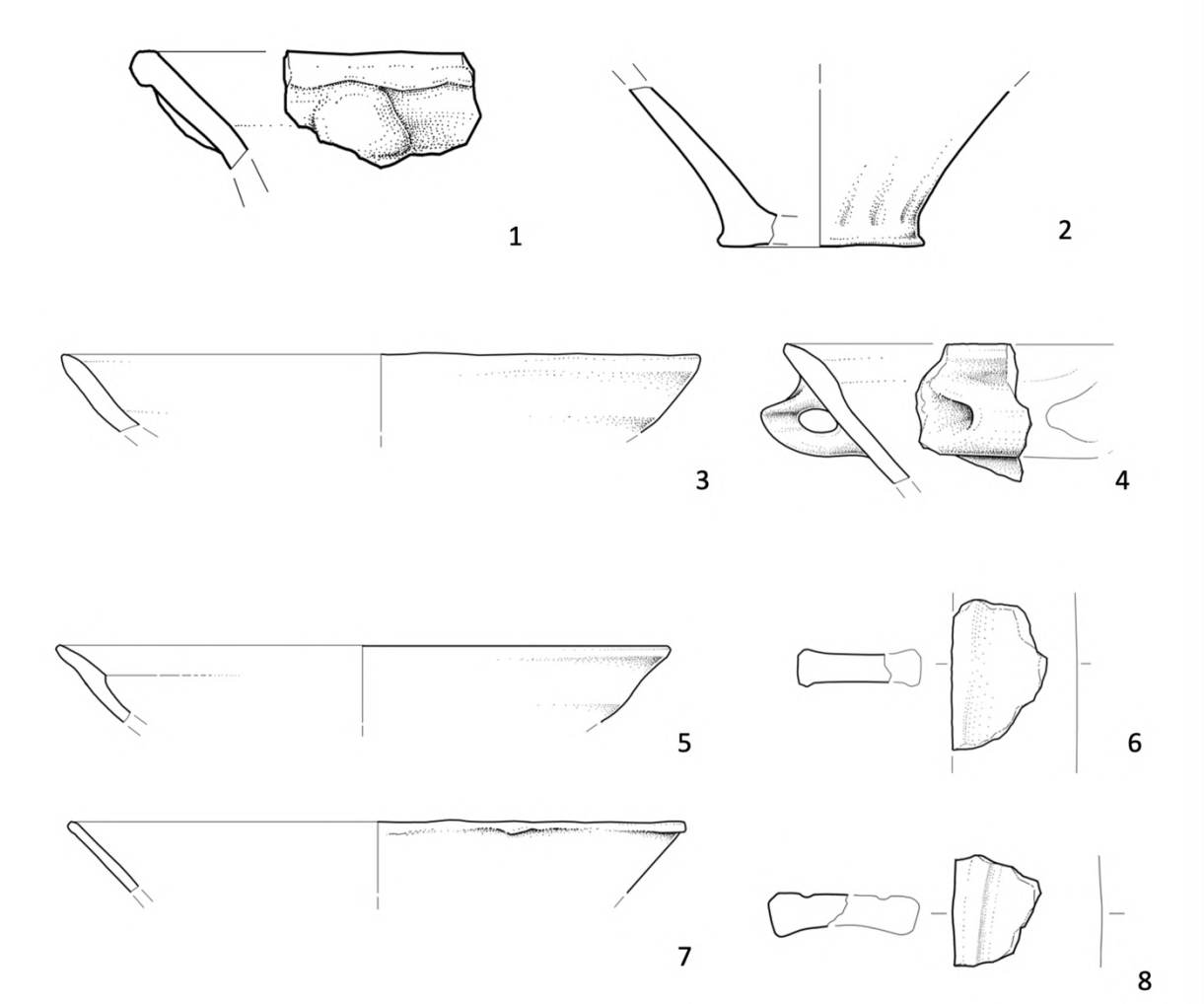

Figure 40. Selection of ceramic vessels from the Trmun site. Pottery found in US12: 1, 2, 5, 7, 8; US21: 3, 4, 6. Drawings by: T. Korošec. (Bernardini et al., 2023, submitted)

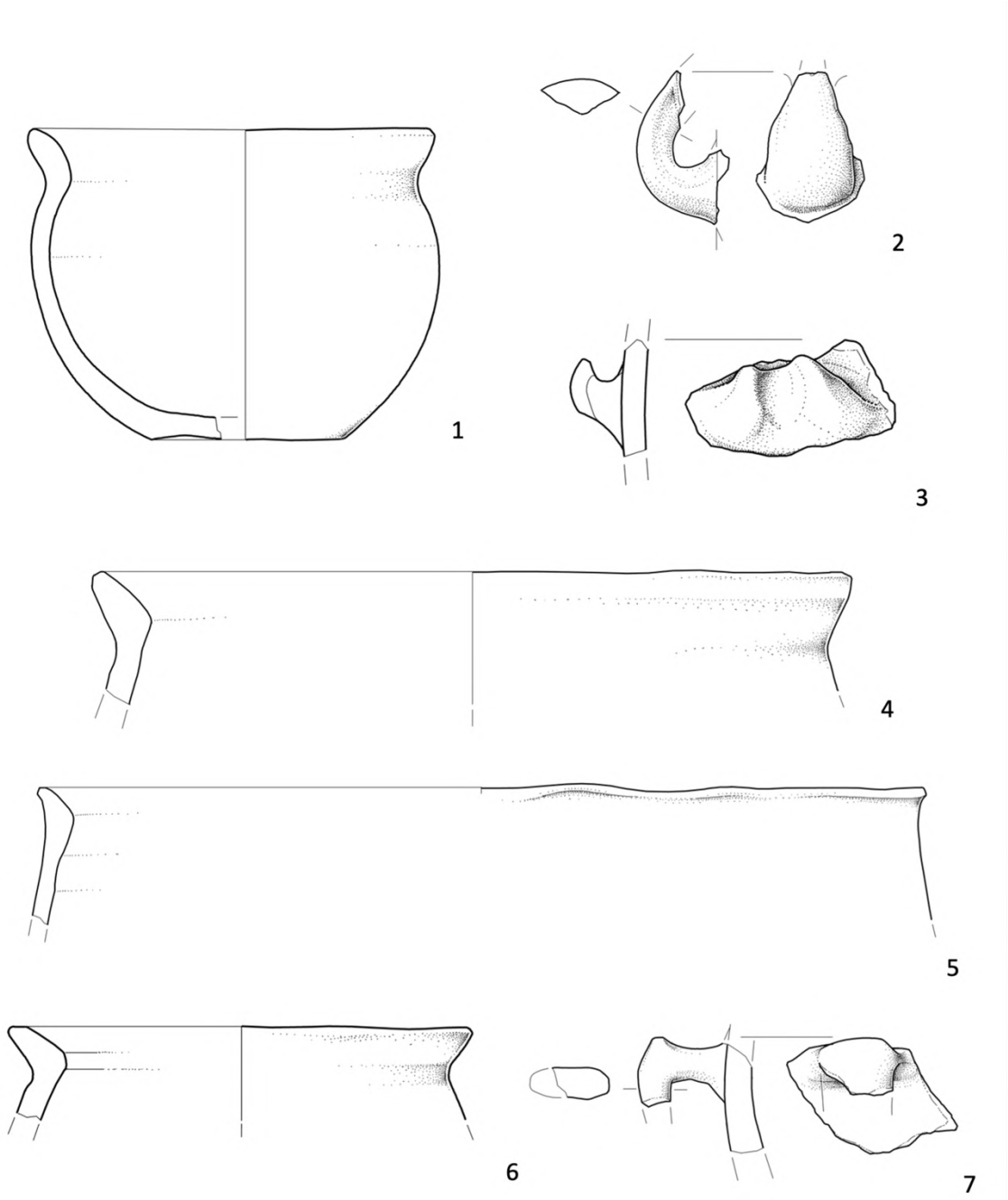

Figure 41. Selection of ceramic vessels from the Trmun site. Pottery found in US12: 2, 4, 5; US21: 1, 3, 6, 7. Drawings by: T. Korošec. (Bernardini et al., 2023, submitted)

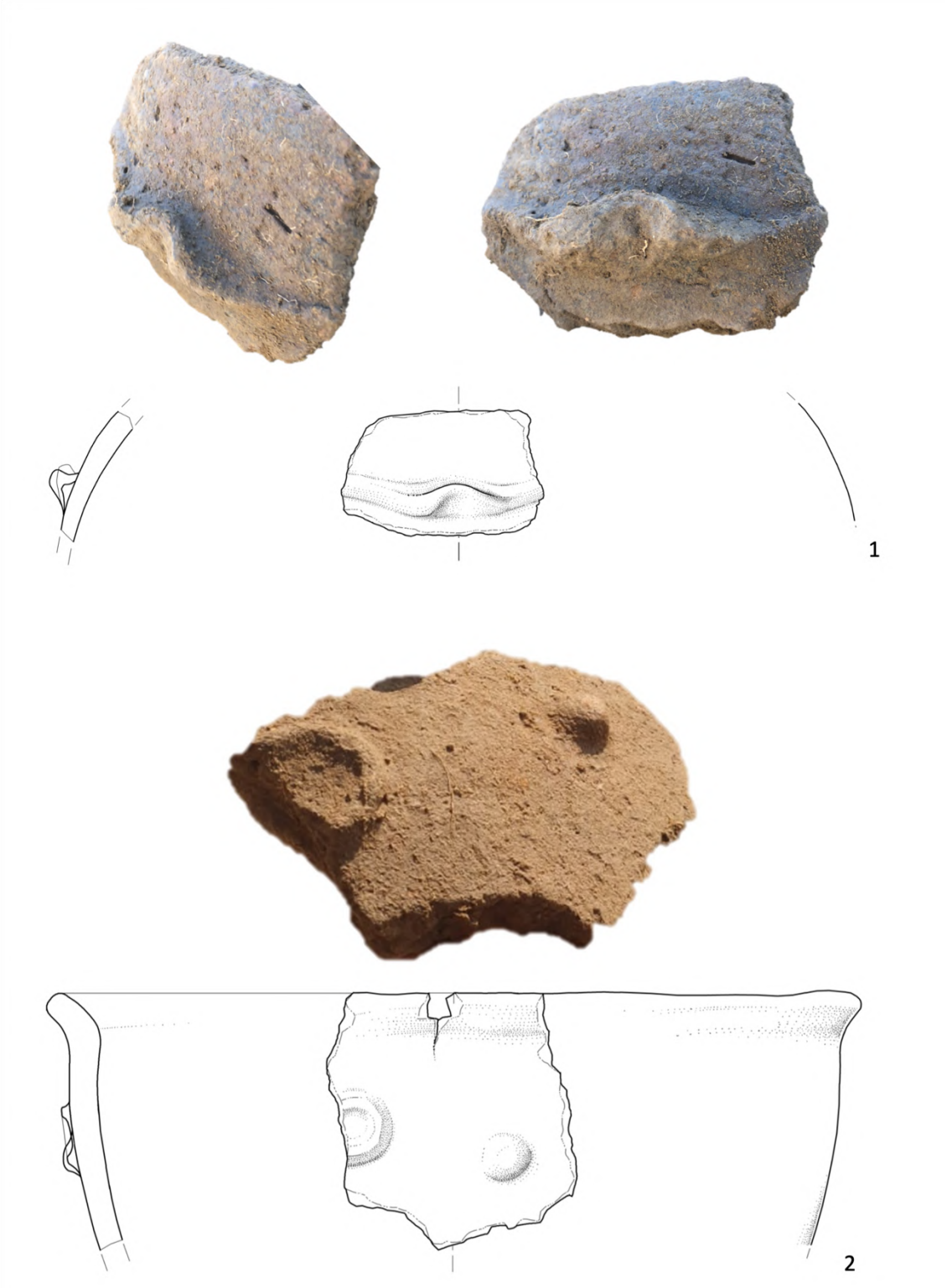

Figure 42. Two pottery fragments found at the Trmun site. These drawings are accompanied by a photo of the actual piece. Top (1): US21; bottom (2): US12. Drawings by: T. Korošec. (Bernardini et al., 2023, submitted)

5. Conclusion

Based on all of the results from the Trmun campaign, the hilltop was occupied more than once throughout history. The earliest settlement, confirmed with the study of protohistoric pottery remains, dates to a period between the late Early Bronze Age and the Middle Bronze Age. After eventual abandonment, evidence pointed to another occupation during the post-Roman period. The site had adequate structure remains and artifacts to build a chronology of the Trmun hilltop.

The protohistoric hillfort covers a relatively flat area and spans approximately five hectares. The preliminary analysis of pottery fragments greatly assisted in establishing a period of occupation. According to results, the Trmun hillfort was built during the earliest phase of the *castellieri* era. The *castellieri* culture featured small, fortified villages scattered throughout the Karst-Istrian region from the late Early Bronze Age, approximately 1800 to 1650 B.C. to the late Iron Age. The initial study of Trmun pottery points to occupation between the late Early Bronze Age and beginning of the Middle Bronze Age, allowing for a deeper, improved understanding of the earliest *castellieri* period.

Looking at Karst-Istrian chronology, the nearby Monte d'Oro hillfort was also active during the same period as Trmun. It is likely that these two hillforts were politically associated and may have controlled route access through the Monte d'Oro ridge that connected the Trieste and Karst areas with northern Istria. The landscape with many minor hilltops allowed hundreds of small, fortified villages to thrive rather peacefully until the shift to larger settlements and changing warfare styles. Towards the end of the Bronze Age, the ramparts that characterized *castellieri* were no longer a sufficient form of protection and dominating forces came in. This aligns with the initial study of protohistoric pottery from Trmun, that infers the site was abandoned by the Late Bronze Age. Additionally, the unearthed stones associated with the wall collapse deduce a purposeful act of destruction and a quick desertion.

A second occupation at the Trmun hilltop occurred during the post-Roman period. The investigative phase results showed three subsurface features and the stratigraphic excavation confirmed the existence of one tower with an opening and an internal area arranged with

sandstone slabs. The fortification appears to exploit the remains of the protohistoric wall. The ALS and SfM photogrammetric DTMs hint at two other structures on the hilltop that resemble the excavated tower that as a whole, created a fortlet. The geological aspects, a hilltop overlooking the Rosanda and Ospo valleys on the Monte d'Oro ridge, suggest the small fortification could have been connected to a military campaign.

As analysis of artifact remains continues, more details of the Trmun hilltop will unfold. The protohistoric pottery and remains of a rampart are expanding the knowledge of the most ancient period of the *castellieri* culture. There are some organic samples taken from the site currently undergoing C-14 dating; the results of this will provide a more precise chronology of the site (Bernardini et al., 2023, submitted).

6. Discussion

The Trmun campaign demonstrates the impact digital methods can have in archaeological studies. The use of traditional methods, such as stratigraphic excavations will certainly remain focal and be a necessary means for attaining certainty of results. However, employing digital methods, especially non-invasive ones such as ALS, SfM photogrammetry, GPR and thermal imaging can provide significant benefits in a campaign. Where physical evidence is scarce to none, but intangible indications suggest historical ties, digital methods can generate high-quality topographic models and detect buried subsurface archaeological features.

Digital practices can also be used to better plan stratigraphic excavations. For the Trmun investigation, an initial ALS-derived DTM that encompassed the whole protohistoric settlement suggested the eastern section was one of the best-preserved areas. Further investigation, that included high-resolution DTMs generated from ALS and SfM photogrammetry, indicated the northwestern sector of the hilltop would be best suited for an excavation and could provide the strongest physical evidence. The use of GPR boosted confidence, as the features detected matched the anomalies found in the DTMs.

The Trmun campaign showed low-cost techniques can compete with more expensive methods. SfM photogrammetry acquisition produced a 0.02m-resolution DTM, while ALS only generated a 0.5m-resolution DTM. A 0.5m-resolution DTM is surely accurate and provides a high-level of detail, but the 0.02m-resolution DTM can strengthen anomaly detection. When a study area is free of vegetation, SfM photogrammetry can be an excellent cost-saving option that produces highly accurate topography.

If possible, utilizing ground-based methods in addition to airborne ones can solidify findings. GPR is a cost-effective method that can be helpful during campaigns relatively free of thick vegetation. This technique detects anomalies to tell an archaeologist *something* is below the surface. GPR cannot reveal the type of material, but remains a useful companion to airborne methods to confirm subterranean archaeological features.

Employing a thermographic survey within an archaeological campaign should continue to be explored. The thermal images produced for the Trmun campaign were a mere extra aspect of

digital study. ALS, SfM photogrammetry and GPR provided sufficient evidence to demonstrate archaeological features. The lack of thermographic feature detection is most certainly due to a lack of a formalized study. For a proper investigation, climate conditions need to be considered and multiple thermographic surveys of the study area should be conducted. The use of thermal images within archaeological campaigns is still in the early stages, due to prior cost restraints and therefore, a standard practice of thermography is yet to be established.

The combination of digital and traditional methods proved essential for the Trmun campaign. This is not an isolated occurrence though; undeniably, other archaeological sites exist that will not be found without the use of digital tools. As these techniques become more affordable and the practice of these methods becomes more mainstream, new sites will be discovered with a strong spatiotemporal analysis.

Acknowledgements

To Prof. Federico Bernardini, thank you for your continuous support and guidance throughout this work. I am beyond grateful for the opportunity to have taken part in the Trmun excavation that initiated the topic for my final studies. I have learned a vast amount of knowledge from you and gained a new passion. To Dr. Massimo Calosi, your expertise and patience during and after the excavation have been much appreciated. You have expanded my perception and understanding of archaeology on and off the field. To Prof. Elena Leghissa, I admire your proficiency in the ancient topics that have aided in further developing sections of this work.

Thank you to the Venice Center for Digital and Public Humanities for offering a diverse program that has allowed me to study various subjects to better understand where my interests lie. The faculty have eagerly encouraged me to broaden my skill set and I am thankful for finding the archaeological side of Digital and Public Humanities.

The most heartfelt thank you goes to my parents who have supported me in all my worldly endeavors. I would certainly not be where I am today without their never-ending love and encouragement.

Bibliography

AeroScientific, “Flight Planning for Aerial Photography | FlightPlanner,” Adelaide, Australia, https://www.aerosci.info/flightplanner/.

Agisoft LLC, St. Petersburg, Russia, https://www.agisoft.com.

Alevizos, E., 2019, *How to Create High Resolution Digital Elevation Models of Terrestrial Landscape using UAV Imagery and Open-Source Software*, DOI: 10.13140/RG.2.2.25616.25603.

Ángel, J., et al., 2020, “Assessing the potential of multispectral and thermal UAV imagery from archaeological sites. A case study from the Iron Age hillfort of Villasviejas del Tamuja (Cáceres, Spain),” in *Journal of Archaeological Science: Reports*, v. 31, 102312.

Apple Inc., 2023, “iPhone 14 Pro,” California, USA, https://www.apple.com/iphone-14-pro/specs/.

Arrowsmith, J.R., Crosby, C., Scott, C., October 4, 2021, *2021 Geological Society of America (GSA) Short Course: Introduction to Structure from Motion Photogrammetry,* OpenTopography, UNAVCO. https://opentopography.org/workshops/GSA2021.

Bemis, S.P., et al., 2014, “Ground-based and UAV-Based photogrammetry: a multi-scale, high-resolution mapping tool for structural geology and paleoseismology,” in *Journal of Structural Geology*, v. 69, 163-178.

Bernardini, F., et al., 2013, “Airborne LiDAR application to karstic areas: the example of Trieste province (north-eastern Italy) from prehistoric sites to Roman forts,” in *Journal of Archaeological Science*, v. 40, 2152-2160.

Bernardini, F., et al., 2015, “Early Roman military fortifications and the origin of Trieste, Italy,” in *Proceedings of the National Academy of Sciences*, v. 112, E1520-E1529.

Bernardini, F., et al., 2021, “Grociana piccolo: a rare example of Republican military fortifications in Italy,” in *Journal of Roman Archaeology*, v. 34(2), 695-712.

Bernardini, F., et al., 2023, *Trmun (north-eastern Italy): multi-sale remote and ground-based sensing of a Bronze Age and post-Roman fortification,* submitted.

Bettinger, P., Merry, K., 2019, "Smartphone GPS accuracy study in an urban environment," in *PLOS ONE*, v. 14(7): e021989, https://doi.org/10.1371/journal.pone.0219890.

Boeser, S.M., 2019, "Global Positioning Systems (GPS)," in Finkl, C.W., Makowski, C., *Encyclopedia of Coastal Science,* Encyclopedia of Earth Sciences Series, 905-907, Springer Cham.

Borgna, E., Càssola Guida, P., Mihovilić, K., Tasca, G., Teržan, B., 2018, "Il *Caput Adriae* tra Bronze Antico e Bronze Recente," in Borgna, E., Càssola Guida, P., Corazza, S., *Preistoria e Protostoria del Caput Adriae*, Firenze: Istituto Italiano di Preistoria e Protostoria, 75-96.

Bratina, P., 2014, "Zemono Near Vipava," in Teržan, B., Črešnar, M., *Absolutno Datiranje Bronaste in Železne Dobe na Slovenskem (Eng. Absolute Dating of the Bronze and Iron Ages in Slovenia)*, Ljubljana: Univerza v Ljubljani, Narodni muzej, 563-567.

Casana, J. et al., 2014, "Archaeological aerial thermography: A case study at the Chaco-era Blue J community, New Mexico," in *Journal of Archaeological Science,* v. 45, 207-219.

Casana, J. et al., 2017, "Archaeological Aerial Thermography in Theory and Practice," in Herr, H., Rieth, C., van der Linde, S., *Advances in Archaeological Practice*, v. 5(4), Cambridge: Cambridge University Press.

Casana, J., Hill, A. C., Jakoby Laugier, E., October 4, 2019, *Archaeological Prospection Using Drone-Acquired Thermal and Multispectral Imagery*, Recording Archaeology, Doug Rocks-Macqueen & CAA Volunteers, https://www.youtube.com/watch?v=H-3N1rWtQVc.

Conyers, L. B., 2016, "Ground-Penetrating Radar," in Gilbert, A.S., *Encyclopedia of Geoarchaeology*, Encyclopedia of Earth Sciences Series, 367-378, Springer Cham.

Conyers, L.B., 2018, "Ground-Penetrating Radar," in *Ground-penetrating Radar and Magnetometry for Buried Landscape Analysis*, SpringerBriefs in Geography, 17, Springer Cham.

DJI, “Mavic 2 Specs,” Shenzhen, China, https://www.dji.com/mavic-2?site=brandsite&from=landing_page.

DJI, “DJI Mini 2,” Shenzhen, China, https://www.dji.com/mini-2?site=brandsite&from=landing_page.

Fassbinder, J.W.E., 2016, “Magnetometry for Archaeology,” in Gilbert, A.S., *Encyclopedia of Geoarchaeology*, Encyclopedia of Earth Sciences Series, 499-514, Springer Cham.

Forte, E., et al., 2021, “Optimised Extraction of Archaeological Features from Full 3-D GPR Data,” in *Applied Sciences,* v. 11(18), 8517, https://doi.org/10.3390/app11188517.

Förstner, W., Wrobel, B.P., 2016, “Bundle Adjustment,” in *Photogrammetric Computer Vision*, Geometry and Computing, v. 11, 643-725, Springer, Cham.

Gajda, A., Harvey, F., Kaim, D., 2014, “Analysis of Historical Change Using Cadastral Materials in the Carpathian Foothills,” in *European Journal of Geography*, v. 5(3), 6-21.

Gilli, E., Montagnari Kokelj, E., 1992, “La Grotta dei Ciclami nel Carso Trestino (materiali degli scavi 1959-1961),” in *Società per la preistoria e la protostoria della regione Friuli-Venezia Giulia*, n. 7, 65-162.

GuidelineGEO, “A History of Leading Geophysical Research,” Malå Sweden, https://www.guidelinegeo.com/about-us/history/.

GuidelineGEO, 2021, *Malå MiniMIA, Ground Penetrating Radar, MIRA – MALÅ Imaging Radar Array for true 3D acquisiton,* Malå Sweden.

Hänsel, B., Mihovilić, K., Teržan, B., 2019, “Fortification Concepts of the Bronze Age Hillforts in Istria,” in Hansen, S., Krause, R., *Bronze Age Fortresses in Europe*, Frankfurt am Main: Goethe-Universität, 99-115.

Harding, A., 2014, “The prehistoric exploitation of salt in Europe,” in *Geological Quarterly*, v. 58(3), 591-596.

Harris Matrix, 2023, “About the Matrix,” http://harrismatrix.com/about-the-matrix/.

Hellmuth Kramberger, A., 2017, *Monkodonja. Istraživanje protourbanog naselja brončanodobne Istra Knjiga 2/2 Brončanodobna kermika s gradine Monkodonja – Katalog,* Pula: Arheološki muzej Istre.

Historic England, 2018, *Using Airborne Lidar in Archaeological Survey: The Light Fantastic*, Swindon: Historic England.

Historic England, n.d., *Using Aerial Photographs,* https://historicengland.org.uk/research/methods/airborne-remote-sensing/aerial-photographs/.

Iglhaut, J., et al., 2019, "Structure from Motion Photogrammetry in Forestry: a Review," in *Current Forestry Reports*, v. 5, 155-168.

Johnston, G., July 18, 2018, *Interpreting GPR Data: The Basics, Part 1*, Sensors & Software Inc., https://www.youtube.com/watch?v=D01oUf1-DvU&t=787s.

Johnston, G., August 11, 2021, *Using GPR to Locate Unmarked Graves Webinar*, Sensors & Software Inc., https://www.youtube.com/watch?v=rV5Z_6AUMUk&t=942s.

Jurkovšek, B., et al., 2016, "Geology of the Classical Karst Region (SW Slovenia-NE Italy)," in *Journal of Maps*, v. 12 (S1), 352-362.

Lonza, B., 1977, "Appunti sui castellieri dell'Istria e della provincia di Trieste," in *Società per la preistoria e la protostoria della regione Friuli-Venezia Giulia*, Quaderno n. 2, Trieste: I. Svevo.

Lonza, B., 1981, "La ceramica del castelliere degli Elleri," in *Società per la preistoria e la protostoria della regione Friuli-Venezia Giulia*, Quaderno n. 4, Trieste: I. Svevo.

Lowe, D., 1999, "Object recognition from local scale-invariant features," in *Proceedings of the International Conference on Computer Vision*, v. 2, 1150-1157.

Lugari, A., 2014, *Active and Passive Remote Sensing Techniques and Artificial Neural Networks in Support of Buildings Seismic Vulnerability Assessment,* Civil and Computer Engineering Department, Tor Vergata University, Rome, Italy, DOI:10.13140/2.1.2200.7682.

Luo, L., et al., 2019, “Airborne and spaceborne remote sensing for archaeological and cultural heritage applications: A review of the century (1907-2017),” in *Remote Sensing of Environment*, 232, 111280.

Marchesetti, C., 1903, “I Castellieri preistorici di Trieste e della regione Giulia,” in *Atti del Museo Civico di Storia Naturale di Trieste*, 10, v. 4, 1-206.

McLeester, M., et al., 2018, “Detecting prehistoric landscape features using thermal, multispectral, and historical imagery analysis at Midewin National Tallgrass Prairie, Illinois,” in *Journal of Archaeological Science: Reports*, v. 21, 450-459.

Mihovilić, K., Hänsel, B., Teržan, B., Matošević, D., 2009, “Redni broj: 152,” in Mesić, et al., *Hrvatski arheološki godišnjak (Eng. Croatian Archaeological Yearbook)*, Zagreb: Ministarstvo culture Uprava za arhivsku djelatnost i arheološku baštinu (Eng. Ministry of Culture: Directorate for Archives and Archaeological Heritage), 347-350.

Mihovilić, K., 2013, “*Castellieri-Gradine* of the Northern Adiratic,” in Fokkens, H., Hardings, A., *The Oxford Handbook of the European Bronze Age*, Oxford: Oxford University Press, 864-876.

Monnet, J.M., 2012, *Airborne laser scanning for forest applications – state of the art,* HAL open science, IRSTEA, hal-02601299.

National Aeronautics and Space Administration (NASA), 2010, “Introduction to the Electromagnetic Spectrum,” *Science Mission Directorate*, http://science.nasa.gov/ems/01_intro.

National Collection of Aerial Photography, 1941, San Dorligo della Valle Friuli Venezia Giulia, NCAP-000-000-050-243.

National Coordination Office for Space-Based Positioning, Navigation, and Timing. 2021. *The Global Positioning System. U.S. Space Force*. https://www.gps.gov/systems/gps/.

National Weather Service, “Beaufort Wind Scale,” U.S. Department of Commerce, https://www.weather.gov/mfl/beaufort.

Novo, A., et al., 2008, *3D GPR in Archaeology: What can be gained from dense Data Acquisition and Processing?*, Proceedings of the 12th International Conference on Ground Penetrating Radar 2008, Birmingham, UK.

Pearson, T. et al., 2015, *Where on Earth Are We? The Role of Global Navigation Satellite Systems (GNSS) in Archaeological Field Survey*, Swindon: Historic England.

Percan, T., 2021, "Sv. Križ – St. Cross (Istria, Croatia): some remarks on the food preparing and storaging during the Bronze Age in the Northern Adriatic Region," in Jallot, L., Peinetti, A., *Use of Space and Domestic Areas: Functional Organization and Social Strategies*, Oxford: Archaeopress, 31-52.

Permanent Delegation of Slovenia to UNESCO, 2015, "Klasicni kras (Eng. Classical Karst)," in *Tentative Lists*, Category: Natural, Ref.: 6072, UNESCO World Heritage Centre.

Regione Autonoma Friuli Venezia Giulia (RAFVG), 2023, "Catalogo dei Dati Ambientali e Territoriali," in *Repertorio dei Dati e dei Servizi Ambientali e Territoriali,* https://www.regione.fvg.it/rafvg/cms/RAFVG/ambiente-territorio/conoscere-ambiente-territorio/FOGLIA7.

Sarris, A., 2016, "Geophysics," in Gilbert, A.S., *Encyclopedia of Geoarchaeology*, Encyclopedia of Earth Sciences Series, 323-326, Springer Cham.

Sharma, M., Sara, R., Jariwala, J., Agarwal, S., 2022, "Study of Camera Sensor Type and Resolution for Georeferencing Point Cloud using Structure from Motion (SfM) and Photogrammetry," in *Indian Journal of Spatial Science*, 13, 44-51.

SONY Electronics Inc., "Alpha 6000 – APS-C Interchangeable Lens Camera 24.3MP, 11FPS, Full HD 1080p," Minato City, Japan, https://electronics.sony.com/imaging/interchangeable-lens-cameras/aps-c/p/ilce6000-b.

Stolt, R.H., 1978, "Migration by Fourier Transform," in *Geophysics*, v. 43(1), 23-48.

Tabbagh, A., 2016, "Electrical Resistivity and Electromagnetism," in Gilbert, A.S., *Encyclopedia of Geoarchaeology*, Encyclopedia of Earth Sciences Series, 211-219, Springer Cham.

Teledyne FLIR LLC, “FLIR Vue Pro,” Oregon, USA, https://www.flir.com/products/vue-pro/?model=436-0015-00S&vertical=suas&segment=oem.

Teledyne FLIR LLC, “FLIR Thermal Studio Suite (TSS),” https://www.flir.com/products/flir-thermal-studio-suite/.

Teledyne FLIR LLC, 2023, “What is the operating temperature for the FLIR ONE?” https://www.flir.com/support-center/flir-one/what-is-the-operating-temperature-for-the-flir-one/.

Thomas, H., 2018, “Some like it hot: The impact of next generation FLIR Systems thermal cameras on archaeological thermography,” in *Archaeological Prospection*, v. 25, 81-87.

Thomas, H., Williams, E., 2019, “High resolution terrestrial thermography of archaeological sites,” in *Archaeological Prospection*, v. 26(3), 189-198.

Turk, I., Modrijan, Z., Prus, T., Culiberg, M., Šercelj, A., Perko, V., Dirjec, J., & Pavlin, P., 1993, “Podmol pri Kastelcu - novo večplastno arheološko najdišče na Krasu, Slovenija (Eng. Podmol Near Kastelec – A New Multi-Layered Archaeological Site on the Karst in Slovenia),” in *Arheološki Vestnik*, v. *44*(1), 45-96.

Vlastelica, G. et al., 2018, “Durability of soft rocks in Eocene flysch formation (Dalmatia, Croatia),” in *Engineering Geology*, v. 245, 207-217.

Zendron, F., 2017, “In cammino verso la storia, I manufatti dell’età del Bronzo e dell’età del Ferro,” in Maggi, P., Pieri, F., Ventura, P., *Monte Castellier, Le pietre di Elleri narrano la storia*, Trieste: Edizioni Università di Trieste, 209-249.